

Recovery of organic solvents from dewaxed oil mixtures using Organic Solvent Nanofiltration technology

by

Alexander Spratt

Thesis presented in partial fulfilment
of the requirements for the Degree



of
MASTER OF ENGINEERING
(CHEMICAL ENGINEERING)

in the Faculty of Engineering
at Stellenbosch University

Supervisor

Prof. P. Van der Gryp

Co-supervisor

Prof. A. Burger

April 2019

DECLARATION

By submitting this thesis electronically, I declare that the entirety of the work contained therein is my own, original work, that I am the sole author thereof (save to the extent explicitly otherwise stated), that reproduction and publication thereof by Stellenbosch University will not infringe any third party rights and that I have not previously in its entirety or in part submitted it for obtaining any qualification.

Date: April 2019

Copyright © 2019 Stellenbosch University

All rights reserved

PLAGIARISM DECLARATION

1. Plagiarism is the use of ideas, material and other intellectual property of another's work and to present it as my own.
2. I agree that plagiarism is a punishable offence because it constitutes theft.
3. I also understand that direct translations are plagiarism.
4. Accordingly, all quotations and contributions from any source whatsoever (including the internet) have been cited fully. I understand that the reproduction of text without quotation marks (even when the source is cited) is plagiarism.
5. I declare that the work contained in this assignment, except where otherwise stated, is my original work and that I have not previously (in its entirety or in part) submitted it for grading in this module/assignment or another module/assignment.

Initials and surname:

Date: April 2019

ABSTRACT

Solvents are valuable chemicals, which are conventionally recovered through energy intensive processes such as distillation. In lube oil dewaxing processes, four times more solvent relative to solute is required. Solvents, such as toluene and methyl ethyl ketone (MEK), are commonly used in the dewaxing process. Due to high-energy costs, potential alternatives to recover these solvents are investigated. An alternative to solvent recovery through distillation is the use of Organic Solvent Nanofiltration (OSN) technology, which incorporates nanofiltration membranes designed to separate solvent-oil mixtures. The Max DeWax operation using OSN technology demonstrated successful recovery of solvent, while providing lower energy usage in solvent recovery. The research documented in this thesis focused on solvent recovery, membrane performance, transport modelling and techno-economic evaluation.

The main aim of the project was to investigate the viability of OSN separation as an alternative method to conventional process separation. OSN viability evaluation was accomplished through demonstrating the recovery of solvent-oil mixtures using novel membranes. Experimental investigations performed in this study focused on recovery of four commercially available solvents used in lube-oil dewaxing processes, namely toluene, methyl ethyl ketone (MEK), methyl-isobutyl ketone (MIBK), di-chloro-methane (DCM) and the solute species which represented long-chain paraffin solutions, n-hexadecane ($C_{16}H_{34}$). Duramem™150, Duramem™200 and Puramem™280 membranes were used for the recovery process. Operating parameters, which include pressure, solute feed concentration, solvent type and membrane type, were varied and the effects thereof on membrane performance were investigated.

The investigation also focused on describing the mass transfer through membranes using transport models, such as solution-diffusion and pore-flow transport models, using Matlab R2013a. Modelling of the mass transfer of MEK and toluene, well-known commercial solvents used in lube-oil dewaxing and processing, was done according to two pore-flow models (PF-1, PF-2) and two solution-diffusion models (SD-1, SD-2) using Duramem™150, Duramem™200 and Puramem™280 membranes. Furthermore, the permeability of hexadecane was regressed to fit the experimental data.

The viability of OSN operations in comparison to distillation operations was determined through a preliminary techno-economic evaluation using simulation software (Aspen Plus V8.8) to describe the mass and energy and provide supporting data for use in cost evaluation. Energy consumption, equipment performance as well as operating and capital costs were investigated.

The main contributions made by this study are threefold: **(i)** to demonstrate the successful recovery of solvent-oil mixtures using novel membranes through experimentation, **(ii)** to describe the transport through membranes using transport models and **(iii)** to investigate the economic feasibility of OSN systems, using simulation software.

i) Recovery of solvents from oil mixtures

This study found that the recovery of MEK from solute was the most successful while providing high membrane fluxes and high rejections over the rest, followed by DCM. Overall, MEK and n-hexadecane, at feed concentrations above 20 wt/wt% separated using Duramem™150 membranes, provided >90% rejection, while permeating at fluxes of approximately 12 L.m⁻².hr⁻¹. Membrane performance and solvent behaviour of permeating species were found to be affected mainly by applied pressure, chemical properties that describe polarity such as di-electric constant and dipole moment as well as properties such as molar volume, viscosity and solubility parameters.

ii) OSN modelling and simulation

The transport of pure solvent and binary solvent-solute mixtures was described using transport models based on literature. Using MEK and toluene, the two-parameter pore-flow model (PF-2) and the classical solution-diffusion model (SD-1) provided relatively good predictions for the transport through the polar stable membranes such as Duramem™150 and Duramem™200, but poor predictive models for non-polar stable membranes such as Puramem™280. The PF-2 model and SD-1 model provided Pearson coefficients of >0.988 and >0.996, respectively, for the Duramem™ series membranes. The SD-1 model was further improved after regressing the estimated permeability parameter of hexadecane which provided an optimized Pearson coefficient of 0.9995.

iii) OSN solvent recovery

For both OSN and distillation systems, while ignoring the cost of raw material, It was found that the energy required to recover a ton of MEK solvent by OSN (i.e. 2.5 kWh.ton_{solvent_product}⁻¹) is approximately 50 times less than that of distillation (135 kWh.ton_{solvent_product}⁻¹) with energy recovery incorporated, which also results in a lower carbon footprint. However, by using the Nelson-Farrar cost index, it was found that the capital costs for OSN (\$0.85 million) in 2015 were approximately ~25% of the capital cost for distillation (i.e. \$3.36 million). The operating costs, while ignoring the cost of raw material and having a total operating feed capacity of 1 ton.hr⁻¹, were approximately \$0.075 million.yr⁻¹ for OSN operation and \$0.155 million.yr⁻¹ for distillation operation with a recycling stream and heat integration, while providing solute rejections as high as 97%. Total operating costs of OSN are less than half the amount required

for distillation with heat integration, where energy and maintenance costs differ significantly between the two processes.

SAMEVATTING

Oplosmiddels is waardevolle chemikalieë wat op gerieflike wyse hernu kan word deur energie intensiewe prosesse soos distillasie. In smeerolie ontwassingsprosesse word vier keer meer oplosmiddel relatief tot opgeloste stof benodig. Oplosmiddels, soos tolueen en metietielketoon (MEK), word algemeen gebruik in die ontwassingsproses. Weens hoë energie kostes, word potensieel alternatiewe prosesse vir die herwinning van hierdie oplosmiddels ondersoek. 'n Alternatief vir oplosmiddel herwinning deur distillasie is die gebruik van Organiese Oplosmiddel Nanofiltrasie (OSN) tegnologie, wat nanofiltrasie membrane inkorporeer wat ontwerp is vir die skeiding van oplosmiddel-olie mengsels. Die Max Dewax proses, wat OSN tegnologie gebruik, is in staat om oplosmiddel suksesvol te herwin terwyl die proses ook laer energieverbruik getoon het. Die navorsing wat beskryf word in hierdie tesis fokus op oplosmiddel herwinning, membraan werksverrigting, transmembraanvervoer modellering en tegno-ekonomiese evaluering van die OSN proses.

Die hoofdoel van die projek was om die lewensvatbaarheid van OSN as 'n alternatief tot konvensionele prosesse te ondersoek. Die evaluering van OSN lewensvatbaarheid is voltooi deur die herwinning van oplosmiddel-olie met nuwe tipes van moderne membrane te demonstreer. Die eksperimentele ondersoeke wat uitgevoer is het gefokus op die herwinning van vier kommersieel beskikbare oplosmiddels deur gebruik te maak van smeerolie ontwassingsprosesse. Die vier oplosmiddels waarvan die herwinning ondersoek is, was tolueen, metietielketoon (MEK), metiel-isobutiel ketoon (MIBK) en dichloormetaan (DCM). Die opgeloste stof, wat langketting paraffien oplossings verteenwoordig het, was n-heksadekaan ($C_{16}H_{34}$). DuramemTM150, DuramemTM200 en PuramemTM280 membrane is gebruik in die herwinningsproses. Bedryfsparameters insluitende druk, opgeloste stof toevoerkonsentrasie, oplosmiddeltipe en membraantipe, is gevarieer en die effek daarvan op die membraan werksverrigting is ondersoek.

Die ondersoek het ook daarop gefokus om die massa-oordrag deur membrane te beskryf deur gebruik te maak van vervoermodelle, soos oplossing-diffusie en porie-vloei modelle in Matlab R2013a. MEK en tolueen is bekende kommersiële oplosmiddels wat gebruik word in smeerolie ontwassing en prosessering. Modellering van die massa-oordrag van hierdie twee oplosmiddels is gedoen volgens twee porie-vloei modelle (PF-1, PF-2) en twee oplossing-diffusie modelle (SD-1, SD-2), deur gebruik te maak van DuramemTM150, DuramemTM200 en PuramemTM280 membrane. Verder is regressie gedoen van die membraan deurlaatbaarheid van heksadekaan om 'n passing met die eksperimentele data te verkry.

Die lewensvatbaarheid van die bedryf van OSN sisteme in vergelyking met distillasie sisteme is vasgestel deur 'n voorlopige tegno-ekonomiese evaluasie te doen. Hiervoor is simulاسie

sagteware (Aspen Plus V8.8) gebruik om die massa en energie te beskryf en om ondersteunende data te genereer vir gebruik in koste evaluasie. Energieverbruik, toerusting werksverrigting asook bedryfs- en kapitale kostes is ondersoek.

Die hoof bydraes wat gemaak is deur hierdie studie is drieledig: (i) demonstrasie deur eksperimentering van die suksesvolle herwinning van oplosmiddel-olie mengsels deur gebruik te maak van nuwe, moderne membrane, (ii) die beskrywing van die vervoer deur membrane deur gebruik te maak van vervoermodelle en (iii) die ondersoek van die ekonomiese lewensvatbaarheid van OSN sisteme deur gebruik te maak van simulاسie sagteware.

i) Herwinning van oplosmiddels uit olie mengsels.

Hierdie studie het gevind dat die herwinning van MEK uit oplossing die suksesvolste was, gevolg deur dié van DCM. Hoë membraanvloei en verwerpings is hiervoor verkry. MEK en n-heksadekaan is geskei deur Duramem™150 membrane by toevoerkonsentrasies bo 20 gew./gew.% en >90% verwerping is gelever teen deursypelingsvloei van ongeveer 12 L.M⁻².h⁻¹. Daar is gevind dat die membraan werksverrigting en oplosmiddelgedrag van die deurdringende spesie hoofsaaklik geaffekteer is deur toegepaste druk, chemiese eienskappe wat polareit beskryf soos diëlektriese konstante en dipoolmoment, asook eienskappe soos molêre volume, viskositeit en oplosbaarheidsparameters.

ii) OSN modellering en simulاسie.

Die vervoer van suiwer oplosmiddel en binêre oplosmiddel-opgeloste stof mengsels is beskryf deur gebruik te maak van vervoermodelle wat gebasseer is op wetenskaplike literatuur. Met MEK en toluen as oplosmiddels, het die twee-parameter porie-vloei model (PF-2) en die klassieke oplossing-diffusie model (SD-1) goeie voorspellings verkry vir die vervoer deur polêr stabiele membrane soos Duramem™150. Die voorspellingsvermoë van die modelle vir die vervoer deur nie-polêr stabiele membrane, soos Puramem™280, was egter swak. Die PF-2 model en SD-1 model het Pearson koëffisiënte van >0.988 en >0.996, respektiewelik, verkry vir die Duramem™ reeks membrane. Die SD-1 model is verder verbeter deur regressie van die geskatte deurdringingsparameter van heksadekaan wat 'n geoptimeerde Pearson koëffisiënt van 0.9995 gelever het.

iii) OSN oplosmiddel herwinning.

Vir beide OSN sowel as distillasie stelsels, terwyl die koste van rou materiaal geïgnoreer word, daar is gevind dat die energie wat nodig is om n ton oplosmiddel te herwin van OSN (2.5 kWh.ton_{solvent_product}⁻¹) ongeveer 50 keer minder is as dié van distillasie (135 kWh.ton_{solvent_product}⁻¹) met energie herwinning ingesluit, wat ook 'n laer koolstofvoetspoor tot gevolg het. Daar is egter gevind, deur gebruik te maak van die Nelson-Farrar koste-indeks, dat die kapitale koste

van OSN (\$0.85 miljoen) in 2015 ongeveer 'n kwart was van die kapitale koste van distillasie (\$3.36 miljoen). Die bedryfskoste, terwyl die koste van rou material geïgnoreer word en 'n totale bedryfskapasiteit van $1 \text{ ton} \cdot \text{hr}^{-1}$ het, was ongeveer $\$0.075 \text{ miljoen} \cdot \text{j}^{-1}$ vir die OSN sisteem en $\$0.155 \text{ miljoen} \cdot \text{j}^{-1}$ vir die distillasie sisteem met 'n hersirkuleringstroom en hitte integrasie, wat verwerpings vir opgeloste stof so hoog soos 97% gelever het. Die totale bedryfskoste van OSN minder as die helfte is van dié van distillasie met hitte integrasie, met energie- en instandhoudingskoste wat die meeste verskil tussen die twee sisteme.

ACKNOWLEDGEMENTS

I would like to thank the Lord for this journey through Stellenbosch University. For providing me the chance to become part of the Eendrag Men's Residence family in my first year, then enrolling for a Bachelor in chemical engineering in my second year, the opportunity to make amazing friends and lastly for providing me the chance to do my Master's Degree in Chemical Engineering in 2016.

I would like to thank my amazing parents for their support, which I needed to complete this thesis over the two years of study. They have always been there for me and I would not have been able to do this without them by my side.

I would like to thank my supervisor, Prof. P. van der Gryp for being supportive and making the Master's journey a fun and exciting one, which I will cherish and take with me on the journey after my Master's. Through some laughs and sad times, we formed a bond that I will forever be grateful for. I will never forget the day you gave me the chance to take on this project. Additionally, I would like to thank Prof. A. Burger for his insight and academic support.

I would like to thank my friends for the great laughs inside the laboratory, outside the laboratory and making my journey fun and enjoyable. My friends made me realize that time is too short to worry about the small things - so enjoy the moments in life as they appear in front of us. Additionally, I would like to thank my dear friend Brandon Wakefield for assisting me with the implementation of transport models in Matlab software.

I would lastly like to thank Sasol for providing me the funding in order to complete this thesis.

Table of Contents

DECLARATION	ii
PLAGIARISM DECLARATION	iii
ABSTRACT	iv
SAMEVATTING	vii
ACKNOWLEDGEMENTS	x
Nomenclature	xiv
Chapter 1: Introduction	1
1.1. Background and motivation	2
1.2. Objectives	4
1.3. Scope of study and thesis layout	5
1.4. References	7
Chapter 2: Literature Study	9
2.1. Theoretical background	10
2.1.1 Principles of OSN	14
2.2 Review of solvent recovery using OSN	15
2.3. Review of transport models in solvent recovery	23
2.3.1. Membrane transport theory	23
2.3.2. Solution-diffusion divergence	27
2.3.3. Pore-flow divergence	28
2.3.4. Combination of solution-diffusion and pore-flow	29
2.3.5. Phenomenological models	30
2.4. Review of cost and energy analysis	31
2.5. Concluding remarks	34
2.6. References	35
Chapter 3: Methodology	39
3.1. Materials	40
3.1.1. Chemicals	40
3.1.2. Membranes	40

3.2. Organic Solvent Nanofiltration (OSN) experimentation	41
3.2.1. Experimental Setup	41
3.2.2. Experimental methodology	43
3.3. Analytical techniques	44
3.3.1. Gas-chromatography	44
3.4. Methodology of membrane transport	46
3.4. Methodology of economic analysis	49
3.5. References	52
Chapter 4: Results and Discussion – Recovery of Solvent	54
4.1. Introduction	55
4.2. Experimental error and reproducibility	55
4.3. Pure species permeation tests	58
4.4. Effect of solvent properties	60
4.5. Binary species permeation and rejection	68
4.6. Concluding remarks	72
4.7. References	73
Chapter 5: Results and Discussion - OSN Characterization and Modelling	75
5.1. Introduction	76
5.2. Pore-flow model	77
5.3. Solution-diffusion model	79
5.4. Regression of P_{c16}^{SD}	81
5.5. Concluding remarks	83
5.6. References	84
Chapter 6: Cost and Energy Evaluation	85
6.1. Introduction	86
6.2. Design base case	87
6.3. Design approach	88
6.3.1. Solvent recovery by distillation	88
6.3.2. Solvent recovery by OSN	91

6.4. Results and feasibility analysis	93
6.5. Concluding remarks.....	94
6.6. References	96
Chapter 7: Conclusions and Recommendations.....	98
7.1. Solvent recovery.....	99
7.2. OSN transport modelling	100
7.3. Energy and economic evaluation.....	101
7.4. Recommendations for future work	101
7.5. References	103
Appendices	104
Appendix A: Detailed experimental procedure.....	105
Appendix B: Analytical procedures and calibrations	108
B.1. Start-up, operational and shutdown procedures	109
B.2. Calibration curves and data.....	109
Appendix C: Sample calculations	111
C.1. Experimental flux and rejection	112
C.2. Transport modelling	113
Appendix D: Raw experimental data	119
D.1. Pure species flux tests	120
D.2. Summary of all experimental calculated data	130
Appendix E: Simulation data	134
E.1 OSN stream data	135
E.2 Distillation stream data	136
E.3. Heat exchanger Aspen Plus™ data.....	137

Nomenclature

Abbreviations	
API	Active pharmaceutical ingredient
Da	Daltons
DCM	Dichloromethane
DMC	Dimethyl carbonate
DMF	Dimethyl formamide
DMMS	Dimethyl methylsuccinate
EtOH	Ethanol
GC	Gas-chromatography
MeCN	Acetonitrile
MEK	Methyl ethyl ketone
MeOH	Methanol
MET	Membrane extraction technology
MF	Microfiltration
MWCO	Molecular weight cut off
NF	Nanofiltration
OSN	Organic solvent nanofiltration
PEG	Polyethyleneglycol
PF	Pore-flow
RO	Reverse osmosis
SD	Solution-diffusion
SFPF	Surface force pore-flow
SRNF	Solvent resistant nanofiltration
TCE	Trichloroethylene
TDA	Tridecylamine
TDDA	Tridodecylamine
TEA	Triethylamine
THeptA	Triheptylamine
THexA	Trihexylamine
THF	Tetrahydrofuran
TOABr	Tetraoctylammonium bromide
TOA	Trioctylamine
TPP	Triphenylphosphine
UF	Ultrafiltration

Symbol	Description	units
A	Surface area	m ²
C _f	Feed solute concentration	mg.L ⁻¹ ((mL.mL ⁻¹)
C _p	Permeating solute concentration	mg.L ⁻¹ (mL.mL ⁻¹)
d	Pore diameter	mm
J	Permeate flux	L.m ⁻² .hr ⁻¹
L _i	Coefficient of proportionality	
P	Pressure	Bar
P ^{sat}	Saturation pressure	Bar
R _{solute}	Rejection of solute	%
R	Universal gas constant	J.mol ⁻¹ .K ⁻¹
t	Time	hr
T	Temperature	°C
V _n	Permeating volume	Litres
x _i	Molar fraction of species i	

Greek Symbols		
ε	Porosity	
φ	Fugacity coefficient of species i	
τ	Tortuosity	
μ	Chemical potential	
dμ _i /dx	Chemical potential gradient of component i	

Chapter 1: Introduction

Overview

This chapter provides a broad overview of the research of this investigation and is divided into three subsections, beginning with background and motivation for this investigation in Section 1.1. The aims and objectives of the research are formulated in Section 1.2, followed by a discussion of the layout and scope of the thesis in Section 1.3.

1.1. Background and motivation

Lubricant production, with more than 100 operations internationally, is one of the most energy intensive processes in the refining industry [21]. Furthermore, lubricating oil is the most commonly used lubricant that is produced by the refining of crude oil to a variety of different oil base stocks. Lubricant production illustrated in Figure 1.1 consists of two main intermediate steps, namely the fractional distillation process and the oil-dewaxing process.

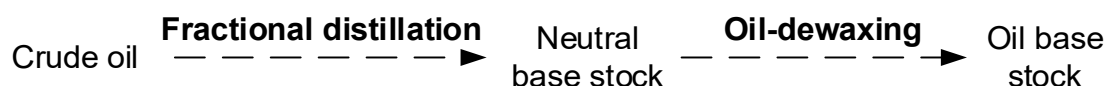


Figure 1.1: main Intermediate processes in lubricant production from crude oil.

Significant amounts of solvent are fed through the process, making solvent recovery an attractive option towards reducing expenses on operating costs. Solvent recovery from the oil-dewaxing step shown in Figure 1.1 is commonly practiced in industry [2]. Conventionally, the waxy feed in the dewaxing process is initially mixed with solvent before being chilled to desired filtration temperatures, allowing the waxy feed components to precipitate. The feed mixture enters a rotatory drum separator, which then separates the feed into slack wax and oil filtrate. The oil filtrate, which consists mostly of solvent, is sent through distillation operations for the recovery of solvent from the oil filtrate [1].

Solvent recovery by distillation is a conventional method used in the separation of mixtures by creation of two or more coexisting zones, which differ in temperature, pressure and composition as well as phase state [3]. High-energy input, capital costs and large space requirements are however associated with distillation processes. Additionally, distillation has the risk of bottlenecking the flow through processes involving slow filtration of waxy components [4]. Distillation can be hydraulically limited or may be constrained by the heat input through steam heaters or fired furnaces [5]. The drawbacks of distillation such as high-energy requirements are a concern that should be dealt with by identifying novel separation technologies.

One novel separation technology, which has been brought to the industrial level, is membrane separation, specifically focusing on Organic Solvent Nano-filtration (OSN). OSN technology has been a promising new separations technology for processes like solvent recovery in lube oil dewaxing [6,7]. Over the past few years researchers have investigated this novel technology with regard to operation performance, energy consumption and economic feasibility. This technology is competing with conventional separation operations as an alternative separation technology. OSN technology, combined with the initial distillation

operation, has the potential to debottleneck the flow through the dewaxing process while recovering solvent at (or near) dewaxing temperatures. Recycled solvent at dewaxing temperatures decreases filter feed viscosity, resulting in higher filtration rates, which reduces the risk of bottlenecking throughout the dewaxing process [5]. Initially the focus had been on the performance of membranes, such as in the work of White and co-workers [8], where membrane performances were tested for the recovery of solvents. Many other research groups [9-11] have since illustrated that the performance of membrane separation of solvents from solutes is highly competitive with that of distillation performances.

Previously available commercial membranes (i.e. Starmem™) have been sufficiently modelled [13,14]. However, currently available commercial membranes, such as Duramem™, Puramem™ as well as PerVap [15,16], have been shown to provide better performance than the Starmem™ membranes. However, modelling of these membranes have not been done sufficiently, and thus a consensus agreement on the best model is not available.

The obstacles associated with OSN systems are commonly found in the design phase of industrial applications. One challenge in the design phase includes choosing a suitable membrane for the specific system in question (i.e. toluene recovery from dewaxed-oil mixture). Another challenge is describing the effect of operating conditions on the performance of a system. This obstacle was observed in the work of Silva *et al.* [12], where a solution-diffusion model was developed to describe the flux and rejection of a TOABr-toluene mixture at one temperature. The use of this solution-diffusion model for other systems creates some uncertainty, as experimentation needs to be done to determine the influence of certain operating parameters, such as temperature, on the performance of the specific membrane. These aforementioned obstacles make it challenging to find an optimal process (i.e. optimal number of modules, retentate and permeate recycling internally, arrangement, etc.)

Over the past decade transport phenomena have been a subject of interest in OSN research. Peeva *et al.* [17] focused on developing transport models for specific membranes. Peeva and co-workers summarized various transport models that have been used such as the solution-diffusion model as well as pore-flow modules. Combining membrane modelling with simulation is complex and only a handful of researchers have demonstrated the crossover between modelling of membranes to simulation. Chowdhury *et al.* [18] modelled a gas separation system through hollow fibre membranes. Darvishmanesh *et al.* [19] also simulated an OSN system using Aspen Custom modeller for Duramem™ membranes. Fontalvo *et al.* [20] chose to link Matlab to excel and Aspen interface in order to model the membrane system.

Economic evaluations have been discussed as early as the implementation of the MAX DEWAX process and have been of interest to many researchers [21,22], who have performed

techno-economic evaluations. With reference to commercial applications, such as the MAX DEWAX process [1], it is evident that the process can be economical and viable. However, to overcome the aforementioned obstacles and challenges, state-of-the-art research should be of importance. State-of-the-art research on novel OSN membrane operation includes investigations on membrane fabrication, membrane performance, transport modelling and economic evaluations.

1.2. Objectives

The aim of this study is threefold: **i)** firstly, to demonstrate the successful utilization of OSN in recovering solvents from solvent-oil mixtures, **ii)** secondly, to describe the mass transport of the solvent-oil system through the membrane using different fundamental models, and **iii)** thirdly, to illuminate on a preliminary level the economic potential of using OSN compared to distillation. The objectives of this study are summarized as follows:

i) Recovery of solvents from oil mixtures

- Experimental investigation on membrane performance for the recovery of various solvents (methyl-ethyl-ketone, toluene, methyl-isobutyl-ketone and dichloromethane) from an oil-solvent mixture.
- Investigate the effect of operating parameters such as pressure, membrane type (Duramem™ (150,200) and Puramem™280), concentration and solvent type on the membrane performance.
- Investigate the OSN separation performances in comparison to those of conventional processes (Aspen Plus™).

ii) OSN Modelling and simulation

- Investigate the use of transport models (pore-flow and solution-diffusion) to describe the transport through an OSN membrane.
- Simulating the membrane system using a simulation program (Aspen Plus™) and evaluate the mass and energy balances involved.
- Comparison between the OSN system and conventional systems with regard to energy usage in conjunction with the sub-objectives set out in part (i) for the recovery of solvents in solvent-oil mixtures.

iii) Technical and economic evaluation

- Preliminary techno-economic evaluation was done for the membrane system and was compared to conventional systems for solvent recovery (MEK, toluene) from a solute component representing dewaxed oil.

1.3. Scope of study and thesis layout

This thesis aims to provide insight and knowledge on the recovery of solvents using OSN membrane separation. The scope of this study is set out in Figure 1.2 in the form of a flow diagram to achieve the objectives listed in section 1.2. These objectives are discussed within the seven chapters in this thesis.

The objectives within the scope of this study are illustrated in Figure 1.2.

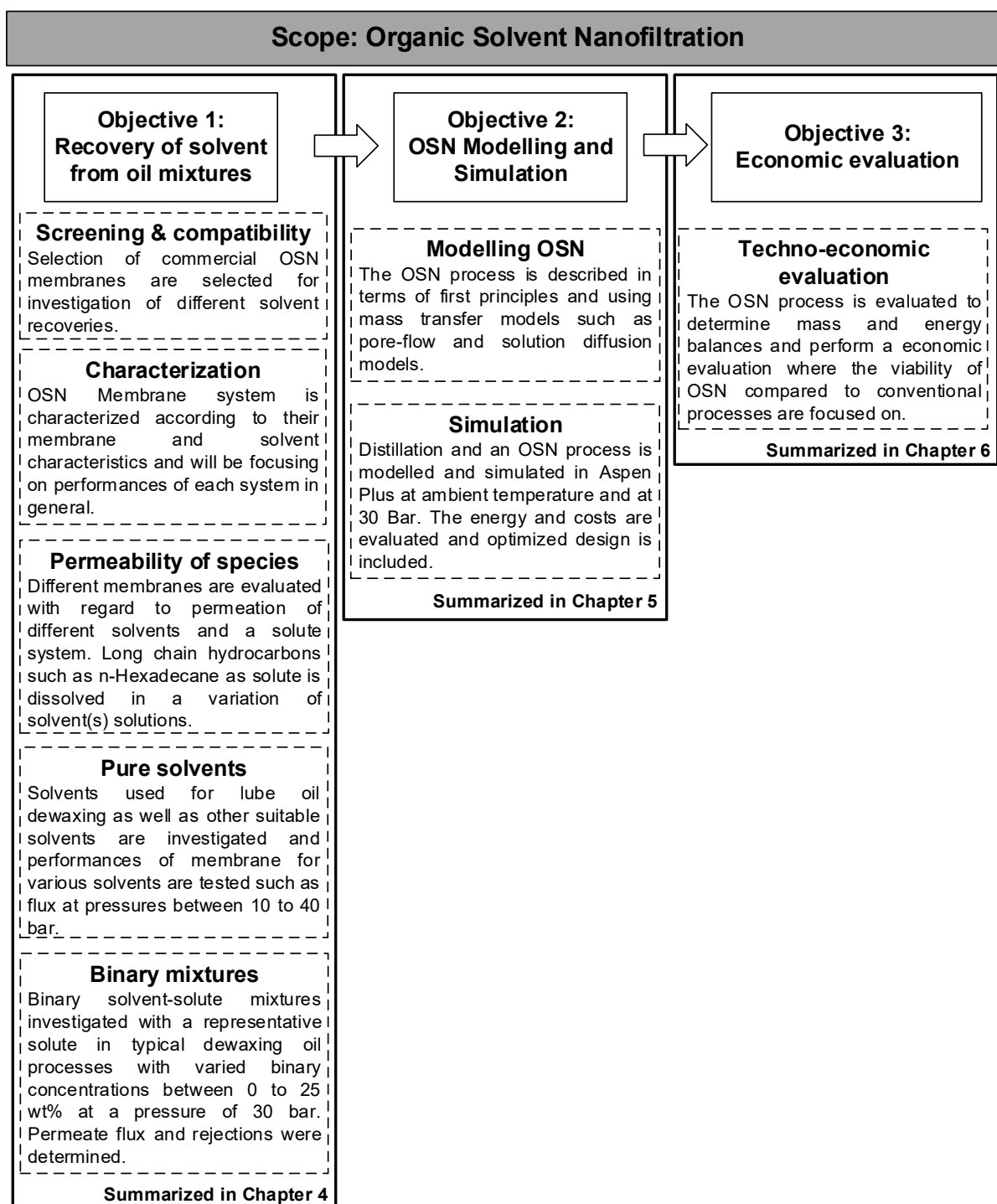


Figure 1.2: Scope of Study illustrated in the form of a diagram

Chapter 2 offers literary support to the investigations of this study, providing insightful and critical knowledge relating to the field of OSN. The purpose of this chapter is to critically review literature relevant to this study. OSN definitions and principles are discussed in this chapter followed by modelling and simulation. A state-of-the-art literature review is critical to understanding the state of current research and has been included with regard to solvent recovery and membrane performances.

Chapter 3 provides a detailed discussion on the practical aspects of this study. The discussion covers various aspects of how each of the investigations were conducted, detailing experimental procedures, approaches to modelling, experimental conditions and parameters used in this study. Materials and chemicals are included in this chapter along with diagrams and photographic illustrations of equipment.

Chapter 4 opens with a result summary to give the reader an overall idea of what is to be expected from this chapter, followed by the illustration of results and the discussion thereof. The discussion depicts the performances of commercial membranes, the influence of the solvent as well as the modelling and simulation of these systems using theory introduced in Chapter 2. Comparison with traditional solvent recovery methods are made by evaluating mass- and energy efficiency

Chapter 5 discusses the OSN modelling and simulation, which describes various transport models investigated with results. With the aid of experimental data, these models were developed and regressed; thereby covering part of objective (ii).

Chapter 6 covers objective (iii) and offers a preliminary techno- economic evaluation on the OSN system by making use of specific operating and capital costing heuristics. A comparison is made with traditional solvent recovery methods in order to determine the viability of OSN separation on an economic scale.

As a last chapter, **Chapter 7** provides a summary of the main findings from the investigations performed in this work and provides conclusions pertaining to the findings in a concise manner. Recommendations follow the conclusions of this work, which provide adequate suggestions for future work to be investigated.

1.4. References

- [1] R.M. Gould, L.S. White, C.R. Wildemuth, *Enviro. Prog.* **20** (2001) 12-16.
- [2] C. Capello, U. Fischer, K. Hungerbühler, *Green Chem.* **9** (2007) 927-934.
- [3] R. H. Perry, D. W. Green, ***Perry's chemical engineers' handbook***, McGraw-Hill, New York, 2008.
- [4] T. Welton, Solvents and sustainable chemistry, **471** (2015) 20150502.
- [5] N.A., Bhore, R.M Gould, S.M., Jacob, P.O., Staffeld, D., McNally, P.H., Smiley and C.R., Wildemuth, *Oil & gas J.*, **97**(1999) 67-72
- [6] M. Priske, M. Lazar, C. Schnitzer, G. Baumgarten, *Chem. Ing. Tech.* (2016) 39-49.
- [7] W.J. Koros, R. Mahajan, *J. Memb. Sci.* **175** (2000) 181-196.
- [8] L.S. White, A.R. Nitsch, *J. Memb. Sci.* **179** (2000) 267-274.
- [9] J.G. Speight, ***The chemistry and technology of petroleum***, CRC press, New York, 2014.
- [10] L.Z. Pillon, ***Interfacial properties of petroleum products***, CRC Press, New York, 2007.
- [11] Z. Zhao, J. Li, D. Zhang, C. Chen, *J. Memb. Sci.* **232** (2004) 1-8.
- [12] P. Silva, L.G. Peeva, A.G. Livingston, *J. Membr. Sci.* **349** (2010) 167.
- [13] X. Yang, A. Livingston, L.F. Dos Santos, *J. Memb. Sci.* **190** (2001) 45-55.
- [14] L. Hesse, J. Mićović, P. Schmidt, A. Górak, G. Sadowski, *J. Memb. Sci.* **428** (2013) 554-561
- [15] S. Ottewell, 'Membranes Target Organic Solvents', *Chemical Processing*, 24 June (2013).
- [16] H.B. Soltane, D. Roizard, E. Favre, *Sep. Purif. Tech.* **161** (2016) 193-201.
- [17] L.G. Peeva, E. Gibbins, S.S. Luthra, L.S. White, R.P. Stateva, A.G. Livingston, *J. Memb. Sci.* **236** (2004) 121-136.
- [18] M.H. Chowdhury, X. Feng, P. Douglas, E. Croiset, *Chem. Eng. & Tech.* **28** (2005) 773-782.
- [19] S. Darvishmanesh, T. Robberecht, P. Luis, J. Degrevé, B. Van Der Bruggen, *J. Am. Oil Chem. Soc.* **88** (2011) 1255-1261.
- [20] J. Fontalvo, *Ingeniería e Investigación* **34** (2014) 39-43.

[21] G. Szekely, M.F. Jimenez-Solomon, P. Marchetti, J.F. Kim, A.G. Livingston, *Green Chem.* **16** (2014) 4440.

[22] P. Schmidt, E.L. Bednarz, P. Lutze, A. Górak, *Chem. Eng. Sci.* **115** (2014) 115.

.

Chapter 2: Literature Study

Overview

The purpose of this chapter is to provide an understanding of terminologies, concepts and principles as well as literature that are relevant to this thesis. General knowledge of membrane separation as well as related concepts are discussed (Section 2.1). State of the art literature reviews on the use of membranes by Organic Solvent Nanofiltration (OSN) were investigated and are discussed in Section 2.2. OSN modelling research follows in Sections 2.3, describing the transport through the membrane. Energy and cost associated with OSN technology are further elaborated on in Section 2.4.

2.1. Theoretical background

According to Mulder [1] a membrane can be described as thick or thin, natural or synthetic as well as neutral or charged, while its structure can be homogenous or heterogeneous.

Membrane separation is a widely discussed topic that has made separation processes more simplistic with regard to lower energy consumption as well as waste generation when compared to conventional processes such as distillation [60,69]. Illustrated in Figure 2.1, membrane separation can be viewed as a selectively permeable membrane barrier separating two phases with a driving force [1].

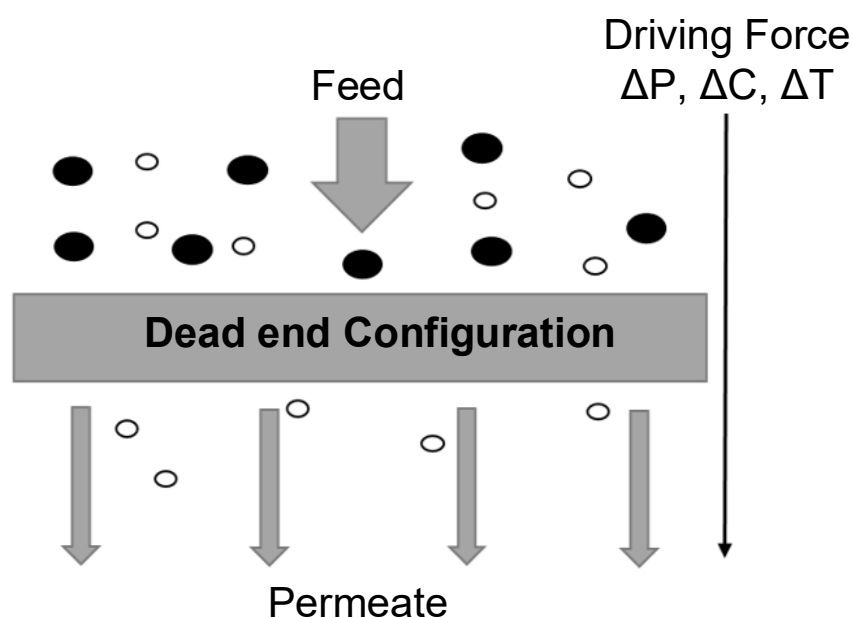


Figure 2.1: Membrane configuration and driving force.

A driving force through the membrane initiates separation through the membrane. Transport can be active or passive. Active transport, initiated by external force, is the movement of molecules or ions from a low concentration to a high concentration. Passive transport is the movement of molecules or ions from a high concentration to a low concentration. Passive transport can be driven as illustrated in Figure 2.1 by a pressure gradient, concentration potential, as well as temperature. Membranes are designed to contain specific properties that control the flow of molecular species through the membrane, i.e. only specific molecules can move through the membrane, hence forcing separation to occur. The design of the membrane takes a specie's molecular size, geometry, polarity as well as viscosity into account [1].

Research conducted over the past few years in the field of membrane technology tends to be application specific [2]. Membranes are system specific due to the process nature such as process conditions as well as material interactions. For this reason, a database of previous

work should be used as reference to determine the most appropriate membrane-system. A recent publication by Schmidt *et al.* [3] provides a thorough discussion on the membrane-system design procedure used to find the best membrane-system integration, which also expands the membrane-system specific database.

Membranes should not be confused with filter separations. By convention, the term filter is limited to structures that separate particulate suspensions ca 1 – 10µm [4]. As previously mentioned in this chapter, a membrane can be described as thick or thin, natural or synthetic as well as neutral or charged, while its structure can be homogenous or heterogeneous [4]. This gives more flexibility and accommodates for the complexity of a wide spectrum of systems. In this regard, the advantages and disadvantages of membranes are summarized in Table 2.1 [1].

Table 2.1: Advantages and disadvantages of membrane systems

Advantages	Disadvantages
Low energy consumption	Membrane fouling/ concentration polarization
Membrane integration	Low membrane lifetime
Easy to scale up	Generally low selectivity

Disadvantages listed in Table 2.1 are dependent on a number of factors. Fouling which occurs on a membrane is one important factor that has a major influence on the membrane performance [4]. Fouling is the surface accumulation on a membrane due to chemical species blocking membrane hollow pores near the surface. The chemical species block the pores forming a coated barrier, which affects the permeation of other chemical species through the membrane [5]. Concentration polarization is a fouling behaviour that affects the selectivity of a membrane. This behaviour can be described as the accumulation of retarded or slow permeating species relative to fast permeating species at the surface of the membrane. This causes a greater concentration of the retarding species at the membrane surface relative to the solution itself, and as a result hinders the permeate flow through the membrane [2]. Both fouling and concentration polarization can be controlled by using specific strategies such as prefiltration, high fluxes, membrane selection and cyclic cleansing of the membrane [5].

Membranes are classified according to their ability to separate specific chemical species from each other by size exclusion. Membranes can be classified as reverse osmosis (RO), nanofiltration (NF), ultrafiltration (UF) and microfiltration membranes. Each membrane classification is represented in Figure 2.2, where different ranges in pore size, pressure, permeability and molecular weight cut off (MWCO). MWCO is further discussed in section

2.1.1. Different molecules and chemical species are shown under each membrane class, which can potentially reject the species noted [6].

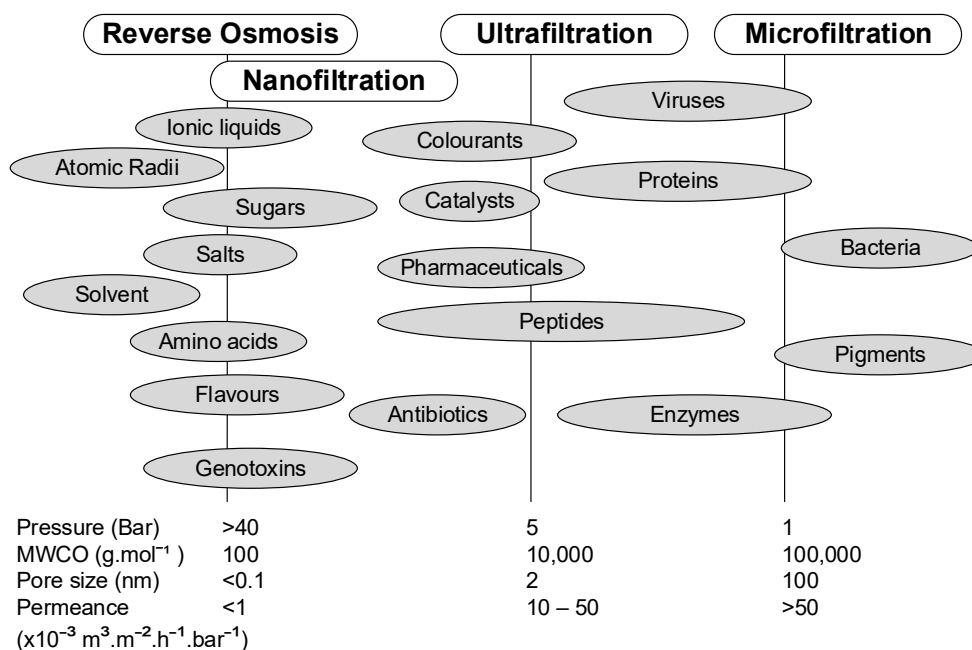


Figure 2.2: Membrane classification and their distinctive class ranges

NF membranes are relatively new to the membrane field and falls between the upper molecular weight range of RO membranes and the lower molecular weight of UF membranes [5]. NF has separation potential for chemical species in the size range of 200 – 1200 g.mol⁻¹, which is useful for separating solvents from organic compounds such as long chained linear and branched alkanes [2,7,8]. The field where solvents are separated from other organic components are classified as Organic Solvent Nanofiltration.

Organic Solvent Nanofiltration (OSN) yields the same advantages as other nanofiltration membranes in the sense that the separations require no phase transition, no additives, minimal thermal damage and are easily combined with other separations to form hybrid systems [2,6]. The integration of OSN membranes with other separation processes is a concern for companies who do not have the practical knowledge of such processes.

There are two flow configurations in which membrane separation of a feed produces a permeate and a retentate stream. The two types of flow configurations, illustrated in Figure 2.3, are commonly used in industry as well as in research facilities.

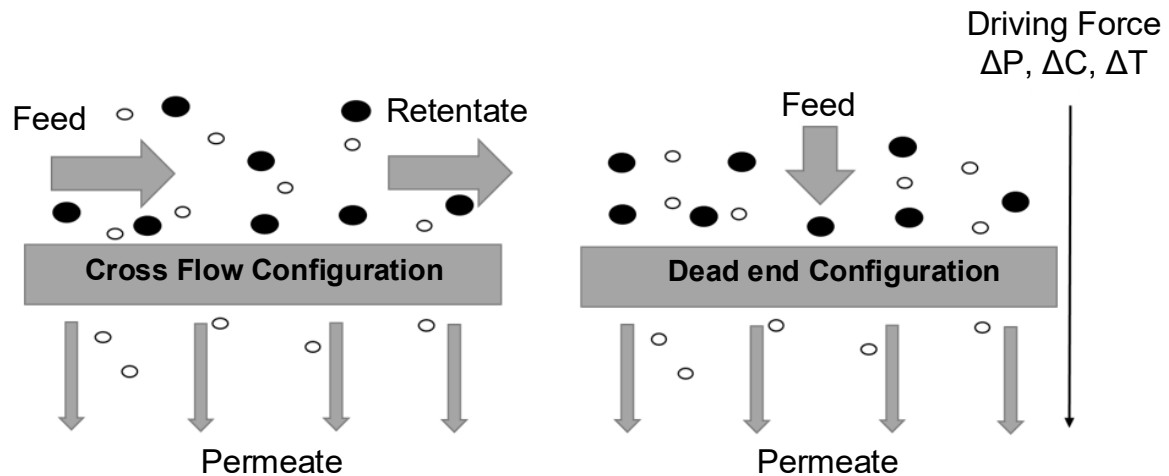


Figure 2.3: Dead end and cross flow configurations

In a dead-end membrane configuration setup, the retentate flows directly into the membrane wall. The retentate piles up against the wall, while the permeate flows through the selectively permeable membrane due to a differential pressure over the membrane. In a crossflow membrane configuration setup, the feed flows tangent to the membrane wall, while allowing the retentate to flow in the same direction and the permeate to leave through the other side of the permeable membrane. The continuous flow is produced using a pump pumping the feed continuously through the system. [9]

Dead-end configuration is useful for screening of membrane systems and is both cost effective and simplistic [10]. However, it is prone to concentration polarization, which can greatly affect performance, and for this reason is adequate for small bench scale experiments but not ideal for large-scale operations. Crossflow configuration has better operating conditions and reduced fouling compared to a dead end configuration setup, but is more sophisticated than a dead end setup [6].

Membranes are manufactured from various materials. Membranes are commonly either polymeric, mixed matrix or ceramic. Polymeric membranes are membranes that consist of polymeric material which are either porous or non-porous, depending on the application. Reverse Osmosis membranes are mostly non-porous, while nanofiltration membranes are mostly porous. Polymeric membranes are formed to become greener, generating less waste from manufacturing and becoming more solvent stable providing high membrane fluxes. However, polymer membranes are not suitable for every OSN system, limiting their scope of application in membrane operations because of their susceptibility to the effects of temperature, solvent type, pressure and operational lifespan [6].

Ceramic membranes are developed from inorganic materials that are expensive to manufacture. These membranes have better mechanical, chemical and thermal stability compared to polymeric membranes. Ceramic membranes do not compact under pressure and do not swell in organic solvent. However, ceramic membranes are difficult to scale up, have high cost and are more brittle compared to polymeric membranes. Mixed matrix membranes are combinations of both polymeric and ceramic material which give both the desired properties of polymeric material as well as ceramic material [11]. Figure 2.4 illustrates the taxonomy of membranes by classifying them according to the material type, membrane type and preparation technique.

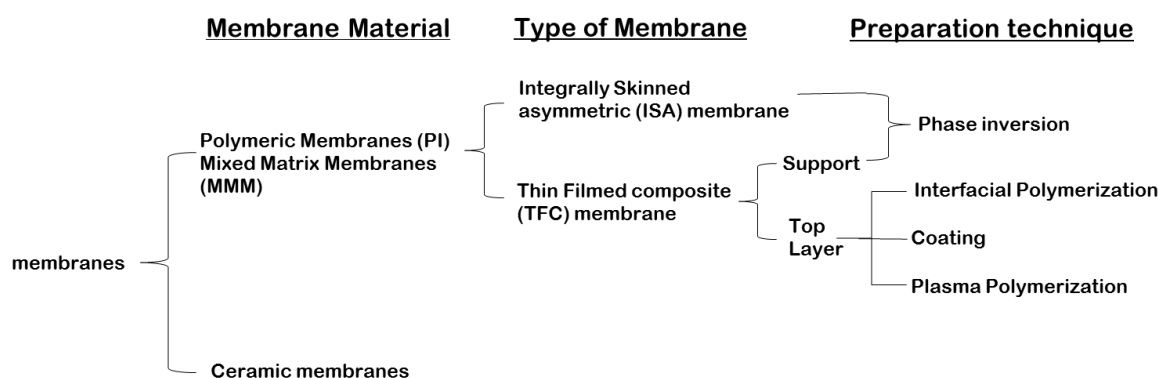


Figure 2.4: Membrane taxonomy

Polymeric membranes can be classified as Integrally Skinned Asymmetric (ISA) types or Thin Filmed Composite (TFC) types of membranes, as illustrated in Figure 2.4. The focus of current membrane manufacturing and development is to make polymeric membranes more robust, with ISA and TFC membranes being some of the products of current research [11]. Additionally, polyimide membranes are more compatible with organic solvents relative to ceramic membranes.

2.1.1 Principles of OSN

Membranes are characterized by their molecular weight cut-off (MWCO) which is, according to Szekely *et al.* [11], defined as the molecular weight of a chemical species which is 90% rejected by the membrane. Characterizing membrane performance solely on MWCO does not give sufficient information on the separating performance. The interactions between solute and solvent influence the solubility of a mixture. The properties that solvents and solutes exhibit (i.e. polarity, solvency, solubility, viscosity, size, etc.) affect the performance of certain types of membranes, such as hydrophilic and hydrophobic membranes. Research focusing on determining MWCO for membranes used alkanes [12] in determining specific rejections,

while other researchers identified the significance of the effect of specific solvents on membrane performances [13].

Membrane performance is a measure of how well a membrane can perform under specific circumstances. These circumstances include process conditions such as temperature, pressure, flowrate, concentration and system configuration. Membrane performance is commonly classified by the flux of permeate and rejection of solute [1]. Membrane flux is defined as the flow of liquid through the membrane over an area during an instance of time. The membrane flux can be expressed using Equation 2.1.

$$J = \frac{V_n}{A \cdot \Delta t} \quad (2.1)$$

Where

V_n – volume of fluid that permeates through membrane normal to the surface area (L)

A – effective membrane surface area (m^2)

t – time interval for which volume V permeates through the membrane (hr)

J – flux of a permeating species through the membrane ($L \cdot m^{-2} \cdot hr^{-1}$)

Rejection is defined as the difference in concentration of solute in the feed (C_{feed}) to the permeate ($C_{permeate}$) over the concentration of initial feed. The rejection can be expressed using Equation 2.2.

$$R_{solute} = \left(1 - \frac{C_p}{C_f}\right) \times 100\% \quad (2.2)$$

Where

C_p – solute concentration in feed permeate ($mL \cdot mL^{-1}$ or $mg \cdot L^{-1}$)

C_f – solute concentration in the feed ($mL \cdot mL^{-1}$ or $mg \cdot L^{-1}$)

R_{solute} – rejection

2.2 Review of solvent recovery using OSN

Solvent recovery using OSN was introduced as early as the 1980's, when Wight *et al.* [14] published a patent on solvent recovery from dewaxed oil in lube oil dewaxing processes. Furthermore, Wright paved the way for the first successful commercial OSN process to be operational in 1991, and it was known as the MAX De Wax process.

OSN research is guided by the works of Schmit *et al.* [3], Livingston *et al.* [15] and Vankelecom *et al.* [16], setting the stage for OSN application and knowledge. In this section, reviews on past literature relating to solvent recovery using OSN technology are investigated. Reviews on past research on OSN membrane performance are listed in Table 2.2. These reviews include those that were done on the performance of both commercial and non-commercial membranes.

Table 2.2: Summary of previous publications regarding the separation of different solutes using Commercial OSN membranes

Company	Membrane	Solute	Solute (g.mol ⁻¹)	MW	solute/solvent ratio	Temperature (°C)	Pressure (Bar)	Solvent	Flux (L.m ² .hr ⁻¹)	Rejection	Ref
Bor Mem tech	GMT-oNF-2	TPP	262.29			20	30	n-hexanal	19.8	39 %	[3]
								Toluene		91 %	
Evonik	Duramem™ 150	steryl esters	650 - 850		10% w/w	20	35	n-hexane		59 %	[17]
		sterols	370-420					2-Propanol		66 %	
		oleic acid	282.4614					DMC		58 %	
		polystyrene oligomers	236-1200					hexane	59.5	94 %	
								hexane		94 %	
	Duramem™ 200	API1	?			30	30	THF	3.1	>93 %	[18]
		API2	?			30	30	Acetone	10	>98 %	
	Duramem™ 300	styrene oligomers	236-1200					DCM	10.5	100 %	[19]
								DCM	10.5	97 %	
	Puramem™ 280	TPP	262.29			20	30	DCM	98	94 %	[3]
								n-hexanal	18.3	73 %	
								Toluene	41.6	97 %	
								n-hexane	20.3	57 %	
								2-Propanol	12.2	83 %	
	Puramem™ S600							DMC	49.9	88 %	[17]
		steryl esters	650 - 850		10% w/w	20	35	hexane	56	92 %	
		sterols	370-420					hexane		82 %	
		oleic acid	282.4614					hexane		82 %	
		Soybean daidzin	416 Da			20	30	H2O	9	94 %	
	Starmem™ 120							MeOH	170	53 %	[7]
								Toluene	15	92 %	
								Toluene	30	>98 %	
						20	30	H2O	20.6	98 %	
								MeOH	320	20 %	
	Starmem™ 122	docosane (TOABr)	310			30	30	DMMS/ MeOH	78	30 %	[21]
		Soybean daidzin	416			20	30	Toluene	72.5	7 %	
						25	30	Toluene	28.3	99 %	
								Toluene	28.9	99 %	
								Toluene	30.7	98 %	
	Starmem™ 122							Toluene	30.5	98 %	[7]
								Toluene	21.1	19 %	
								Isopropanol	4.48	79 %	
								Ethanol	17.4	96 %	
								Acetone	56.6	70 %	
	Starmem™ 228	Soybean daidzin	416			20	30	H2O	2	95 %	[7]
								MeOH	21.9	79 %	
								H2O	9	98 %	
	Starmem™ 240	Soybean daidzin	416			20	30	MeOH	164	51 %	[7]

Company	Membrane	Solute	Solute (g.mol ⁻¹)	MW	solute/solvent ratio	Temperature (°C)	Pressure (Bar)	Solvent	Flux (L.m ² .hr ⁻¹)	Rejection	Ref
Koch	MPF-44	Polystyrene	200 -1200					toluene		>90 %	[23]
		Soybean daidzin	416 Da			20	30	n-heptane		>90 %	[7]
								Water	27	89 %	
								MeOH	7.4	72 %	
								EtOH	1.4	44 %	
	MPF-50	Soybean daidzin	416 Da					Acetone	0.86	56 %	
								Ethyl Acetate	0.55	24 %	
								Water	6.6	34 %	
								MeOH	42	83 %	
								EtOH	25	86 %	
	MP-50/MPF-60	(TOABr)	546			30	30	Acetone	267	72 %	[21]
						Room temp	30.4	Ethyl Acetate	197	32 %	
								DMMS/MeOH	60	10 %	
								Water	10	\	
								Pentanol	31	\	[24] [25]
HP Polymer	Lenzing P84	n-Decane	142.28			50	41.4	Butanol	50	\	
			142.2					Propanol	70	\	
			226.44					Ethanol	119	\	
			246.43					Methanol	175	\	
		1-Methyl-naphthalene	142.2					Octane	349	\	[8]
		n-Hexadecane	226.44					Acetone	490	\	
		1-Phenyldodecane	246.43					Toluene	35.58	44 %	
		Pristane	268.51					Toluene	35.58	1 %	
		n-Docosane	310.61					Toluene	35.58	79 %	[26]
		styrene oligomers	236-1200			30	30	Toluene	35.58	95 %	
		styrene oligomers	236-1200			20	30	Toluene	35.58	66 %	
		PEG-400	400			22	10	Toluene	35.58	92 %	
		PEG-2000	2000					DMF/Dioxane	>120	>90 %	[27]
Osmonics	SEPA DK							DMF	87	>90 %	
	SEPA DL							MeCN	29	66 %	
	SEPA GH							MeCN	29	99 %	
Solvay	NF 030306	soybean oil			25% w/w	40	30	hexane	0.1	no data	[29]
		Cooking oil	914.9					hexane	0.1	no data	
								hexane	12	67 %	
					10% w/w	23		Ethanol	4.89	78 %	
	NF 030306F	Degummed soybean oil	862.7					Acetone	16.6	78 %	[22]
								Cyclohexane	0.54	64 %	
								Hexane	0.55	38 %	
								hexane	3.9	56 %	
		steryl esters	650 - 850		35% w/w	30	20	hexane	0.385	27 %	[30]
		sterols	370-420		10% w/w	20	35	hexane		35 %	
		oleic acid	282.4614					hexane		30 %	
		steryl esters	650 - 850					hexane	2.59	88 %	
	NF 030306F	sterols	370-420					hexane		71 %	[17]
		oleic acid	282.4614					hexane		69 %	

Company	Membrane	Solute	Solute (g.mol ⁻¹)	MW	solute/solvent ratio	Temperature (°C)	Pressure (Bar)	Solvent	Flux (L.m ² .hr ⁻¹)	Rejection	Ref
Sulzer	NF 070706	steryl esters	650 - 850		10% w/w	20	35	hexane	2.695	83 %	[17]
		sterols	370-420					hexane		0 %	
		oleic acid	282.4614					hexane		3 %	
	PERVAPTM 4060	n-Tetracosane (C24)	338.65			30	15	Toluene		40 %	[31]
		n-Triacontane (C30)	422.81					Toluene		61 %	
HaiHang Industry Co.		n-Pentacontane (C50)	703.34					Toluene		100 %	
	Matrimid 5218	100N			20 % w/w	-10	41.37	MEK, Toluene	12.9	96 %	[32]
GKSS,		Mobil light neutral base oil			20 % w/w	-10	41.37	MEK, Toluene		98 %	[12]
	PEBAX	free fatty acids	280			20	10	Acetone	3	35 %	[33]
		Palm oil						Acetone	3.3	86 %	
		rapeseed oil						Acetone	4.2	81 %	
		Sunflower oil						Acetone	0.5	90 %	
	Cellulose	Palm oil						Acetone	1.8	93 %	
		rapeseed oil						Acetone	2	>98 %	
		Sunflower oil						Acetone	1.8	97 %	
		Sunflower + PPhLipids						Acetone	1.6	93 %	
		Sunflower + Beeswax						Acetone	1.5	92 %	
	PAN/PDMS composite	Sunflower oil			8% w/w	20	7	n-hexane	12	92 %	[34]
		polyisobutylene	1300		8% w/w	24	7	n-hexane	12.5	90 %	[35]
Shanghai petrochemicals Unknown Sigma Aldrich, UK	PAN/PDMS , PAN/PEO-PDMS-PEO composite	sunflower oil			8% w/w	24	30	n-hexane	\	95 %	[36]
								toluene	50	80 %	
	PAN/MMA composite	dewaxed oil	450		17% w/w	20	20	MEK, Toluene	12	73 %	[37]
	6FDA	Lube oil			20% w/w	20	30	MEK, Toluene	>12	96 %	[38]
	TFC-MPD-NP (wout/treatment)	polystyrene oligomers	236-1200			30	30	MeOH	7	95 %	[18]
	TFC-MPD-NP (with/treatment)	polystyrene oligomers	236-1200					MeOH	23	>95 %	
								DMF	8.6	>90 %	
	TFC-MPD (wout/treatment)	polystyrene oligomers	236-1200					MeOH	15	>97 %	
								Acetone	0.3	>96 %	
	TFC-MPD (with/treatment)	polystyrene oligomers	236-1200					MeOH	46	>97 %	
								DMF	46.1	>90 %	
								Acetone	71	>95 %	
								Ethyl acetate	26	>85 %	

Company	Membrane	Solute	Solute (g.mol ⁻¹)	MW	solute/solvent ratio	Temperature (°C)	Pressure (Bar)	Solvent	Flux (L.m ² .hr ⁻¹)	Rejection	Ref
Solvay	TFC-PIP (with/treatment)	Alkanes	220 -380					toluene	4.2	>96 %	
								THF	45	100 %	
		polystyrene oligomers	236-1200					THF	35.6	>90 %	
		Alkanes	220 -380					Acetone	65	>90 %	
								THF	80.2	>80 %	
	TFC-HDA (with/treatment)	polystyrene oligomers	236-1200					Acetone	64	>90 % (MWCO >300 Da)	
	TMC - MPD and Silica particles	dewaxed oil	550		20% w/w	ambient	15	MEK +Toluene	10.4	95 %	[39]
	TMC + MPD	dewaxed oil			20% w/w	ambient	15	MEK +Toluene	\	95 %	[40]
	TFC	dewaxed oil			20% w/w	ambient	15	MEK +Toluene	10.4	95 %	[41]
	TFN0.02								13.85	96 %	
	TFN0.05								14.53	95 %	
	TFN0.1								15.05	88 %	
	TFN0.2								16.93	50 %	
	PVDF-10SI	Degummed soybean oil	862.7		25% w/w	30	20	hexane	20.1	77 %	[30]
	PVDF-12SI						15	hexane	15.9	85 %	
	PVDF-15SI						10	hexane	7.8	81 %	
	PVDF-CA					40	20	hexane	19	55 %	

One of the first membranes to be used for solvent recovery was the MPF – series. Research using these membranes has been done by Machado *et al.* [24,25], who demonstrated that membrane performance was different for various solvents as well as different operating conditions. As shown in Table 2.2, Machado *et al.* demonstrated that solvents, such as acetone, provided higher fluxes compared to other solvents, such as butanol, for the MPF-50 membrane series mainly due to lower surface tension and lower viscosity. Furthermore, the work from Machado *et al.* explains how the rise in temperature, change in pressure and varying solvent concentration can influence the permeate flow by changing a permeating species properties such as viscosity, hence the recovery of valuable chemicals.

Yang *et al.* [13] stated that the MPF-series was an undesirable choice for organic systems. Yang and co-workers demonstrated in their research that the membrane performance for the MPF series was not entirely predictable when using organic solvents. Methanol permeation through MPF-50 and MPF-80 membranes as investigated by Yang *et al.*, was compared to the works of Machado *et al.* [24,25] and Whu *et al.* [41]. These research groups obtained different permeation fluxes. Yang *et al.* states that the reason for such variation in fluxes is due to dead end cell setup as this relates to the membrane active area, while Whu *et al.* suggests that the major fluctuations in permeate flux is due to the reversibility of the membrane.

White *et al.* [12] used the matrimid membrane series to recover solvents from lube oil. White *et al.* focused on the membrane performance with regard to membrane resistance and determined how economical the membrane separation performances were. Furthermore, White *et al.* demonstrated that, with binary solvent (MEK and toluene) and using matrimid membranes, it is possible to obtain a solvent purity of greater than 99 wt% and a steady permeation rate.

Peeva *et al.* [20] used another type of commercially available membrane known as the Starmem™ series. Peeva *et al.* focused on the effect of concentration polarisation on the system with solvent and solute present. Peeva *et al.* determined that at higher solute concentrations, concentration polarisation has a large effect on the recovery of solvent. Peeva *et al.* used these results to model the system by incorporating activity coefficients into the transport models used.

A new plasma grafted membrane to recover solvent from dewaxed oil was introduced through the work of Zhao *et al.* [37]. Zhao *et al.* demonstrated that the new non-commercial membrane could recover solvent well. However, it obtained low rejection of solute reaching around 72.8%. Plasma grafted membranes were shown not to provide competitive membrane performance

to that of traditional technologies, such as distillation, where purities of solvent are around 98 wt%.

In 2005, Kong *et al.* [38] demonstrated that the polyimide nanofiltration membranes were competitive with traditional technologies for separating and recovering solvent (MEK and toluene) from dewaxed lube oil filtrates. The PI membrane used was shown to reject 96% of the oil, and produce high permeate fluxes of around $12 \text{ L.m}^{-2}.\text{h}^{-1}$. Kong *et al.* demonstrated that variation in operating conditions, such as temperature, pressure, feed concentration and the binary mixture of solvents, has a definite effect on the solvent recovery capacity. However, the investigations by Kong *et al.* showed that high purities of solvents were obtained by permeation through the non-commercial membranes that were used in his research. Further research is required to investigate the recovery of solvents through commercial membranes, such as the Starmem™ series.

Silva *et al.* [21] compared the solvent transport of methanol and toluene mixtures for two different membranes (Starmem™122 and MPF-50). Silva *et al.* demonstrated that Starmem™122 had better performance characteristics compared to that of MPF-50 membranes. Fluxes for toluene were found to be higher for MPF-50 series membranes than for the Starmem™ series. However, the rejection of TOABr ranged at around 80% through MPF-50 compared to the 99% rejection through a Starmem™122 membrane. Silva *et al.* demonstrated that the MPF-50 membranes were not able to provide reproducible results. Hence, further modelling of the OSN system was performed using Starmem™ series membranes.

Zhao *et al.* [7] investigated the influence that aqueous and organic solvents have on membrane performances. Experiments were conducted using Starmem™ series membranes obtained from W.R. Grace, MPF series membranes from Koch and Desal-DK membranes from Osmotics. The results for MPF membranes were in line with the findings of other research groups [13,21], indicating that rejection of solute was more uncommon in organic solvent than in water. With regard to solvent flux, organic solvents provided higher fluxes through the commercial membranes used.

Zhao *et al.* [7] also demonstrated in the same year that the pretreatment of a membrane with a solvent can influence the membrane performance significantly. The performance of Starmem™ and Desal-DK membranes were affected significantly, while the commercial Koch membranes (MPF-50) were not significantly affected in methanol.

Polar aprotic solvents were used in membrane characterisation in research conducted by Toh *et al.* [26]. The influence of aprotic solvents on the lenzing membrane, provided good

separation and recovery of both the solute and solvent. The DMF permeability was shown to range between 1 – 8 L.m⁻².h⁻¹.bar⁻¹ at temperatures below 100°C.

Toh *et al.*, in the same year, made use of various solvents with a solute to characterize Starmem™ membranes. Molecular Weight Cut Off (MWCO) tests were performed using various solvents, such as toluene and ethyl acetate. Solvent permeability tests were included in the tests and illustrated fluxes ranging between 5 – 210 L.m⁻².h⁻¹ at 30 bar. Silva *et al.* [21] reported similar fluxes for Starmem™122. Toh *et al.* found that the observed flux of solvent increased with increasing MWCO of the membrane, resulting in a MWCO variability which is dependent on the solvent system used.

Various non-commercial membranes were investigated in order to understand their characteristics and impact on the performance of an OSN system. Soroko *et al.* [27] investigated the influence of TiO₂ nanoparticles on the morphology and performance of cross-linked polyimide OSN membranes. The solvents included DMF and isopropanol and they determined that the fluxes through these membranes varied between 160 and 50 L.m⁻².h⁻¹. The performance results of these membranes in the presence of TiO₂ nanoparticles showed improved compaction resistance as well as unaltered rejection and solvent flux.

Apart from the Starmem™ series, Evonik provides other commercially available membranes known as Puramem™ and Duramem™. Research on Duramem™ membranes were initiated in 2012 through the work of Solomon's group [18]. The Group demonstrated that the performances of Duramem™150 membranes are well above the MWCO of 90% for polystyrene oligomers dissolved in acetone and THF solvents.

Siddique *et al.* [19] later demonstrated that the Duramem™ series membranes performed well in DCM solvent systems separating Active Pharmaceutical Ingredients (API) at high rejections and at moderate flux rates.

Another commercial membrane available from Evonik, known as Puramem™ membranes, were shown to successfully separate triphenylphosphine (TPP) using a variety of different solvents, such as toluene and DMC, and these membranes provided similar results to the Starmem™ series [43].

Recent reviews from Marchetti *et al.* [6], Szeleky *et al.* [11] and Cheng *et al.* [44] have provided state of the art overviews of the knowledge on OSN in general and the current state of research [6,44] on the subject. They also discuss the sustainability of OSN compared to conventional processes [11].

2.3. Review of transport models in solvent recovery

In order to understand the membrane transport mechanism, modelling of the OSN system is necessary. Modelling can be used for two purposes: design and prediction. Design of a membrane system can occur at three levels: (i) membrane scale, (ii) module scale and (iii) process scale. According to Peshev *et al.* [45], 91% of membrane modelling focused on membrane scale up until 2013. Designing at membrane scale is accomplished by using experimental data for solvent-solute systems, and then obtaining unknown parameters through analytical and numerical regression of the experimental data. Industries use these models in order to understand the rate of permeation [46] and adapt the industrial process accordingly in order to meet an objective, thus using modelling based on membrane operation. These models can be used to describe the movement of solvents and solutes through the OSN membranes [6].

There are three types of models that are commonly used at present for OSN modelling and these are known as the solution-diffusion model, pore-flow model and the phenomenological model [20]. These models can be used to model the flux through a membrane and this has been investigated in literature [47- 50]. This section discusses the above-mentioned models with regard to their applicability and uses.

2.3.1. Membrane transport theory

The first solution-diffusion model was developed by Lonsdale *et al.* [46,50]. He investigated the diffusion coefficients of reverse osmosis membranes, in order to acquire data for developing a solution-diffusion model. The work of Lonsdale was later reviewed by Wijmans *et al.* [47], providing a critical evaluation on the solution-diffusion model as well as pore-flow models.

The classic solution-diffusion model is described by Wijmans *et al.* [47] as a transport model which portrays how permeate dissolves into the membrane material and then diffuses through the membrane down a concentration gradient, and is shown in Equation 2.3 as well as in Figure 2.5.

$$J_{n,i} = \frac{D_i K_i}{l} \left[c_{i,FM} - c_{i,P} \cdot \frac{\gamma_{i,p}}{\gamma_{i,MP}} \exp \left(- \left(V_{m,i} \cdot \frac{P_{MP} - P_P}{RT} \right) \right) \right] \quad (2.3)$$

where

$J_{n,i}$ – partial molar flux of species i ,

$c_{i,FM}$ – feed concentration of species i ,

$c_{i,PM}$ – permeate concentration of species i ,

D_i – diffusion coefficient of species i ,

K_i – the sorption coefficient,

γ_i – the surface tension

V_m – the molar volume of species i ,

l – the membrane thickness

A concentration gradient is produced as the permeate diffuses through the membrane. The properties of each permeating species influence the permeation rate of that specific species. Due to the different properties of permeating species through the membrane, separation is enforced [47].

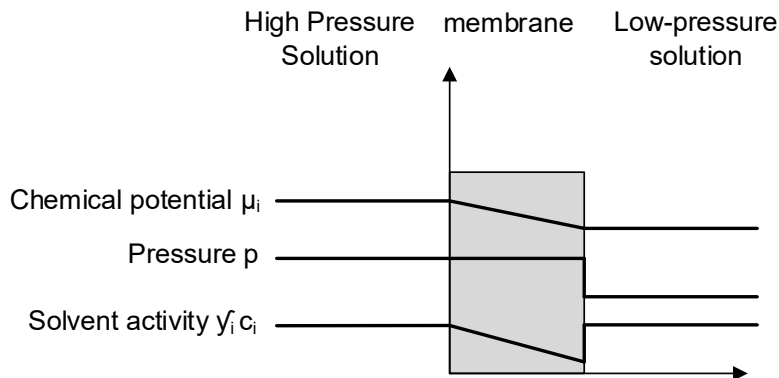


Figure 2.5: Solution-diffusion model through a membrane [46,47]

The chemical potential gradient illustrated in Figure 2.5, is used to formulate a general flux equation as described in Equation 2.4.

$$J = -L_i \frac{d\mu_i}{dx} \quad (2.4)$$

Where

J – flux of a permeating species through the membrane

L_i – coefficient of proportionality

$d\mu_i/dx$ – chemical potential gradient of component i

In many membrane processes a combination of driving forces are applied to produce a permeate-retentate separation. Pressure and chemical potential are two driving forces commonly used to describe transport models, such as the pore-flow and solution-diffusion models. Chemical potential for organic solvents through a membrane is described by Equation 2.5, which incorporates the effect of various parameters such as constant pressure, concentration and fugacity coefficient of species i [46].

$$\mu_i(T, P) = \mu_{0i}^{id}(T, P^{sat}) + RT \ln\left(\frac{P}{P^{sat}}\right) + RT \ln(C_i) + RT \ln(\phi) \quad (2.5)$$

Where

- μ – chemical potential
- p^{sat} – saturated vapour pressure
- T – temperature
- R – universal gas constant
- C_i – the molar concentration of species i
- ϕ – the fugacity coefficient of species i

Wijmans *et al.* [47] provided assumptions with the solution-diffusion model, which govern the transport mechanism through the model. The following assumptions are made for the solution-diffusion model:

- *Fluids on either side of the membrane are in equilibrium with the membrane surface interface.*
- *Pressure through a membrane is uniform.*

Applications where the solution-diffusion model is used adopt Equation 2.5 to the specific system. It is difficult to formulate a model to suit every system. Generally, the solution-diffusion model is well suited for dense membranes. Bhanushali *et al.* [51] illustrated that the solution-diffusion model gave a good description of the transport mechanism for hydrophobic membranes in alcohols and alkane. Bhanushali and co-workers showed that separation of solutes in a system which uses dense membranes, requires understanding of polymer-solvent, solvent-solute and solute-polymer interactions.

Pore-flow models describe systems where the permeate is separated by pressure driven convective flow through the tiny pores [47]. Research investigations are seldom done on transport through nanofiltration membranes due to the heterogeneous nature of the porous matrix that surrounds the polymer. The pore-flow model is well known as the Hagen-Poiseuille pore-flow model, as shown in Equation 2.6. The Hagen-Poiseuille equation assumes that the membrane consists of a number of cylindrical pores, which are parallel or oblique to the membrane surface, and that these capillaries are uniform and cylindrical.

$$J^{PF} = \left(\frac{\epsilon_m \cdot d_{\text{pore}}^2}{32 \cdot \eta \cdot \tau} \right) \left(\frac{\Delta P}{\Delta X_m} \right) \quad (2.6)$$

Where

- J^{PF} – Flux ($\text{L} \cdot \text{m}^{-2} \cdot \text{hr}^{-1}$)
- ΔP – Pressure difference (Pa)
- ΔX_m – Membrane thickness (m)
- η – Viscosity of liquid ($\text{Pa} \cdot \text{s} \cdot \text{m}^{-2}$)
- ϵ_m – Surface porosity

τ – Membrane tortuosity,

d_{pore} – Membrane pore diameter

The parameters that characterize the complex polymeric porous structure are not generally available, which necessitates experimentation in order to obtain them. Widely used parameters include tortuosity (τ), porosity (ϵ) and the average pore diameter (d). The general pore-flow model is illustrated in Figure 2.6.

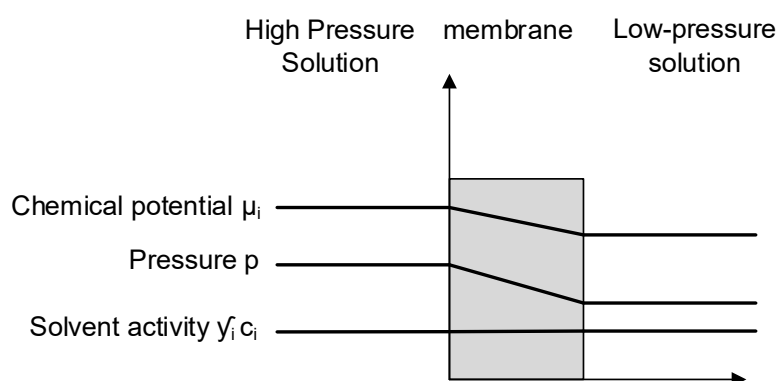


Figure 2.6: Pore-flow model through a membrane [47]

The permeate transport through a porous membrane can be described as in Figure 2.6, where there is a linear pressure gradient throughout the membrane, while the solvent activity is constant. One of the earliest pore-flow transport models, known as the *surface force pore-flow model*, was developed by Matsuura and Sourirajan [52]. This was later adapted by Mehdizadeh and Dickson [53] to obtain a model known as the *modified surface pore-flow model*.

According to Soltane *et al.* [31], there is no currently accepted model or transport mechanism that can be used to describe the solvent and solute transport through OSN processes. This statement by Soltane and co-workers' can be justified from perusal of research done in the past decade and late 1900's. Various solution-diffusion models as well as pore-flow models [52, 53] have been developed, but they do not apply to a broad spectrum of systems but rather only to specific ones. Paul and co-workers [48] investigated fluid transport through membranes initially using the pressure driven principles. In further studies, Paul *et al.* [48] re-evaluates the solution-diffusion model by using volume fractions of the solvent in the membrane, rather than taking the traditional pressure gradient concept. Paul *et al.* [48] observed that the results they obtained with swelling tests for transport of solvent using volume fractions were different from those obtained using pressure gradients. Further clarity on the three main models discussed in this section (i.e. solution-diffusion, pore-flow and phenomenological), is provided in the following sections.

2.3.2. Solution-diffusion divergence

Modelling of the transport through OSN membranes have been done since as early as 1995, when J.G. Wijmans *et al.* [47] developed a classic solution-diffusion model (i.e. Equation 2.3), that could model the transport through a membrane according to certain assumptions. The validity of his model ranged from dialysis to gas pervaporation. However, the Wijmans *et al.* [47] transport model lacks validation in other membrane processes such as OSN membrane modelling. Membrane modelling is diverging to many types of models which is why there is still potential to develop suitable transport models for general OSN systems. Variations of the solution-diffusion model are discussed in this study as supported from literature by a number of researchers.

Peeva *et al.* [20] have developed a derived model from the classic diffusion model, which relies on experimental data, as shown in Equation 2.7.

$$J_i = P_{i,M} \left[c_{i,M} - \frac{J_i}{J_i + j_j} \frac{\gamma_{i,P}}{\gamma_{i,FM}} \exp \left(-\frac{v_i p}{RT} \right) \right] \quad (2.7)$$

Peeva *et al.* demonstrated that permeation of a solvent mixture through Starmem™ 122 series membranes can be predicted fairly well. This model received attention from other researchers such as Silva *et al.* [54]. Silva *et al.* investigated the transport of various solvents through Starmem™ 122 series membranes. They demonstrated that the solution-diffusion model shown in Equation 2.7 was able to predict the permeation of solvent mixtures through the membrane. The model parameters were based on pure solvent permeabilities and did not take membrane properties such as swelling and porosity into account. Furthermore, the solution model was found to have the most accurate predictions, although membrane interaction was not considered.

Geens *et al.* [55] demonstrated that solvent flux is dependent on membrane properties such as molecular size, viscosity and difference in surface tension and this can be mathematically portrayed by Equation 2.8.

$$J \sim \frac{V_m}{\mu \Delta\gamma} \quad (2.8)$$

The developed model introduced a correction to the Bhanushali model, illustrated in Equation 2.9 [51], which showed high correlation with experimental data and describes the solvent transport through relatively dense membranes adequately.

$$J \sim \left(\frac{V_m}{\mu} \right) \left(\frac{l}{\phi^n \gamma_m} \right) \quad (2.9)$$

The models described by Bhanushali *et al.* [51] were tested on a variety of commercial membranes including MPF-44, 50 and Solsep-030505. Geens *et al.* [55] illustrated that

membrane-solvent interaction plays a larger role in the solvent permeability through hydrophobic membranes (MPF-50, Solsep-030505) than through hydrophilic membranes (MPF-44, Desal-5-DL) with increasingly polar solvents.

According to Silva *et al.* [56], predictive modelling was demonstrated by describing the transport through the spiral-wound membranes. Silva *et al.* used a spiral-wound Starmem™122 to perform the OSN investigations for the separation of toluene from tetraoctylammonium bromide (TOABr). They found that membrane performances for the spiral-wound membranes were accurately determined by using the membrane transport parameters determined from flat-sheet membrane tests.

From another perspective, Stafie *et al.* [34] also focused on modelling composite membranes using the solution-diffusion model. The system that was modelled was a n-hexane/ sunflower oil system, with various feed concentrations and pressures. They found that the solution-diffusion model described the hexane solvent transport system well, and determined that one of the main parameters governing hexane transport is the apparent viscosity and membrane swelling in a composite membrane system. Stafie *et al.* [34] focused on low pressure operation and explained that further work is required at higher pressures of up to 30 bar.

2.3.3. Pore-flow divergence

The pore-flow model can be described as a one-parameter model where the permeability term $\left(\frac{\varepsilon d_{pore}^2}{32l\tau}\right)$ for each solvent was determined by arithmetic averages. The experimental results for mixtures were described poorly using the one-term Hagen-Poiseuille model. Silva *et al.* [54] used this model in order to further develop an improved model known as the two-parameter Hagen-Poiseuille model, given in Equation 2.10.

$$J = \left(\frac{\Delta P}{\eta_{mix}}\right) \left[v_1 c_{1(m)} \left(\frac{\varepsilon d_{pore}^2}{32l\tau}\right)_1 + v_2 c_{2(m)} \left(\frac{\varepsilon d_{pore}^2}{32l\tau}\right)_2 \right] \quad (2.10)$$

According to Silva *et al.*, the model given as Equation 2.10 has demonstrated improvement in the accuracy of experimental results compared to the one-parameter model. According to Mulder *et al.* [1], the Hagen-Poiseuille pore-flow model bases its predictions on the assumption that the membrane consists of cylindrical pores that are homogeneous throughout the membrane. Mulder *et al.* also states that if the assumption is made that the membrane consists of closely packed spheres, the Kozeny-Carmen equation, shown in Equation 2.11, can be used to describe the transport of a species through a membrane.

$$J_v = \frac{\varepsilon^3}{Kls^2(1-\varepsilon)^2} \times \frac{P_0 - P_z}{\eta} \quad (2.11)$$

One of the earliest variations of the pore-flow model came from the work of Jonsson and Boesen *et al.* [57] and this model was developed for reverse osmosis systems. Jonsson *et al.* developed the model based on the combination of viscous flow and frictional models in order to determine the permeate flux. The model's variation is given in Equation 2.12, which includes a new parameter in the equation, known as the molecular weight.

$$J_v = \frac{\varepsilon d_{pore}^2}{32\eta\tau} \left[\frac{1}{1 + \frac{d_{pore}^2 x_{smc}}{32\eta MW}} \right] \times \frac{\Delta P}{\Delta z} \quad (2.12)$$

Robinson *et al.* [58] investigated the influence of organic solvents on composite membranes. The transport through the membranes can be interpreted using the Hagen–Poiseuille equation. However, with binary mixtures there are limitations. Robinson *et al.* [58] states that an investigation towards a deepened understanding of pore-flow and solution-diffusion models in composite membranes is not warranted, due to a lack of sufficient knowledge on their use in such systems.

In 1999, Machado *et al.* [24,25] developed a transport model for MPF membranes. The model focuses on membrane properties such as viscosity, surface tension and membrane hydrophobicity and is presented in Equation 2.13.

$$J = \frac{\Delta P}{\Phi[(\gamma_c - \gamma_L) + f_1] + f_2\mu} \quad (2.13)$$

The models developed by Machado's research group illustrated that it is possible to model membrane systems. However, the solvent properties and interactions are not fully understood, which is why some of Machado's modelling parameters, such as the dielectric constant, is not valid for certain systems, such as the acetone – water system.

Another variation of the pore-flow model, which describes the influence of the solute-membrane interactions of a binary system is discussed through the work of Matsuura *et al.* [52]. The model which Matsuura *et al.* describes is given in Equation 2.14

$$J_{n,i} = -\frac{RT}{x_{i,j}b_f} \frac{dc_i}{dx} + \frac{v_{m,i}C_i}{bf} \quad (2.14)$$

In later years, the model developed by Matsuura *et al.* [52] was disproven by Mehdizadeh and Dickson [53], who stated that there was a flaw in the model's mass balance and that it was inconsistent in relating to the cylindrical pore geometry.

2.3.4. Combination of solution-diffusion and pore-flow

In literature, there are models that have been derived from the combination of both pore-flow and solution-diffusion models, by using both conceptual modelling ideas and implementing a

new mechanism for these models. The solution-diffusion-imperfection model, described in the work of Mason *et al.* [59], integrates viscous transport with diffusive transport, which may occur due to inconsistent imperfections in the membrane. This model is given in Equation 2.15.

$$J = \frac{c_{iM} D_{iM} v_i}{RTl} \Delta P + \frac{c_{iM} B_o}{\eta l} \Delta P \quad (2.15)$$

White *et al.* [8] understood the lack of information on characterizing Lenzing P84 membranes and focused on transport properties of various solutes dissolved in toluene. Applying the solution-diffusion model to the organic solvent resistant membrane system, using various solute molecules, this group could provide predictable performance for nanofiltration. White *et al.* [8] also states that alternative solvents, such as ketones and alcohols, are viable options for use in an asymmetric membrane system where predictable solution-diffusion models are applicable.

2.3.5. Phenomenological models

Vankelecom *et al.* [49] investigated the physio-chemical interpretation of PDMS - composite membrane with the commercially available MPF-50 membranes. Since using MPF-series membranes with organic solvents are debatable, Vankelecom *et al.* demonstrated that convective flow is the main driving force for MPF membranes and membrane swelling the main driving force through PDMS composite membranes. Vankelecom *et al.* [49] also stated that it is impossible to provide a generalized expression of solvent resistant nanofiltration transport mechanisms. Many models are derived from the classical solution-diffusion and pore-flow models. The derived models are discussed further in this section and a summary of the reviewed transport models have been illustrated in Table 2.4.

Table 2.4: Summary of reviewed OSN transport models

Model	Equation
Solution-diffusion	
Classic solution-diffusion	$J_{n,i} = \frac{D_{i,K_i}}{l} \left[c_{i,FM} - c_{i,P} \cdot \frac{\gamma_{i,P}}{\gamma_{i,MP}} \exp \left(- \left(V_{m,i} \cdot \frac{P_{MP} - P_P}{RT} \right) \right) \right]$
Peeva <i>et al.</i>	$J_i = P_{i,M} \left[c_{i,M} - \frac{J_i}{J_i + J_j} \frac{\gamma_{i,P}}{\gamma_{i,FM}} \exp \left(- \frac{v_i P}{RT} \right) \right]$
Bhanushi <i>et al.</i> model	$J \sim \left(\frac{V_m}{\mu} \right) \left(\frac{l}{\phi^n \gamma_m} \right)$
Geens <i>et al.</i> model	$J \sim \frac{V_m}{\mu \Delta \gamma}$
Pore-flow model	
One term hagen Poiseuille	$J = \left(\frac{\varepsilon_m \cdot d_{pore}^2}{32 \cdot \eta \cdot \tau} \right) \left(\frac{\Delta P}{\Delta X_m} \right)$

Model	Equation
Jonsson and Boedien model	$J_v = \frac{\varepsilon d_{pore}^2}{32\eta\tau} \left[\frac{1}{1 + \frac{d_{pore}^2 x_{smc}}{32\eta MW}} \right] \times \frac{\Delta P}{\Delta z}$
Two term hagen-Poiseuille	$J = \left(\frac{\Delta P}{\eta_{mix}} \right) \left[v_1 c_{1(m)} \left(\frac{\varepsilon d_{pore}^2}{32l\tau} \right)_1 + v_2 c_{2(m)} \left(\frac{\varepsilon d_{pore}^2}{32l\tau} \right)_2 \right]$
Kozeny Carmen	$J_v = \frac{\varepsilon^3}{Kls^2(1-\varepsilon)^2} \times \frac{P_0 - P_z}{\eta}$
Combinations of Solution-diffusion and Pore-flow	
Solution-diffusion-with imperfections	$J = \frac{c_{iM} D_{iM} v_i}{RTl} \Delta P + \frac{c_{iM} B_o}{\eta l} \Delta P$
Machado <i>et al.</i> model	$J = \frac{\Delta P}{\Phi[(\gamma_c - \gamma_L) + f_1] + f_2 \mu}$

2.4. Review of cost and energy analysis

The potential that Organic Solvent Nanofiltration (OSN) has to reduce operating and capital costs has been well demonstrated by the MaxDewax Process [60]. The success of the MaxDewax process contributed to the research field focusing on the economic potential as well as sustainable growth of this technology. Thus, for OSN to be feasible, the separation process needs to be energy efficient, green technology and cost efficient. According to Buonomenna M. [61] and Drioli *et al.* [62], feasibility of membrane technology has demonstrated sustainable growth in many solvent recovery applications performed in industry.

Hybrid systems, which combine membranes with other operations, have been shown to be beneficial. Micovic *et al.* [63] demonstrated that membrane-distillation hybrid systems yield promising, energy-efficient and intensified processes. Micovic *et al.* further stated that the hybrid system may be more economical than the stand-alone distillation process, which was applied to investigate the separation of heavy boilers from low- and middle- boilers in a mixture from hydroformylation processes. Pink *et al.* [64] reported another membrane hybrid system, which provides better separation of contaminants from adsorber unit operations when a membrane stage was introduced to the system. The Palladium concentration in typical solvents, such as toluene and ethyl acetate, was brought down by 8.5 times in the permeate of the hybrid process using 10 times less adsorbent compared to an adsorbent only process.

Werth *et al.* [65] discusses how membrane processes can be both economical and less energy-intensive. Werth *et al.* further discusses, based on a model-based process analysis, how the potential of OSN for solvent recovery has been shown to be high and that OSN is an important investment technology for future processes.

Werth *et al.* demonstrates, using a model-based approach and a flowrate of 2000 kg/hr of non-edible oil, that the total energy demand for the OSN-evaporator hybrid process was between 200 - 600 kW compared to 1400 kW for the base case evaporator system. The total annualized costs for the OSN-evaporator hybrid system was approximately \$1.0 million compared to \$1.2 million for the base-case evaporator system. There is a \$0.2 million difference between the two processes, which is a substantial amount economically saved for an individual process unit. Furthermore, Werth demonstrates graphically that there is a potential optimal point where both energy and total annualized cost can be optimized based on the membrane area.

Werth further discusses that more than 70% of energy can be saved throughout OSN-assisted evaporation processes. From an economically competitive point of view, membrane prices should be \$70/m². Substantial economic advantages were also illustrated at lower membrane areas.

The feasibility of OSN does not only rely on economic and energy initiatives, but also green technology initiatives. A recent review by Szekely *et al.* [11] made a comparison between the energy consumption of a nanofiltration system and a total reboiler for distillation. Szekely summarizes an adequate energy requirement based on pressure difference and this is given in Equation 2.16.

$$Q_{OSN} = \frac{F_f \Delta P_{TM}}{\varepsilon_{pump}} \quad (2.16)$$

Where:

F_f - Feed flow through membrane

ΔP_{TM} - Pressure difference over trans-membrane

ε_{Pump} - Pump efficiency

The energy required in a throughput distillation is given in Equation 2.17.

$$Q_{distillation} = Q_{heating} + Q_{vaporisation} + Q_{condensation} \quad (2.17a)$$

$$Q_{heating} = F_{molar} c_p \Delta T \quad (2.17b)$$

$$Q_{vaporization} = Q_{condensation} = F_{molar} \Delta H_{vap} \quad (2.17c)$$

Where:

F_{molar} - Molar flowrate

c_p - Heat capacity at constant pressure

ΔT - Temperature difference between feed and the boiling point

ΔH_{vap} - Latent heat of evaporation

Szekely illustrates, using Equations 2.16 and 2.17, the energy consumption for the recovery of methanol within a process time of 1371 hr at a feed flowrate of 417 L.hr⁻¹ and an operating pressure of 15 bar. The total energy consumption for distillation and OSN was 1123 GJ and 2.8 GJ, respectively. OSN energy consumption was shown to be 200 times less than that of the distillation column, indicating that a membrane process is advantageous in terms of energy.

Abejón *et al.* [66] investigated the ultra-purification of hydrogen peroxide through multistage reverse osmosis. They performed an economic evaluation on the operating costs for the membrane unit, providing suitable equations that can be used in determining the operating costs of the OSN unit in this study. The equations used were similar to the heuristic equations found in Turton *et al.* [67], which is given in Equation 2.18.

$$TOC = C_{\text{raw}} + C_{\text{labour}} + C_{\text{energy}} + C_{\text{maint}} \quad (2.18a)$$

$$C_{\text{raw}} = FY_{\text{raw}} \quad (2.18b)$$

$$C_{\text{labour}} = 24Y_{\text{labour}} \quad (2.18c)$$

$$C_{\text{energy}} = \frac{\sum(Q_{\text{INi}}\Delta P)}{36\eta} Y_{\text{elec}} \quad (2.18d)$$

$$C_{\text{maint}} = A \cdot C_{\text{capital}} \quad (2.18e)$$

Where:

- F – Feed flow (kg/day)
- C – Operating costs: raw material, maintenance, labour, energy (\$/day)
- Y_{raw} – Price of MEK (\$/kg)
- Y_{labour} – Salary (\$/h)
- Y_{elec} – Electricity price (\$/kWh)
- ΔP_i – Differential pressure across the membrane (Bar)
- Q_{INi} – Stage Flow of inlet stream (m³/s)
- η – Pump efficiency
- A – Maintenance constant ranging between 0.01 - 0.06 (this study: 0.01)

The level of detail that Abejón *et al.* provides using Equation 2.18(a-e) is used as an approximation of operating costs on a basic level, since many assumptions are made. For the purpose of this study, this equation will be used with heuristics obtained from Turton *et al.* [67] to determine the operating costs for both processes, while the capital costs are determined using capital cost estimation formulas provided in Turton *et al.* [67]

2.5. Concluding remarks

The concept of OSN in general is simple to understand, as feed is separated through membrane permeation over a differential pressure. However, the complexity of operation is very application specific and empirical evaluations on OSN systems have been developed, as shown in past literature. There is a lack of knowledge on the understanding of interactions between solvents, solutes and membranes, which are the core factors for developing models for describing the transport in OSN systems. However, as is shown in this chapter, continuous progress is being made towards a better understanding. New membrane systems are continuing to emerge, providing more potential to better understand the OSN technology as a whole.

In the past, while Starmem™ series membranes were still commercially being used, research performed by many research groups showed the recovery of solvents from membranes. The focus has shifted to newly commercialized membranes, such as Duramem™ and Puramem™ series membranes manufactured by Evoniks. However, the recovery of commercially used solvents through polyimide Starmem™ membranes [32, 60,68] have been demonstrated to be successful, while providing rejection of solutes of close to 95%. Cost and energy evaluation from literature has demonstrated that the energy needs of processes can be reduced greatly. Furthermore, the recovery of solvent can drastically lower the operating costs of unit operation, which results in a higher annual profit margin.

2.6. References

- [1] M. Mulder, **Basic Principles of Membrane Technology**, Kluwer Academic Publishers, The Netherlands, 1991.
- [2] P. Vandezande, L.E.M. Gevers, I.F.J. Vankelecom, *Chem. Soc. Rev.* **37** (2008) 365–405.
- [3] P. Schmidt, E.L. Bednarz, P. Lutze, A. Górak, *Chem. Eng. Sci.* **115** (2014) 115–126.
- [4] R.W. Baker, **Membrane Technology and Applications**, 3rd Ed., John Wiley & Sons, Ltd., England, 2012.
- [5] J.L. Humphrey, G.E. Keller, **Separation Process Technology**, McGraw-Hill & Hall, New York, 1997.
- [6] P. Marchetti, M.F.J. Solomon, G. Szekely, A.G. Livingston, *Am. Chem. Soc.* **114** (2015) 10735-10806.
- [7] Y. Zhao, Q. Yuan, *J. Memb. Sci.* **279** (2006) 453–458.
- [8] L.S. White, *J. Membr. Sci.* **205** (2002) 191–202.
- [9] R. H. Perry, D. W. Green, **Perry's Chemical Engineers' Handbook**. McGraw-Hill, New York, 2008.
- [10] D.A. Patterson, L.Y. Lau, C. Roengpithya, E.J. Gibbins, A.G. Livingston, *Desal.* **218** (2008) 248-256.
- [11] G. Szekely, M.F.J. Solomon, P. Marchetti, J.F. Kim, A.G. Livingston, *Green Chem.* **16** (2014) 4440-4473.
- [12] L.S. White, A.R. Nitsch, *J. Memb Sci.* **179** (2000) 267-274.
- [13] X. Yang, A. Livingston, L.F. Dos Santos, *J. Memb. Sci.* **190** (2001) 45-55.
- [14] W.W. Wight (1988), European Patent No. EP0125907B1 .
- [15] A. Livingston, L. Peeva, S. Han, D. Nair, S.S. Luthra, L.S. White, L.M. Freitas Dos Santos, *An. N. Y. Aca. Sci.* **984** (2003) 123-141.
- [16] I.F. Vankelecom, *Chem. Rev.* **102** (2002) 3779-3810.
- [17] A.R.S. Teixeira, J.L.C. Santos, J.G. Crespo. *J. Memb. Sci.* **470** (2014) 138-147.

- [18] M.F.J. Solomon, Y. Bhole, A.G. Livingston, *J. Memb. Sci.* **423** (2013) 371-382.
- [19] H. Siddique, E. Rundquist, Y.L. Bhole, L.G. Peeva, A.G. Livingston, *J. Memb. Sci.* **452** (2014) 354-366.
- [20] L.G. Peeva, E. Gibbins, S.S. Luthra, L.S. White, R.P. Stateva, A.G. Livingston, *J. Memb. Sci.* **236** (2004) 121-136.
- [21] P. Silva, A.G. Livingston, *J. Memb. Sci.* **280** (2006) 889-898.
- [22] S. Darvishmanesh, T. Robberecht, P. Luis, J. Degrevè, B. Van Der Bruggen, *J. Am. Oil Chem. Soc.* **88** (2011) 1255-1261.
- [23] D. Fritsch, P. Merten, K. Heinrich, M. Lazar, M. Priske, *J. Memb. Sci.* **401** (2012) 222-231.
- [24] D.R. Machado, D. Hasson, R. Semiat, *Part I, J. Memb. Sci.* **163** (1999) 93-102.
- [25] D.R. Machado, D. Hasson, R. Semiat, *Part II, J. Memb. Sci.* **166** (2000) pp.63-69.
- [26] Y.H. See-Toh, M. Silva, A. Livingston, *J. Memb. Sci.* **324** (2008) 220-232.
- [27] I. Soroko, A. Livingston, *J. Memb. Sci.* **343** (2009) 189-198.
- [28] J.F. Kim, A.M.F. Da Silva, I.B. Valtcheva, A.G. Livingston, *Sep. Purif.* **116** (2013) 277-286.
- [29] A.P.B. Ribeiro, J.M. de Moura, L.A. Gonçalves, J.C.C. Petrus, L.A. Viotto, *J. Memb. Sci.* **282** (2006) 328-336.
- [30] L.R. Firman, N.A. Ochoa, J. Marchese, C.L. Pagliero, *J. Memb. Sci.* **431** (2013) 187-196.
- [31] H.B. Soltane, D. Roizard, E. Favre, *Sep. Purif. Tech.* **161** (2016) 193-201.
- [32] L.S. White, I. Wang, B.S. Minhas, US Patent No. US5264166A (1993).
- [33] H. Zwijnenberg, A. Krosse, K. Ebert, K. Peinemann, F. Cuperus, *J. Am. Oil Chem. Soc.* **76** (1999) 83.
- [34] N. Stafie, D. Stamatialis, M. Wessling, *J. Membr. Sci.* **228** (2004) 103.
- [35] N. Stafie, **Poly (dimethyl siloxane)-based composite nanofiltration membranes for non-aqueous applications**, University of Twente, 2004.
- [36] D. Stamatialis, N. Stafie, K. Buadu, M. Hempenius, M. Wessling. *J. Membr. Sci.* **279** (2006) 424.
- [37] Z. Zhao, J. Li, D. Zhang, C. Chen. *J. Membr. Sci.* **232** (2004) 1.

- [38] Y. Kong, D. Shi, H. Yu, Y. Wang, J. Yang, Y. Zhang, *Desalination* **191** (2006) 254.
- [39] M. Namvar-MAhboub, M. Pakizeh, *Sep. Purif. Tech* **119** (2013) 35-45.
- [40] M. Namvar-MAhboub, M. Pakizeh, *Kor. J. Chem. Eng.* **31** (2014) 327-337.
- [41] M. Namvar-MAhboub, M. Pakizeh, S. Davari, *J. Memb. Sci.* **459** (2014) 22-32.
- [42] J. Whu, B. Baltzis, K. Sirkar, *J. Membr. Sci.* **170** (2000) 159.
- [43] P. Schmidt, T. Köse, P. Lutze, *J. Memb. Sci.* **429** (2013) 103-120.
- [44] X.Q. Cheng, Y.L. Zhang, Z.X. Wang, Z.H. Guo, Y.P. Bai, L. Shao, *Adv. Polym. Tech.* **33** (2014) 21455.
- [45] D. Peshev, A.G. Livingston, *Chem. Eng. Sci.* **104** (2013) 975.
- [46] L. Hesse, J. Mićović, P. Schmidt, A. Górak, G. Sadowski, *J. Memb. Sci.* **428** (2013) 554-561.
- [47] J.G. Wijmans, R.W. Baker, *J. Membr. Sci.* **107** (1995) 1–21.
- [48] D.R. Paul, *J. Membr. Sci.* **241** (2004) 371–386.
- [49] I.F.J. Vankelecom, K. De Smet, L.E.M. Gevers, A. Livingston, D. Nair, S. Aerts, S. Kuypers, *J. Membr. Sci.* **231** (2004) 99–108.
- [50] H.K. Lonsdale, U. Merten, R.L. Riley, *J. Appl. Polym. Sci.* **9** (1965) 1341–1362.
- [51] D. Bhanushali, S. Kloos, C. Kurth, D. Bhattacharyya, *J. Membr. Sci.* **189** (2001), 1-21.
- [52] T. Matsuura, S. Sourirajan, *Ind. Eng. Chem.* **20** (1981) 273-282.
- [53] H. Mehdizadeh, J.M. Dickson, *J. Memb. Sci.* **42** (1989) 119–145.
- [54] P. Silva, S. Han, A.G. Livingston, *J. Membr. Sci.* **262** (2005) 49.
- [55] J. Geens, B. Van der Bruggen, C. Vandecasteele, *Sep. Purif. Tech* **48** (2006) 255.
- [56] P. Silva, L.G. Peeva, A.G. Livingston, *J. Membr. Sci.* **349** (2010) 167.
- [57] G. Jonsson, C. Boesen, *Desal* **17** (1975) 145.
- [58] J. Robinson, E. Tarleton, C. Millington, A. Nijmeijer, *J. Membr. Sci.* **230** (2004) 29.
- [59] E. Mason, H. Lonsdale, *J. Membr. Sci.* **51** (1990) 1.
- [60] R.M. Gould, L.S. White, C.R. Wildemuth, *Enviro. Prog.* **20** (2001) 12-16.
- [61] M.G. Buonomenna, *RSC advances* **3** (2013) 5694.

- [62] E. Drioli, A. Brunetti, G. Di Profio, G. Barbieri, *Green Chem.* **14** (2012) 1561.
- [63] J. Micovic, K. Werth, P. Lutze, *Chem. Eng. Res. Des.* 2014, **11** (2014) 2131-2147.
- [64] C.J. Pink, H. Wong, F.C. Ferreira, A.G. Livingston, *Org. Proc. Res. Dev.* **12** (2008) 589.
- [65] K. Werth, P. Kaupenjohann, M. Skiborowski, *Sep. Purif. Tech.* **182** (2017) 185.
- [66] R. Abejón, A. Garea, A. Irabien, *Chem. Eng. Res. Design* **90** (2012) 442.
- [67] R. Turton, R.C. Bailie, W.B. Whiting, J.A. Schaeiwitz, **Analysis, Synthesis, and Design of Chemical Processes**, 3rd Ed., Prentice Hall, Boston, 2009.
- [68] M. Priske, M. Lazar, C. Schnitzer, G. Baumgarten, *Chem. Ing. Tech.* **1-2** (2016) 39-49.
- [69] T. Welton, Solvents and sustainable chemistry, **471** (2015) 20150502.

Chapter 3: Methodology

Overview

This chapter discusses the experimental methodology used to complete the objectives at hand. Section 3.1 discusses the chemicals and membranes that were used to investigate the separation performances. Section 3.2 provides a summary of the experimental procedures that were used throughout the experimental investigations. Section 3.3 discusses the approach that was followed to investigate membrane transport. Analytical evaluation using gas-chromatography as well as other equipment is briefly discussed in Section 3.4.

3.1. Materials

The solvents used in this study were Toluene, Methyl Ethyl Ketone (MEK), Methyl-isobutyl-ketone (MIBK) and Dichloromethane (DCM). Toluene and MEK have been selected in this study based on their commercial use throughout the lube oil dewaxing operations [1]. Additionally MIBK has been mentioned by Priske *et al.* [2] to be a suitable solvent alongside MEK and toluene and is therefore investigated in this study.

Previous studies involving DCM and Duramem™200 membranes demonstrate the use of DCM in solvent recovery [3]. DCM is investigated in this study, comparing its suitability as solvent for solvent recovery operations relative to the other solvents investigated in this study.

3.1.1. Chemicals

Toluene (>99.5 wt%), Methyl Ethyl Ketone (>99.5 wt%), Methyl-isobutyl-ketone (99 wt%) and Dichloromethane (>99.5 wt%) were purchased from Ace Chemicals (South Africa). For GC analysis Decane (>99 wt%) obtained from Sigma Aldrich was used as the external standard while n-hexadecane was used as the internal standard. High purity nitrogen, used in the OSN experiments, was supplied by Afrox.

3.1.2. Membranes

The commercially available membranes that were used in this study were of the Puramem™® and Duramem™® membrane series obtained from Evonik [4]. These membranes were supplied as A4 size sheets soaked in preservation oil as a measure of preventing the membranes from drying out. Properties of each membrane type are specified in Table 3.1.

Table 3.1 : List of commercial membranes used in this study and their properties.

Membrane:	Puramem™	Duramem™	Starmem™228
Membrane material:	P84 polyimide	P84 polyimide	Polyimide
MWCO (Da):	280	150, 200	280
Membrane type	Hydrophobic	Semi-hydrophobic	Hydrophobic
Compatible solvents:	Apolar hydrocarbon-type solvents: Toluene Heptane Hexane MEK MIBK Ethyl acetate	Polar solvents: MIBK MEK Methanol	Solvents: Butanol Hexane Toluene MEK MIBK Acetone

Puramem™ and Duramem™ series membranes were chosen due to their stability in the solvents that were used in this study, while a Starmem™228 membrane was used only to test pretreatment solvent type. In order for a membrane to be suitable for solvent recovery, it needs to be able to resist damage and degradation from solvents and other chemical solutes. Additionally, membranes need to resist large degrees of swelling to prevent loss of their separation capabilities [5].

Previous studies have shown that these membranes were successful in recovering valuable solvents, such as toluene and DCM, from systems containing Hoveyda–Grubbs catalysts and activated pharmaceutical ingredients (API), respectively [3,6]

Both membranes mentioned in Table 3.1 are organic solvent-compatible and stable in polar and polar aprotic solvents such as acetone, tetrahydrofuran (THF) and ethanol. These solvent compatibilities indicate that ketones as well as alcohols are adequate solvent species to be used with the Duramem™ series. However, in literature [7-9], the Duramem™ membrane series were used to recover solvents such as DCM, acetone and tetrahydrofuran (THF) from oligomers and other solutes.

Puramem™ membrane series are also P84® polyimide membranes that are hydrophobic by nature and compatible with apolar hydrocarbon-type solvents such as toluene [10]. Like the Duramem™ series, Puramem™ membranes operate at pressures ranging between 20 – 60 Bar. In general, Puramem™ series membranes are compatible with solvents such as toluene as well as ketones, but are not ideally suited for chlorinated solvents such as DCM and amines.

3.2. Organic Solvent Nanofiltration (OSN) experimentation

3.2.1. Experimental Setup

The separation performances (i.e. rejection and flux) of the OSN system as well as the influence of operating parameters (i.e. pressure, feed concentration, temperature) on the system were evaluated using a dead end membrane cell system, as illustrated in Figure 3.1. Previous studies have also used this system to investigate separation performances [11- 13].

The experimental setup consists of a cell chamber (**3**) with a volume capacity of 180 ml. In addition, there is a nitrogen tank (**1**) that supplies nitrogen to the system in order to provide the necessary pressure gradient through the membrane. Furthermore, the inlet valve (**10**), outlet valve (**9**), pressure relieve valve (**7**) and pressure gauge (**6**) are attached to the cell. The membrane chamber has an inner diameter of 46 mm, which provides an active surface area of 16.6 cm². The membrane disks that provide the active surface area are cut from A4 sheets obtained from membrane manufacturers.

The membrane is placed in the chamber holder with the smooth lustrous side facing upwards while the sinter plate supports the membrane from beneath. O-rings are inserted at both ends of the membrane cell before bolts can be fastened.

Concentration polarization, as defined by Vandezande *et al.* [17], occurs on the surface of the membrane as retained solutes begin to accumulate, resulting in an increase in osmotic pressure and a decrease in the permeate flux. This phenomenon was reported in the findings of Stamatialis *et al.* [15] and Peeva *et al.* [16], who both recommend crossflow operations over dead-end cell operations in order to minimize concentration polarization.

The teflon-coated magnetic stirrer bar is placed inside the membrane about 3 mm above the membrane surface, which is in effect once the magnetic stirrer (4) is switched on. The stirring bar is used to accentuate cross flow conditions.

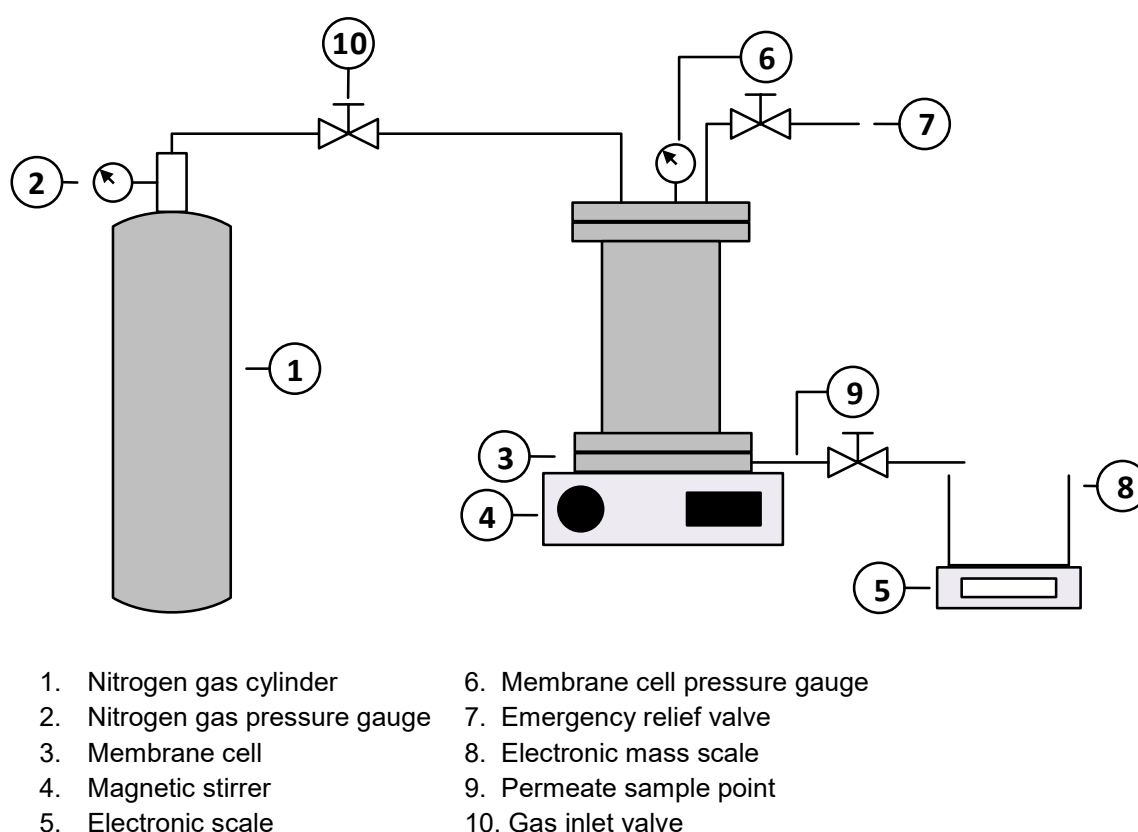


Figure 3.1: Dead-end membrane cell apparatus

The permeate is collected from the outlet valve in a glass beaker (8) that is stationary on an electronic laboratory mass scale (5). The solvent-solute mixture is inserted into the membrane cell after which the cell is tightly sealed and nitrogen is pressurized through the membrane cell. The active experiments are then commenced to allow the rejection and permeate characterization.

3.2.2. Experimental methodology

3.2.2.1. Introduction

In this study experiments were done to obtain membrane performance data that could be used to demonstrate the successful recovery of solvent from oil-solvent mixtures. Pure species permeation, binary component permeation and separation for various membranes and various solvents were investigated using the experimental procedures discussed in this section. The general experimental phases in this study involved: 1) membrane pretreatment, 2) membrane conditioning tests, 3) membrane flux tests and 4) separation evaluation.

3.2.2.2. Pretreatment of membranes

Before any experimentation could occur, membranes were treated in order to remove any contaminants from the membrane and flush the membrane with solvent, to create a homogeneous membrane fluid throughout the membrane. Subjecting the membrane to pretreatment provided homogeneous membrane properties. The solvent that was evaluated through experimentation in this study, was also used as the solvent for pretreatment of the Duramem™ and Puramem™ series membranes.

For pretreatment, 150 ml of the solvent under investigation was loaded into the cell, after which permeation occurred at a continuous transmembrane pressure of 30 bar for 5 to 8 hours. Observing the colour of the permeate provided an indication of the amount of oil removed from the membrane matrix. Approximately 50 ml of the solvent in question had to permeate through to ensure that the oil was completely removed. The pretreatment was repeated for solvents that had very high fluxes (i.e. MEK, DCM) for permeate collection.

3.2.2.3. Membrane conditioning

It is common practice for the conditioning of membranes to be performed prior to experimentation. According to Vandezande *et al.* [17], membrane performance can be influenced significantly without proper membrane conditioning prior to experimentation. The effect of membrane compaction can be minimized by subjecting the membrane to the break-in procedure prior to experimentation.

Membrane conditioning was performed by exposing the membrane to the set of conditions, such as pressure and solvent, which would be used in the experimental runs. This allowed the membrane to compact and swell to the extent that it would during the experimental runs, which minimizes error and external influence on membrane performance. Prior to conditioning of the membrane, the membrane cell was rinsed with roughly 5 ml of the solvent that would be used in the experimental runs in order to remove unwanted species and provide a more consistent experimental run. The cell was then loaded with solvent or solvent mixture and sealed. The cell was pressurized to the desired pressure and roughly one third of the feed solution was

allowed to permeate. For steady state consistency, the permeate was recycled back into the feed, and the process was then performed again for 6 to 8 hours for the membrane to provide steady state.

3.2.2.4. Binary species separation and solvent recovery

Rather than characterizing OSN membrane operation with regard to pure solvent feed, it was evaluated in terms of solvent recovery and rejection of solute.

Binary mixtures considered in this study consisted of the selected solvent and one solute (i.e. n-hexadecane), which was evaluated at solute feed weight fraction percentages. Only one solute species was used to represent the dewaxed oil composition typically found in industry.

The membrane was pretreated initially with the pure solvent that was also used in the binary mixture according to the procedure provided in Section 3.2.2.2. Once pretreated, the solvent-oil mixture was loaded into the cell at a volume of 150 ml and at the solute feed weight fractions that were being evaluated. The cell was pressurized and 60 ml (40 vol%) of the binary feed was allowed to permeate in order to obtain a consistent, steady membrane environment, providing data that is characteristic to the experimental conditions. Once 60 ml of feed solution had permeated, the cell was depressurized and the permeate was thrown back into the feed mixture. This was because if more than 40 vol% of the feed mixture had permeated, the experimental data obtained would have been inconsistent at the implemented experimental conditions. Permeate was recycled back into the feed solution until steady state flux was achieved. Once steady state was achieved, the cell was depressurized in order to take a 4 ml feed sample, after which the cell was pressurized and ready to begin the experimentation phase.

Once steady state was achieved for the binary mixture, the experimentation could commence where 15 ml of feed was allowed to permeate. Once 15 ml of feed had permeated, three samples of 4 ml each were withdrawn from the permeate into a 4 ml vial. The three permeate samples and the initial feed sample were then prepared for GC analysis. The GC was used to determine the concentrations of the three permeate samples as well as the collected feed sample.

3.3. Analytical techniques

3.3.1. Gas-chromatography

The analytical technique that was used to analyse the composition of the permeate and retentate was gas-chromatography (GC). The analytical equipment that was used was a Thermo Scientific (No. 423130) Trace GC Ultra, with analytical separations done on a 30 m x 0.32 mm x 0.25 μm ZB5 capillary column coupled to a flame ionization detector. The

developed method had an initial hold time of 1 minute at 50°C. The temperature of the GC oven was then raised from 50°C to 250°C at 15°C.min⁻¹, with a final hold time of 10 minutes at 250°C. A mixture of helium, hydrogen and air was used as the detector make-up gas. The make-up gas flowrate for helium, air and hydrogen was 20 ml.min⁻¹, 300 ml.min⁻¹ and 30 ml.min⁻¹, respectively.

Standard solutions of hexadecane, having different concentrations, were used to obtain calibration curves which were used to obtain a GC response factor. The standard solutions were made up so that the standard curve range comprised of 10, 20, 30, 80 and 100 µL of each analyte used in this study. The solution contained 30 µL of decane, which was used as the internal standard for this study. The prepared samples were then placed in the GC autosampler, followed by injection on the analytical column for separation of sample components to obtain retention times. The response factor is defined in this study as the ratio between the concentrations of a compound being analysed relative to the ratio between peak areas of these compounds obtained from the GC detector. The peak areas are obtained from the chromatogram. The response factor for n-hexadecane was determined to be 0.9994 using the standard solution concentration curve data. The GC calibration curve and response factor for n-hexadecane is shown in Figure 3.2

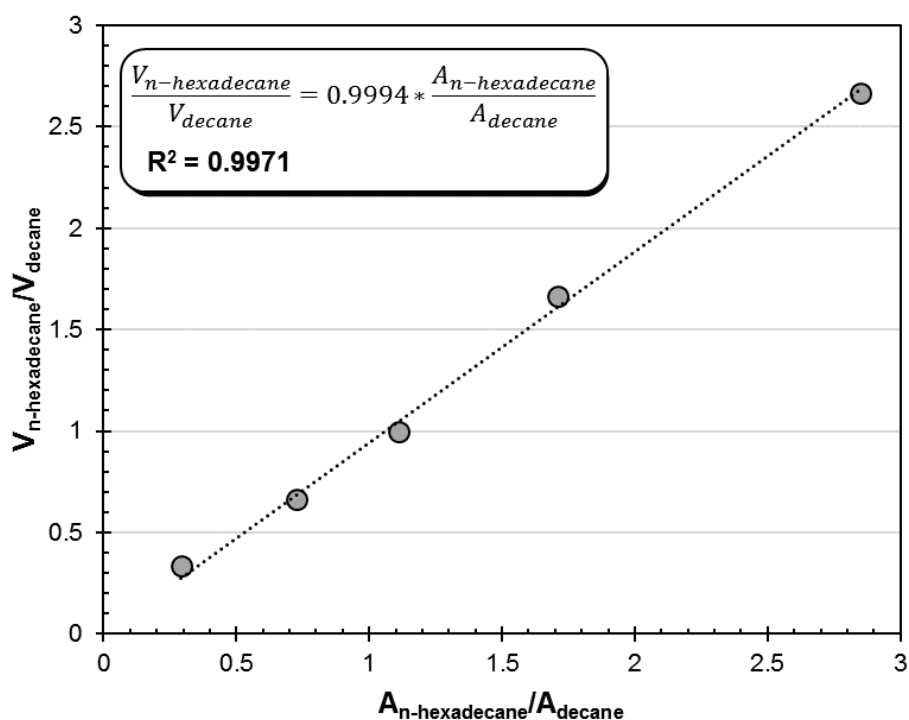


Figure 3.2: GC calibration curve for n-hexadecane

For sample preparation, 80 µL n-hexadecane (i.e. $V_{n\text{-hexadecane}}$) was added to 4 ml of DCM in a 4 ml sample vial and 30 µL of internal standard (i.e. decane, V_{decane}) was added to the solution

as well. The sample was diluted by taking 300 μL of sample solution and adding it to 1.5 ml of DCM in a 2 ml sample vial. The samples were then put into the GC autosampler, injected on the GC column and sample components were separated on the GC column. The resulting GC peak areas of n-hexadecane and the internal standard on the GC chromatogram, as shown in figure 3.3, were then used to determine the response factor of n-hexadecane. Once the response factor was known, the volume of n-hexadecane could be determined from the calibration curve shown in Figure 3.2.

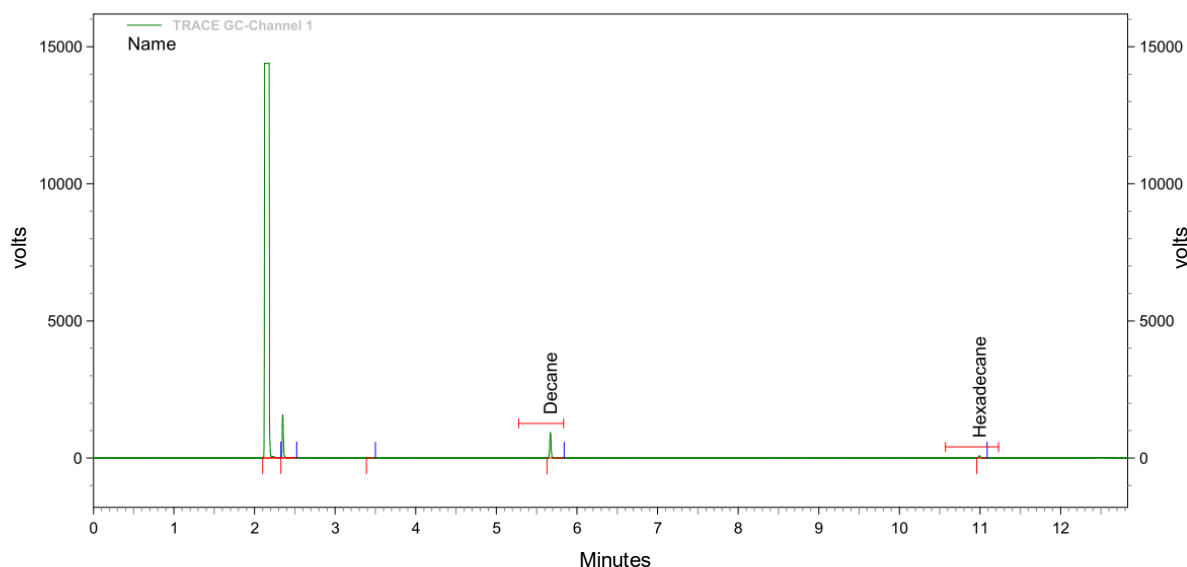


Figure 3.3: Chromatogram for n-hexadecane

As shown in Figure 3.3, the retention time for n-hexadecane and decane is approximately at 11 min and 5.5 minutes, respectively. Combining the internal standard volume with the relative peak areas, results in the formation of Equation 3.1:

$$V_{n\text{-hexadecane}} = V_{\text{decane}} \times \left(\frac{A_{n\text{-hexadecane}}}{A_{\text{decane}}} \right) \times RF \quad (3.1)$$

Equation 3.1 was used to determine the volume of solute in each binary mixture evaluated in this study. Once the concentration had been determined, the rejection of solute could thus be determined.

3.4. Methodology of membrane transport

Objective 2 in this study, which involves the investigation and evaluation of membrane transport mechanisms, was successfully accomplished by obtaining transport models to describe the transport through the membrane, as discussed in Chapter 2.2. A step-by-step procedure to validate, compare and fit the membrane models was developed. The approach that was used to develop models for these membranes can be classified as a three level approach.

Before experimentation is executed, a basic understanding of describing flux mathematically is evaluated through a level 1 approach. Flux described through Equation 2.1 was used to mathematically understand the influence of pressure, flowrate and membrane area. The level 1 approach provides a good foundation towards moving onto level 2 and 3 modelling.

Level 2 modelling requires empirical data from literature as well as modelling results from well-known transport models (i.e. the classic solution-diffusion and pore-flow models) to the existing literature experimental data. Eventually the outcome of level 2 was to obtain flux and rejection as a function of different parameters, as shown in Equation 3.2 and Equation 3.3.

$$J_V = f(T, \Delta P, \omega, P_i) \quad (3.2) \quad R = f(\omega, C_p, C_f) \quad (3.3)$$

Flux and rejection can be shown as a function of various parameters in Equation 3.2 and Equation 3.3. After identifying important model parameters (i.e. permeability) from the classic solution-diffusion and pore-flow models, level 3 modelling makes use of experimental data from this study and incorporates it into the models evaluated in the level 2 modelling. The manipulated variables that were used in investigating the transport through the membrane are given in Table 3.2.

Table 3.2: Manipulated operating variables

Manipulated variables	Range	Description
Feed Pressure	10, 20, 30, 40 Bar	Pressure influences are typical conditions in an OSN system affecting the permeate rate and they have an effect on rejection. Finding the optimum pressure is therefore required.
Solvent species	Toluene, MEK, DCM, MBIK	These solvents are typical solvents used in industry and were tested with a variety of membranes to determine the most suitable solvent(s) for a specific membrane separation.
Solute concentration (n-hexadecane)	10, 15, 20, 25 wt/wt %	The concentrations of oil are typical to what is found in literature applications and in industrial processes, such as the dewax plant. Hexadecane was chosen based on its

Manipulated variables	Range	Description
		properties and represents the oil in this study.
Membrane	Duramem™(150, 200), Puramem™280	Membranes used in commercial application were studied in this investigation.

The manipulated variables listed in Table 3.2 were used in order to produce a variety of output variables, which in turn were used to model and optimize the OSN system. The output variables collected from the experiments are listed in Table 3.3.

Table 3.3: Experimental output variables obtained.

Experimental output variables	Method of acquisition	Description
Permeate concentration	GC analysis	The permeate concentration was required to determine the rejections and modelling equations that needed to be further developed in this study.
Retentate concentration	GC analysis	For modelling and validation purposes the retentate stream concentration was determined.
Permeate rate	Cumulative mass over time	The permeate rate was experimentally determined using a weight mass scale to determine the flux.

The variables from Table 3.2 and Table 3.3 were incorporated into the level 3 modelling. They were used to evaluate the system by identifying the effects of all manipulating variables on the experimental output variables that were required to produce separation performance curves. Once the output performance parameters were obtained for the various membranes, the separation performances of the membrane systems could be compared to conventional separation systems, such as distillation solvent recovery.

The approach of using theoretical models, such as the solution-diffusion and pore-flow models, is a standard approach that requires the necessary parameters both from literature and from experimental data. Chemical properties for this study were based on literature values, while the permeability parameter for each model was experimentally determined in this study. After incorporating the parameters into the models, the response variables (i.e. flux) could be determined.

3.4. Methodology of economic analysis

To determine the feasibility of solvent recovery by OSN membrane operation, a comparative preliminary economic evaluation between distillation and OSN membrane operation was done. The economic evaluation made use of process simulation data, where process simulation was developed from the simplest system to a more complex system. Energy usage was determined for both systems through process simulation, while cost evaluation was determined based on the heuristics found in literature [9,19,20,21]. The simulation of the process conditions was developed using Aspen Plus software. The focus of the simulation was to determine the energy balances as well as mass balances throughout the OSN membrane unit and distillation unit.

In order to provide the same operating conditions as the experimental OSN operation for both distillation and OSN systems, the assumption that the system was continuous for a binary solvent-solute system needed to be made in Aspen Plus. A calculator block was used in order to keep track of rejection and purity of the permeate and distillate streams with regard to the solvent recovered. Once the operating conditions were met, the energy that was required to operate the system was obtained. Energy usage for the OSN system was determined based only on the pump work required in order to provide the necessary pressure into the membrane.

The operating costs depend on a number of operating variables as discussed in Chapter 2. In order to provide a reasonable economic evaluation, the economic evaluation was performed for a system without a recycle stream, which was then compared to the separation units where a recycle stream had been included.

Capital costs were determined based on previous process plant data, such as unit size and unit cost in the provided year. Using the heuristics provided in Turton *et al.* [19], the capital costs were determined. The manipulated variables used to perform the energy and cost analysis are provided in Table 3.5.

Table 3.5: Manipulated operating variables

Manipulated variables	Range	Description
Feed flowrate	1000 kg.hr ⁻¹	The feed flowrate is a design base condition, which was used for the comparison of OSN and distillation in this study.
Organic solvent concentration	75, 80, 85, 90 wt/wt %	The concentration of solvent influences the cost of raw feed material, which influences the recycle ratio, reflux rate, purity and operating costs significantly.
Distillation column stages	10 - 25	The number of stages are based on a typical distillation column design, as illustrated in Coulson <i>et al.</i> [19]
Reflux ratio	0 – 5	A selected input variable, that is required in order to provide the standard purities of solvent recovery obtained in industry for distillation operation.
Split ratio of recycle stream back to OSN feed	0 – 100	The split stream of recycle is determined to provide the ideal amount of solvent that can be placed into the feed, while providing an output stream of high purity solvent recovery at sufficient output flowrates.
Membrane area	10 – 100 m ²	The membrane area influences the size of the OSN unit and is used to determine the capital cost of the membrane unit.

Based on the variables used in Table 3.5, the output variables obtained for comparative analysis of the two systems (i.e. Distillation and OSN operations) in question, are summarized in Table 3.6.

Table 3.6: Economic output variables obtained

Experimental output variables	Method of acquisition	Description
Solute rejection	Aspen calculator block	Using the calculator block as well as the stream concentrations, the rejection can be determined.
Energy consumption	Aspen Plus simulation	Using Aspen Plus simulation software, the energy consumption can be determined for each individual piece of equipment that was used.
Permeate/distillate flowrate	Aspen Plus simulation	From Aspen Plus, the distillate and permeate flowrates were determined for both streams.
Capital Cost	Nelson-Farrar cost indexes	The cost information for the unit equipment was adjusted using appropriate scaling factors, in order to accommodate capacity scaling as well as inflation, which provides the estimated capital cost.
Operating Costs	Cost of manufacturing estimate	Determining the cost of manufacturing relies on five elements, which include labour, energy, fixed capital costs, raw materials, waste, utilities and maintenance.

Economic performance of OSN operation and distillation operation were compared and discussed based on the output variables provided in Table 3.6. The observed effects of manipulated variables demonstrate the flexibility of both systems and as a result indicate which variables have more influence than others.

3.5. References

- [1] R.M. Gould, L.S. White, C.R. Wildemuth, *Enviro. Prog.* **20** (2001) 12-16.
- [2] M. Priske, M. Lazar, C. Schnitzer, G. Baumgarten, *Chem. Ing. Tech.* (2015).
- [3] H. Siddique, E. Rundquist, Y. Bhole, L. Peeva, A. Livingston, *J. Membr. Sci.* **452** (2014) 354.
- [4] Evonik Industries AG, Germany. [Online], (2017). <http://Duramem™.evonik.com>
- [5] D.R. Machado, D. Hasson, R. Semiat, *J. Membr. Sci.* **163** (1999) 93.
- [6] D. Ormerod, B. Bongers, W. Porto-Carrero, S. Giegas, G. Vijt, N. Lefevre, *et al.*, *RSC Advances* **3** (2013) 21501.
- [7] J. Li, M. Wang, Y. Huang, B. Luo, Y. Zhang, Q. Yuan, Part A, *RSC Advances*, **4** (2014) 40740.
- [8] M.F.J. Solomon, Y. Bhole, A.G. Livingston, *J. Membr. Sci.* **423** (2012) 371.
- [9] P. Schmidt, E.L. Bednarz, P. Lutze, A. Górak, *Chem. Eng Sci.* **115** (2014) 115.
- [10] K. Hendrix, M. Van Eynde, G. Koeckelberghs, I.F. Vankelecom. *J. Membr. Sci.* **447** (2013) 212.
- [11] K. Xiao, Y. Shen, X. Huang, *J. Memb. Sci.* **427** (2013) 139–149.
- [12] Y.H. See Toh, F.W. Lim, A.G. Livingston, *J. Memb. Sci.* **301** (2007) 3–10.
- [13] P. Van der Gryp, A. Barnard, J.P. Cronje, D. de Vlieger, S. Marx, H.C.M. Vosloo, *J. Memb. Sci.* **353** (2010) 70–77.
- [14] X. Yang, A. Livingston, L.F. Dos Santos, *J. Memb. Sci.* **190** (2001) 45-55.
- [15] D. Stamatialis, N. Stafie, K. Buadu, M. Hempenius, M. Wessling, *J. Memb. Sci.* **279** (2006) 424-433.
- [16] L.G. Peeva, E. Gibbins, S.S. Luthra, L.S. White, R.P. Stateva, A.G. Livingston, *J. Memb. Sci.* **236** (2004) 121–136.
- [17] P. Vandezande, L.E.M. Gevers, I.F.J. Vankelecom, *Chem. Soc. Rev.* **37** (2008) 365–405.
- [18] Y. Kong, D. Shi, H. Yu, Y. Wang, J. Yang, Y. Zhang, *Desal* **191** (2006) 254.

- [19] R. Turton, R.C. Bailie, W.B. Whiting, J.A. Schaeiwitz, **Analysis, Synthesis, and Design of Chemical Processes**, 3rd Ed., Prentice Hall, Boston, 2009.
- [20] R. Abejón, A. Garea, A. Irabien. *Chem. Eng. Res. Design* **90** (2012) 442.
- [21] D. Peacock, J.F. Richardson, Chemical Engineering, **Chemical and Biochemical Reactors and Process Control**, Volume 3, Elsevier, Oxford, 2012.

Chapter 4: Results and Discussion – Recovery of Solvent

Overview

This chapter discusses all the experimental results that were obtained for the OSN system relating to the pure species and binary species recovery. The membranes investigated were Duramem™150, Duramem™200 and Puramem™280. The experimental validation, repeatability and experimental error are reported in Section 4.2. Membrane performances are discussed in Sections 4.3 and 4.4, demonstrating the effect of solvent, solute and membrane properties on separation performances.

4.1. Introduction

Membrane performance is usually categorized in terms of permeance and rejection parameters. The membrane performance of an industrial system has a significant effect on its economic viability, energy consumption and green-initiatives. The results discussed in this section elaborate on membrane performance in terms of flux and rejection. Flux and rejection data was obtained using Equation 4.1 and Equation 4.2.

$$J = \frac{V_n}{A \cdot \Delta t} \quad (4.1)$$

$$R_{solute} = \left(1 - \frac{C_p}{C_f}\right) \quad (4.2)$$

Where:

V_n – volume of fluid that permeates through membrane normal to the surface area (L)

A – effective membrane surface area (m^2)

t – time interval for which volume V permeates through the membrane (hr)

J – flux of a permeating species through the membrane ($L \cdot m^{-2} \cdot hr^{-1}$)

C_p – solute concentration in feed permeate ($ml \cdot ml^{-1}$ or $mg \cdot L^{-1}$)

C_f – solute concentration in the feed ($ml \cdot ml^{-1}$ or $mg \cdot L^{-1}$)

R_{solute} – rejection

Interactions between solvents, solutes and membranes were observed, which influenced membrane performance, and these interactions are further discussed in this chapter.

4.2. Experimental error and reproducibility

This section presents the reproducibility and experimental validation of all experimental data for the OSN experiments obtained with the dead-end cell. In order to obtain reasonable experimental results for the dead-end cell system, steady state conditions needs to be met. Silva *et al.* [1] states that membrane compaction and steady state operation is a slow process, and that describing the membrane operation at short time periods between 1 - 3 hours does not provide reliable performance for long-term operation. White *et al.* [2] provides a supporting argument, stating that a lined-out steady state was achieved through spiral-wound membranes after 100 hours of membrane operation. Whu *et al.* [3] achieved steady state for methanol at two different pressures for two sets of 8 hour experimental runs using a dead-end-cell setup. Whu *et al.* furthermore stated that membrane compaction is demonstrated as the initial impermanent stage, having a duration of approximately 12 hours.

Using the break-in procedure, discussed in Section 3.2.2.2, the validation of experiments was addressed while achieving steady-state conditions over a 6-hour period, using Puramem™280 and toluene at 20 bar (as shown in Figure 4.1).

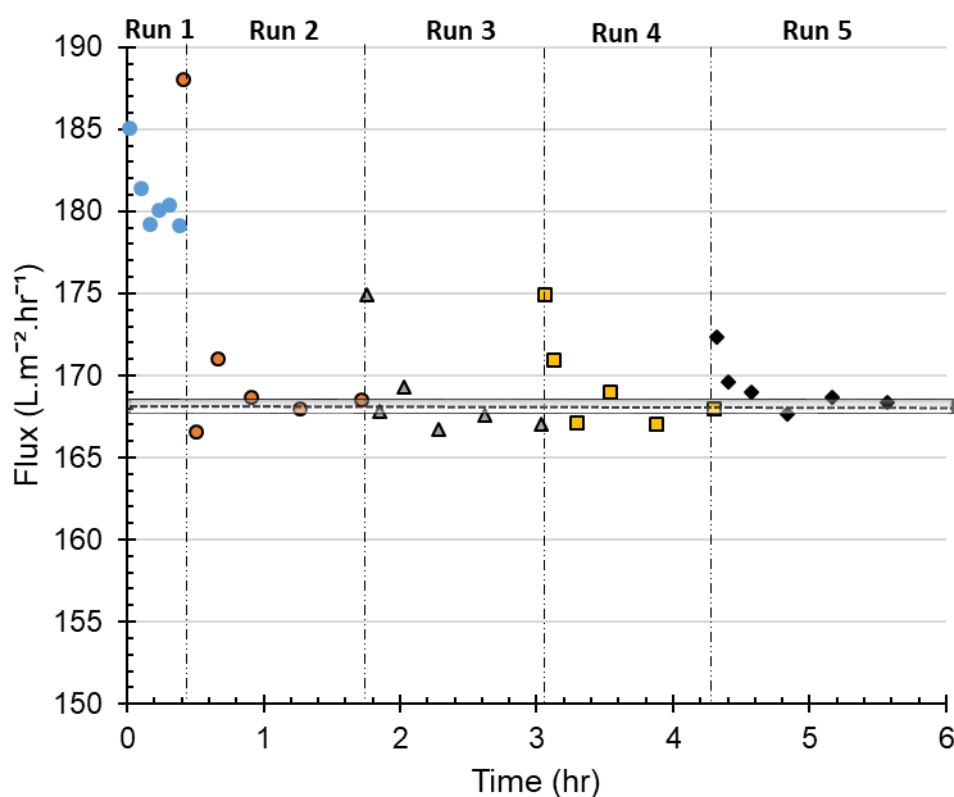


Figure 4.1: Acquisition of steady state flux through Puramem™280 for pure toluene at 20 bar.

OSN experimental runs were performed five consecutive times. During each run the dead-end cell was depressurized, refilled and pressurized again to the desired pressure. This process is depicted in Figure 4.1 by the vertical lines intersecting the different operations, representing the 5 repeated runs. As shown in Figure 4.1, steady state started to be observed from Run 2 onwards. Over five consecutive runs, an average flux of 168 L.m⁻².hr⁻¹ was obtained, as illustrated by the grey horizontal line in Figure 4.1. The steady state phenomenon demonstrated over the five consecutive operations illustrate that steady state had been achieved over 6 hours of operation. Run 1 is the operation where the break-in procedure occurs, resulting in a distributed compaction over the surface of the membrane, which from then onwards, induces a lower flux. Runs 2 – 5 illustrate the lower flux caused by compaction, but also show how the pressure drop over the membrane occurs after pressurizing the cell during each consecutive run. According to Van der Gryp *et al.* [4], a new membrane disc takes approximately three days for solvent flux to reach steady state. However, as shown by Whu *et al.* [3] as well as in Figure 4.1, steady state can be achieved over a shorter duration.

The Starmem™228 membrane was used in this study only to demonstrate the influence that the pretreatment solvent type has on the membrane performance for pure species flux, using pure 1-octene species. The experimental flux obtained was compared to literature flux values. Van der Gryp *et al.* [4] performed 1-octene pure species flux tests on Starmem™228, which is illustrated in Figure 4.2.

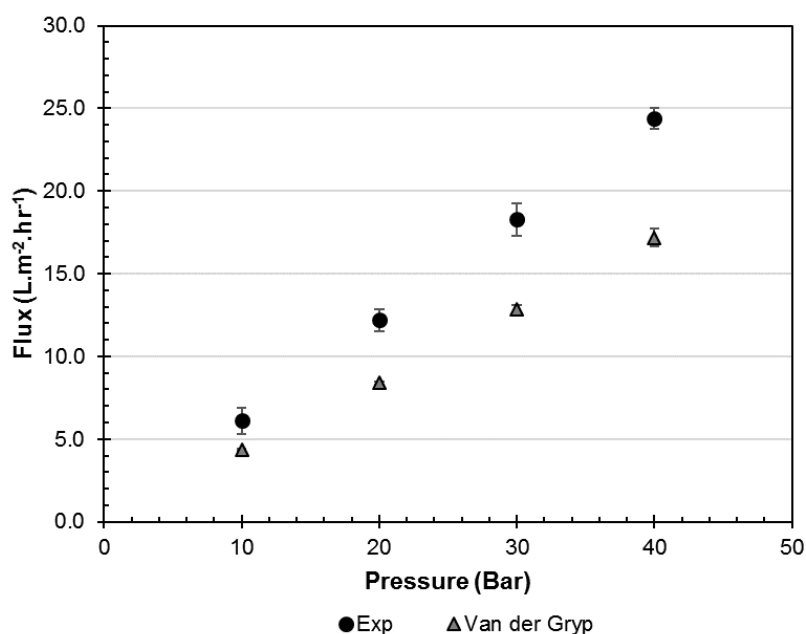


Figure 4.2: 1-Octene Pure Species Flux through Starmem™228

There are differences between the fluxes obtained from experimental work in this study and those obtained by Van der Gryp *et al.* [4], as shown in Figure 4.2. The solvent used for pretreatment of the Starmem228™ membrane in the work of van der Gryp *et al.* [4] was toluene. The solvent used for the pretreatment of the Starmem™228 membrane in this study is 1-octene

According to Zhao *et al.* [5], the membrane structure and membrane hydrophobicity are reorganized depending on the type of solvent used for pretreatment. Additionally, Jeżowska *et al.* [6] state that pretreatment increases the homogeneity of properties of flat sheet membranes. Hence, the difference seen in Figure 4.2 is mainly due to the type of solvent used for pretreatment. For the purpose of this study, the solvents that were used for pretreatment of Duramem™150, Duramem™200 and Puramem™280, are the solvents that were being used in pure species and binary species experimentation, namely MIBK, MEK, toluene or DCM.

Experimental runs for a binary mixture were repeated in order to validate the reproducibility of the experimental results by determining the experimental error for each experimental

operation. Three consecutive runs for the toluene/n-hexadecane mixture were conducted at different solute feed weight fraction percentages (10, 15, 20 and 25 wt%). Experimental error, which is based on the deviation of rejection for binary species, was determined and is summarized in Table 4.1.

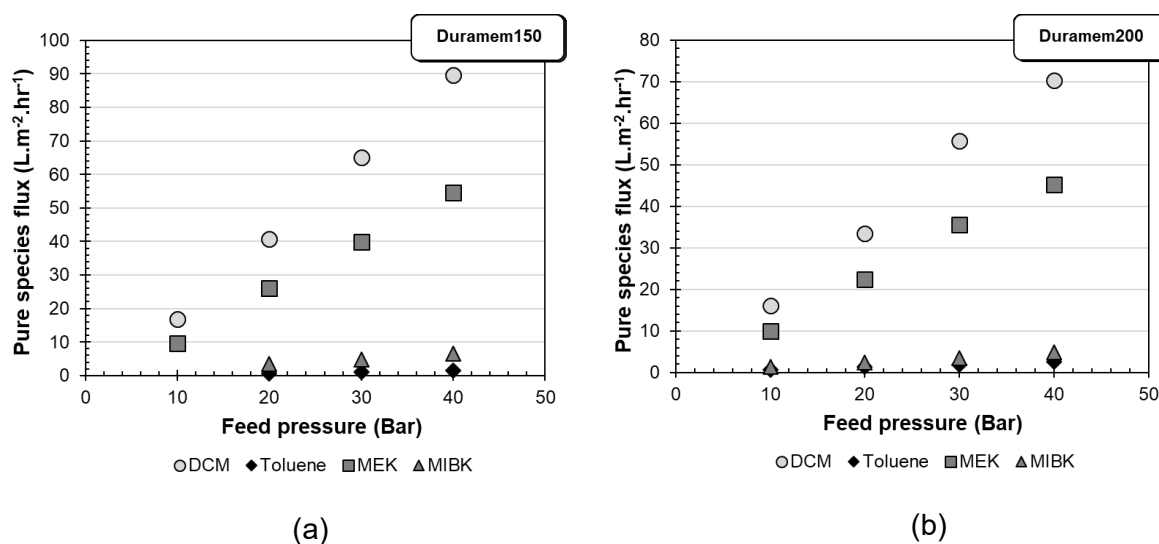
Table 4.1: Experimental error and repeatability for a toluene/n-hexadecane binary mixture through Puramem™280 at 30 bar.

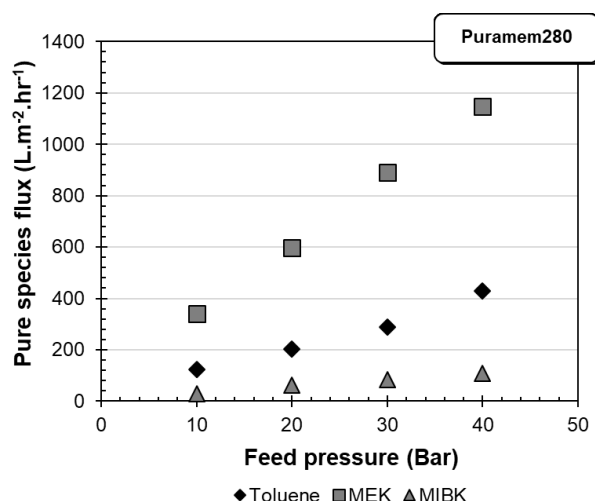
C16 (wt%)	C16 Con feed (mg/L)	C16 Conc Perm (mg/L)	Average Rej (%)	Stdev (σ)	Std error (%)
10	0.100	0.060	39.57 +/- 5.0	4.3	2.5
15	0.127	0.116	8.910 +/- 2.3	2.0	1.1
20	0.173	0.128	26.17 +/- 5.6	4.0	2.8
25	0.287	0.204	29.06 +/- 4.6	3.9	2.3

Table 4.1 shows that for dead-end cell operation the standard error is on average 2.5 %. Furthermore, it can be assumed that all rejection experiments specific for binary mixtures will have the same standard error of 2.5 %.

4.3. Pure species permeation tests

Pure solvent fluxes were experimentally determined through Puramem™ and Duramem™ series membranes at various pressures and the results are illustrated in Figure 4.3.





(c)

Figure 4.3. Pure solvent flux through membranes (a) DuramemTM150, (b) DuramemTM200 and (c) PuramemTM280 at various pressures and ambient room temperature.

As shown in Figure 4.3, the smaller molecular sized species, such as MEK and DCM, permeate at higher fluxes through DuramemTM150 than larger species, such as toluene and MIBK. Other properties besides molecular weight have an influence on the membrane performance. This is evident, for instance, when comparing the fluxes of MIBK and toluene. MIBK has a molecular weight of 100.16 g.mol⁻¹ and a molar volume of 125.8 m³.mol⁻¹, which is larger than that for toluene. However, MIBK has a higher flux relative to toluene, as shown in Figure 4.3 (a) and (b). The reason why the flux of MIBK is higher than that of toluene, lies in the polarity of MIBK resulting in it having a better affinity to the DuramemTM series membranes than toluene. The DuramemTM membranes interact better with polar compounds, giving solvents like MEK, DCM and MIBK a higher flux due to these polar interactions compared to non-polar molecules such as toluene.

The permeance values obtained from various fluxes at different pressures were used to model the transport through the membranes and the permeance of each species for DuramemTM150, DuramemTM200 and PuramemTM280 is shown in Table 4.2.

Table 4.2: Pure species permeance for DuramemTM150, DuramemTM200 and PuramemTM280 at a room temperature of 20°C.

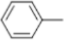
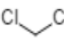
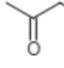
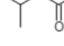
Species	Permeance (L.m ⁻² .hr ⁻¹ .Bar ⁻¹)		
	Duramem TM 150	Duramem TM 200	Puramem TM 280
DCM	2.1700	2.0725	-
MEK	1.3329	1.1403	29.323
MIBK	0.1638	0.1217	2.7660
Toluene	0.0378	0.0655	10.365

The data shown in Table 4.2 can be used in modelling within the pore-flow and solution-diffusion models, as described in chapter 2. Chapter 5 of this thesis will elaborate further on this. As discussed previously, DCM and MEK have higher permeance values compared to the larger species, which are non-polar (i.e. toluene and MIBK).

4.4. Effect of solvent properties

Solvent properties are important when it comes to describing transport of a solvent-solute mixture through a membrane. Some of the solvent properties of interest in this study are shown in Table 4.3.

Table 4.3: Summary of solvent properties used in this study

Species/ Structure	MW (g.mol ⁻¹)	V _m (m ³ /mol)	Viscosity (cP)	Dipole Moment (μ _D)	Polarity	δ ^(a) (MPa) ^{0.5}	ε ^(b)
Toluene 	92.14	106.85	0.55	0.31	Non-polar	18.2	2.32
DCM 	84.93	64.50	0.437	1.6	Fairly polar	20.2	8.93
MEK 	72.11	89.44	0.428	2.78	Highly polar	19.1	18.5
MIBK 	100.16	125.8	0.58	2.7	Highly polar	17	13.1

(a) Solubility Parameters based on Hansen Solubility parameters

(b) Dielectric constant

As shown in Figure 4.3, solvents with larger molecular weights relative to membrane MWCO tend to have lower fluxes. Referring to Table 4.3 and Figure 4.3, MIBK and MEK have molecular weights of 100.16 g.mol⁻¹ and 72.11 g.mol⁻¹, respectively. It is clear that the impact of the molecular size differences of MEK and MIBK on their respective fluxes were significant. Looking at Puramem™280 alone, MEK has a larger flux relative to MIBK and toluene. As mentioned before, the size of a species influences the degree of steric hindrance which that solvent species will experience with itself and with the membrane. When considering only the impact of molecular size, one would expect that the larger molecules would result in lower fluxes through a membrane. However, when arranging the molecules from largest molecular size to smallest: MIBK>Toluene>DCM>MEK, there is no clear explanation why some species, such as DCM, have higher fluxes to that of MEK, as illustrated in Figure 4.3 (b and c). This demonstrates that molecular size is not the only factor which influences the transport of a species through a membrane.

Darvishmanesh *et al.* [8] reported that molecular size alone does not have significant effects on the flux through a membrane. According to these authors, this is due to the fact that other parameters, such as a combination of solvation and hydration effects as well as

solvent-solute-membrane interactions, play an important role. The interactions of solvent with a membrane influence the geometric shape of the membrane which affects its structure and degree of swelling to some degree.

According to Zheng *et al.* [9], molecular size is the most easily accessible parameter to use but is not the most accurate size parameter. Zheng *et al.* further states that the molecular size parameter can be defined in various ways, with most of these assuming a spherical shape and rigid molecule. Focusing rather on describing the transport through a membrane that is based on the molecular shape, provides a better understanding of the molecular size parameter. When one looks from a molecular shape viewpoint, the length and width as well as geometrical conformation is taken into account, based on the molecular mass distribution. Zheng *et al.* defines the molecular shape parameter as the distribution of molecular bulk according to the geometrical conformation of a given molecule.

Zheng *et al.* reported that the retention of solutes with similar molecular shapes increased with increasing molecular size. More importantly, Zheng *et al.* further mentions that for molecules of similar molecular weight, the transport through the membrane is most preferential towards linear molecules, followed by branched molecules and lastly molecules with cyclic groups. Previous studies have also shown preferential transport through membranes for linear molecules compared to branched- and cyclic molecules [8,10,11].

When looking at the solvents in this study, MIBK and toluene have nearly similar molecular weights (MIBK: 100.16 g.mol⁻¹, Toluene: 92.14 g.mol⁻¹). Toluene is classified as a cyclic compound and MIBK is classified as a branched compound. As illustrated in Figure 4.3, the fluxes of MIBK is higher than those of toluene through Duramem™150 and Duramem™200. According to Zheng *et al.* [9], branched molecules have a preferential permeance in comparison to cyclic compounds. This illustrates that even though toluene has a lower molecular size in comparison to MIBK, the molecular shape does influence the transport through the membrane. The molecular shape influences solvent transport through a membrane because of the inter- and intramolecular interactions that the permeating species has with the membrane and other permeating species, irrespective of whether the mixture is homogeneous or heterogeneous.

One solvent property that can describe the pure species flux through a membrane is viscosity. On evaluating the influence that viscosity has on the transport through each membrane, a definite link between the viscosity of a species and the solvent flux is identified. The following fluxes through Puramem™280 have been demonstrated experimentally (organized from highest to lowest flux): MEK>toluene>MIBK. The reported experimental fluxes through Puramem™280 perfectly reflect the viscosities of each pure species in order of smallest to largest viscosity: MEK<toluene<MIBK. For Duramem™150 and Duramem™200, a similar phenomenon occurs, since both MIBK and toluene, which exhibit higher viscosity, provide lower fluxes compared to MEK and DCM.

The Pearson correlation, given in Equation 4.3, is a measure of the strength of the association between two quantitative variables. The nearer the scatter of points are to a straight correlation line, the higher the strength of association between the variables.

$$r = \frac{\sum(x-\bar{x})(y-\bar{y})}{\sqrt{\sum(x-\bar{x})^2 \sum(y-\bar{y})^2}} \quad (4.3)$$

Using the correlation given in Equation 4.3, viscosity can be considered an important property that influences flux through Puramem™280, Duramem™200 and Duramem™150, with Pearson correlations of 0.9995, 0.994, and 0.9423, respectively. The dependence between viscosity, molar volume and flux signifies that the transport across a membrane is controlled by diffusive properties. Figure 4.4 demonstrates how the Pearson correlation closely relates the viscosity to flux.

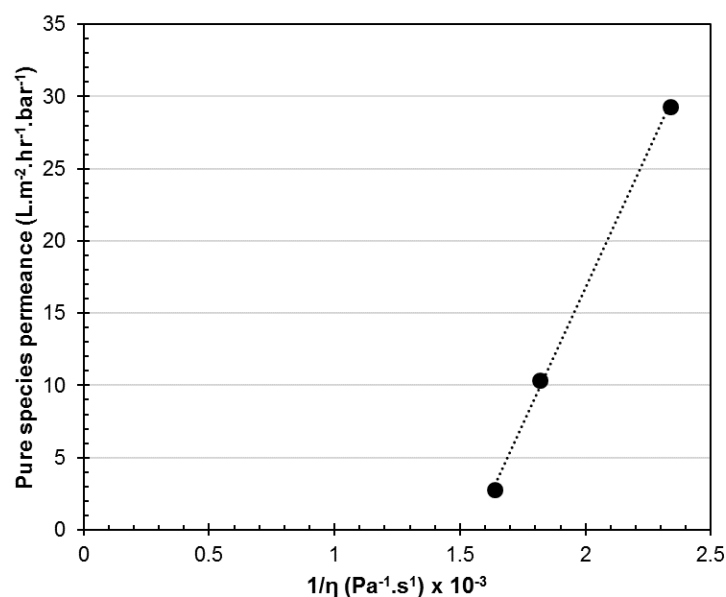


Figure 4.4: Flux vs inverse of viscosity for pure species permeation

The influence that viscosity has on the pure solvent flux through the membrane was shown to be inversely proportional, which has also been reported by other researchers [12-14].

Bhanushali *et al.* [15] proposed a correlation between solvent properties and the experimental fluxes observed. Properties such as viscosity, surface tension, molar volume and sorption terms were included, as described in Equation 4.4.

$$J \propto A \propto \left(\frac{V_m}{\eta \phi^n} \right) \quad (4.4)$$

Where:

V_m – molar volume ($\text{m}^3 \cdot \text{mol}^{-1}$)

η – Viscosity (Pa.s)

The relationship between the solvent properties and solvent transport is described through more than just viscosity and molar volume. According to Geens *et al.* [16], other properties besides viscosity influence the transport of solvents through membranes.

Solvent polarity is an important parameter that is defined as the separation of electric charge, resulting in a molecule or its chemical groups having few or multiple electric dipole moments. Polar molecules are considered to have intermolecular dipole-dipole forces that interact with hydrogen bonds or atoms with low electronegativity. The degree of polarity can be described by three properties, (1) the dipole moment, (2) dielectric constant and (3) miscibility with water.

The dipole moment of a species refers to the measurement of separation of two opposite electrical charges on the species and describes the polarity of a species based on the distribution of electrons between two bonded atoms. The solvents that were used in this study, can be arranged from those with the largest to smallest dipole moments: MEK > MIBK > DCM > toluene. The relationship between solvent dipole moment and solvent permeance is illustrated in Table 4.4.

Table 4.4: Solvent dipole moment and solvent permeance

Species	Dipole moment	Permeance ($\text{L} \cdot \text{m}^{-2} \cdot \text{hr}^{-1} \cdot \text{Bar}^{-1}$)		
		Duramem™150	Duramem™200	Puramem™280
MEK	2.78	1.33	1.14	29.32
MIBK	2.7	0.16	0.12	2.76
DCM	1.6	2.17	2.07	-
Toluene	0.31	0.04	0.07	10.36

On evaluation of the relationship between solvent dipole moment and solvent flux through Duramem™ series membranes presented in Table 4.4, it becomes clear that higher fluxes

are observed for solvents with high dipole moments (MEK, DCM and MIBK) compared to solvents with low dipole moments (toluene). There is no clear relationship between the solvent dipole moment and the pure solvent flux through the Puramem™280 membrane.

For both Duramem™150 and Duramem™200 membranes the following solvent fluxes were observed, arranged from highest to lowest: DCM > MEK > MIBK > toluene. On comparison of the experimental fluxes with the dipole moment arrangement, the most notable observation is that the non-polar molecule, toluene, has a dipole moment of 0.31 and a low solvent flux which can be considered a fair correlation. However, DCM provides high fluxes through Duramem™ series membranes but has a much lower dipole moment of 1.6 compared to those of MEK and MIBK of 2.78 and 2.7, respectively. It is clear from this observation that the dipole moment is a solvent property which is not well correlated with solvent flux for solvents with different functional groups.

The dielectric constant is another parameter that can describe transport of solvent through the membrane. The dielectric constant is a measure of a substance's ability to insulate charges from each other, which can be considered a measure of solvent polarity [16]. Solvents with high dielectric constants generally have high polarity, while solvents with low dielectric constants are classified as non-polar. The relationship between solvent dielectric constant and solvent permeance is illustrated in Table 4.5.

Table 4.5: Solvent dielectric constant and solvent permeance.

Species	Dielectric Constant	Permeance (L.m ⁻² .hr ⁻¹ .Bar ⁻¹)		
		Duramem™150	Duramem™200	Puramem™280
MEK	18.5	1.33	1.14	29.32
MIBK	13.1	0.16	0.12	2.76
DCM	8.93	2.17	2.07	-
Toluene	2.32	0.04	0.07	10.36

From Table 4.5 one compares the dielectric constant gradation (from highest to lowest) of the solvent species used in this study: MEK > MIBK > DCM > toluene, with the apparent experimental permeance (DCM > MEK > MIBK > toluene), the correlation fits well for non-chlorinated species through the Duramem™ series membranes. However, this correlation is not obvious for the solvent permeance through the Puramem™280 membranes.

The solubility between two species can be used to describe the affinity of two species towards each other (i.e. solute, solvent, membrane), hence giving an indication of a species' miscibility as reported by previous researchers [10,17 – 21]. Equation 4.5 is a representation of the difference between the solubilities of two species.

$$\Delta\delta = |\delta_i - \delta_m| \quad (4.5)$$

Where δ_i is the solubility parameter for species i and δ_m is the solubility parameter of the membrane material. According to Li *et al.* [22], the membrane flux and separation can be represented by the solubility parameter and molarity. The model that Li *et al.* developed, provided a good fit for Duramem™ series membranes and is discussed further in Chapter 5. The correlation of the solubility parameter of each solvent with the experimental flux can be evaluated by arranging the solvents from largest to smallest with regard to solubility: DCM > MEK > toluene > MIBK. The major discrepancy comes from the rearrangement of toluene and MIBK on comparison of their apparent fluxes for Duramem™ series membranes (arranged from largest to smallest flux): DCM > MEK > MIBK > toluene.

The solubility of a species can be used to describe the polarity of the species. The solubility parameter for Duramem™ series membranes are found in literature to be 26.8 MPa^{0.5} [22,23]. According to Robertson *et al.* [20], the closer the solubility parameter of the solvent is to that of the membrane, the higher the flux will be. This holds true for DCM and MEK, having Hansen solubility parameters of 20.2 MPa^{0.5} and 19.1 MPa^{0.5}, respectively. However, this is not true in the case of MIBK and toluene. Although toluene has a higher solubility parameter than MIBK, MIBK has a higher permeance than toluene. This indicates that the Hansen solubility parameters do not provide a good correlation with permeance for larger molecules.

According to the Evoniks membrane manufacturers [24], chlorinated solvents, such as dichloromethane (DCM), are not recommended for use with Duramem™ series and Puramem™ series membranes. In this study, the effect of DCM solvent on the Evonik membranes was investigated. DCM was found to be an acceptable solvent for use with the Duramem™ series membranes, but not suitable for use with Puramem™280 membranes. Figure 4.5 is a visual comparison of a Puramem™280 membrane that had been exposed to either a non-chlorinated solvent or a chlorinated solvent.

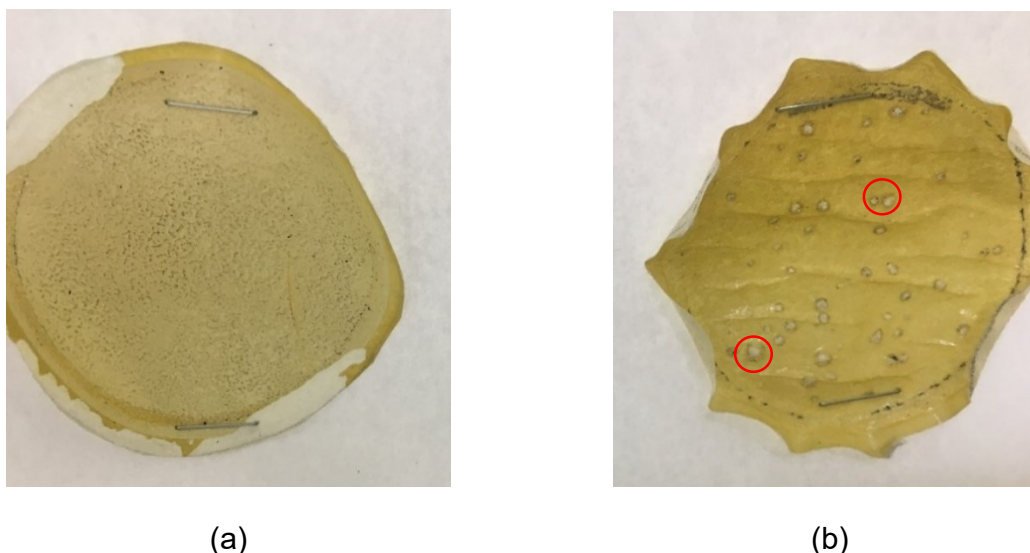


Figure 4.5: Visual presentation of Puramem™280 membrane after (a) non-chlorinated solvent or (b) chlorinated solvent has permeated through at 30 bar and ambient room temperature.

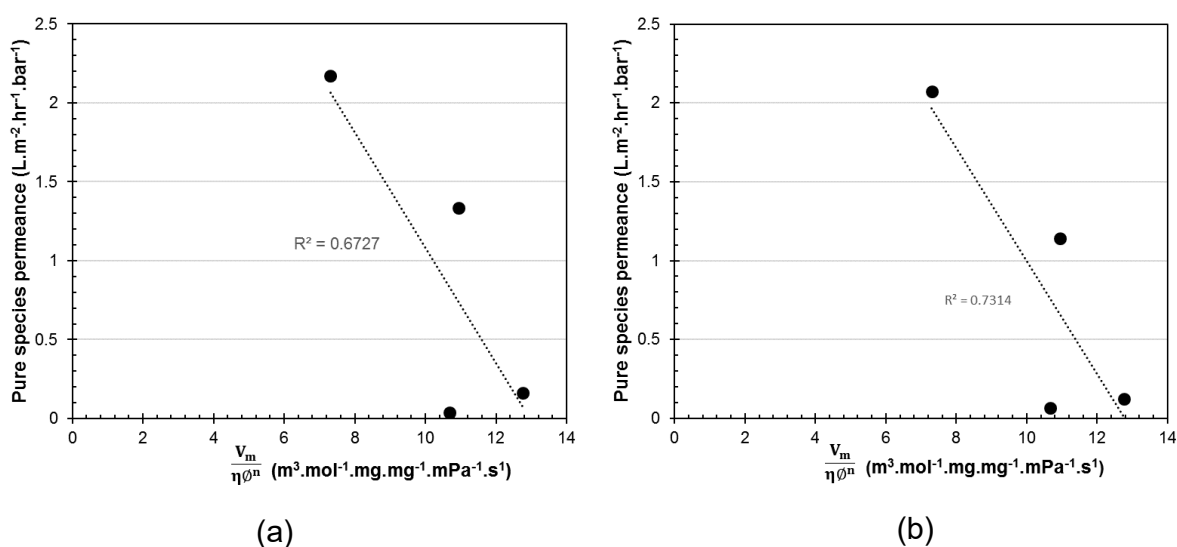
As shown in Figure 4.5(b), the use of chlorinated solvents with Puramem™280 membranes can have a huge impact on the membrane condition. As is visible in Figure 4.5, the chlorinated solvent perforates the membrane, which is undesirable. Perforation causes the membrane to provide little to no separation and in the process the membrane is damaged. According to Lau *et al.* [25], the suitability of commercial polyimide (PI) membranes for use with certain solvents are limited by their susceptibility to degradation through contact with chlorine. This is due to chemical changes that take place in the nature of the PI membranes when they are exposed to chlorine, which affects membrane performance. Furthermore, over the long term chlorine exposure shortens the membrane life span.

Konagaya *et al.* [26] performed research on improving the resistance of Reverse Osmosis (RO) membranes towards chlorine. They demonstrated that it is possible to develop chlorine resistant membranes while providing high RO membrane performance. With regard to nanofiltration membranes, Buch *et al.* [27] investigated the chlorine stability of NF membranes by interfacial polymerization. Buch *et al.* reported that the performance of membranes decreased drastically after exposing the membranes to chloride solution for 24 hours. Buch *et al.* further comments that membrane technology has not reached maturity yet and that more research work needs to be done to enhance the further development of membranes.

In summary, various solvent properties, such as viscosity, dielectric constant, molar volume, dipole moments and solubility parameters, have an impact on membrane transport of the permeating species. However, one parameter alone cannot predict the species flux through the membrane since there are still other interactions with the membrane that have to be taken into account. Various other parameters, such as surface tension, have been reported in literature to have an effect on the flux and membrane performance of the permeating species [16,29 - 31]. In literature, models have been developed [15,16] that take a combination of solvent properties into account, as shown in the relation given in Equation 4.6.

$$permeability \propto \left(\frac{molecular\ size}{1} \right) \times \left(\frac{1}{viscosity} \right) \times \left(\frac{1}{affinity} \right) \quad (4.6)$$

The relationship between permeability and solvent properties given in Equation 4.6 have provided good results for past membranes such as Starmem™ and MFP series membranes. However, fitting this correlation to the solvents and membranes used in this study gives an unfitted trend, as illustrated in Figure 4.6.



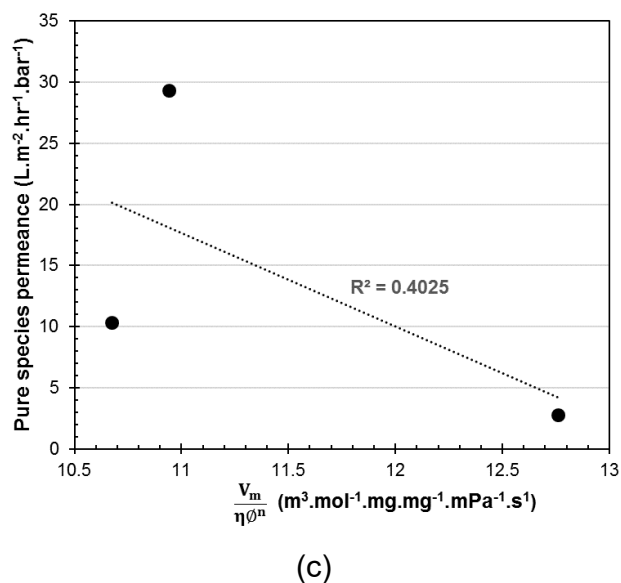


Figure 4.6: Correlation between molar volume, viscosity and solubility constant of solvents in relation to permeance through (a) Duramem™150, (b) Duramem™200 and (c) Puramem™280.

From Figure 4.6 it is clear that the correlations obtained from models proposed in literature, using various forms of Equation 4.6, fit the Puramem™280 series the least and the Duramem™ series membranes, with special reference to Duramem™200, the best. However, for none of the three membranes the correlation is positive, with Pearson correlations for Duramem™150, Duramem™200 and Puramem™280 of -0.82, -0.855 and -0.63, respectively. This shows that there is a negative correlation between the solvent properties and solvent permeance through membranes, indicating that the solvent properties have a low strength of association with the solvent permeance through the membrane.

4.5. Binary species permeation and rejection

n-Hexadecane has been used as a solute marker in past OSN research published by White *et al.* [2], in which toluene was recovered from a toluene-hexadecane system through a polyimide Lenzing P84 membrane. The rejection obtained for this system was found to be 78% hexadecane using Lenzing P84 membranes. Comparing literature to the results obtained from this study, there is a major difference in the performance between the two membranes and solvent types used. The recovery of solvents used in this study from a hexadecane solvent system is illustrated in Figure 4.7.

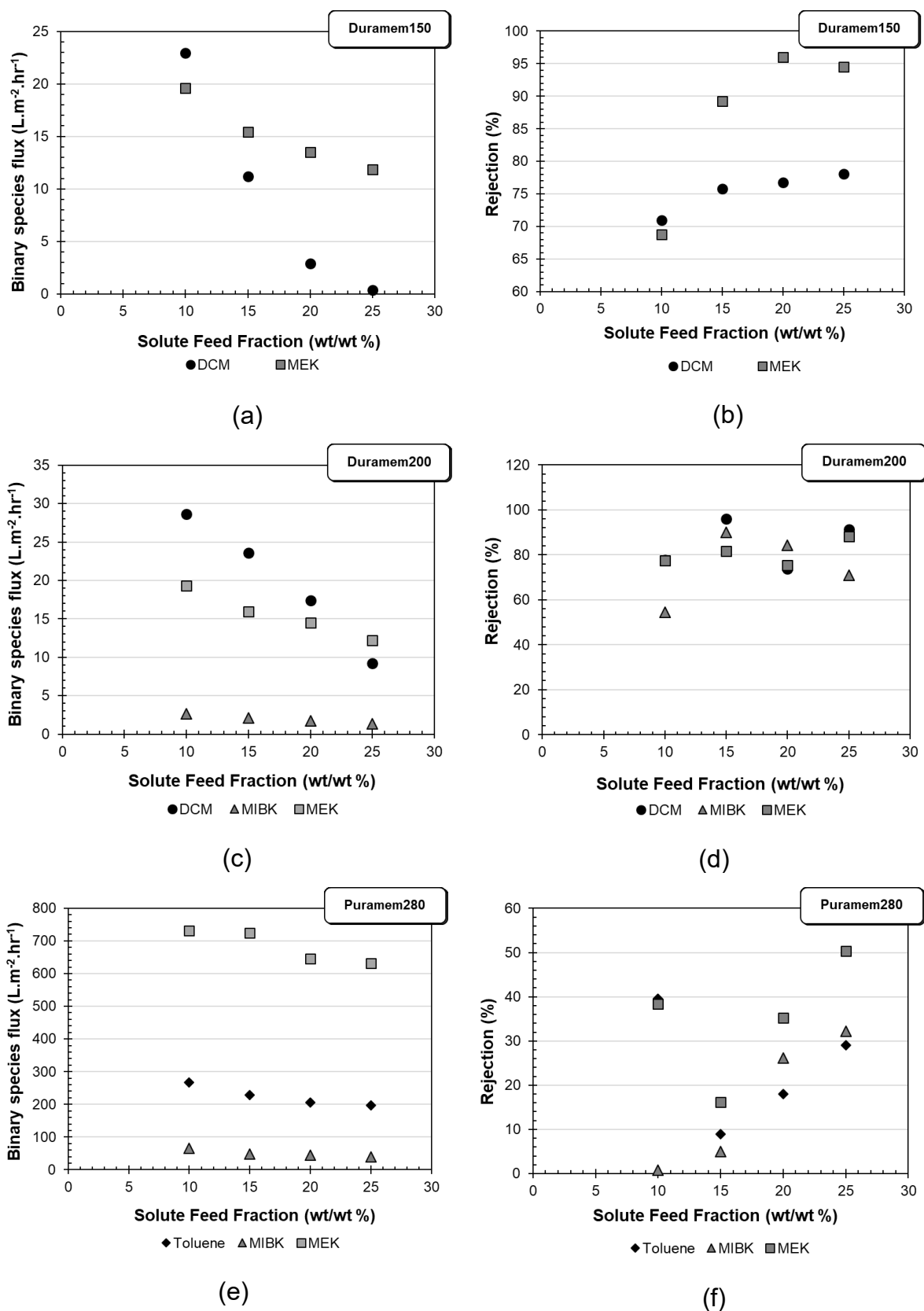


Figure 4.7: Binary permeation and rejection of n-hexadecane from different solvents through three membranes (a-b) Duramem™ 150, (c-d) Duramem™ 200 and (e-f) Puramem™ 280 at various feed concentrations, ambient room temperature and 30 bar feed pressure.

As illustrated in Figure 4.7, MEK had a higher flux than DCM, while both tended to decrease in flux as the concentration of hexadecane increased in the feed. The fact that permeate flux decreased with increasing feed solute concentration, was due to the higher hindrance that the solute has in the membrane, causing higher densities of concentration polarization and more obstruction of pathway through the membrane. Over time the flux decreased due to this hindrance and for this reason only smaller molecules, such as MEK and DCM, were allowed to pass through. One reason for MEK having a higher binary flux, is that MEK has a higher dipole moment, which allows MEK to pass through the membrane more easily. Kong *et al.* [32] demonstrated, with a binary solvent mixture and solute, that the permeation is influenced by the concentration of solute in the feed. A steady decrease of permeate was demonstrated and conclusions made by Kong *et al.* entail that concentration polarization decreases the MEK permeation.

The major discrepancy between MEK and DCM is the difference in their dipole moments of $\Delta\mu_o = 1$. This large difference and the fact that MEK has a larger molar volume (i.e. occupying more space), can be the reason for higher rejection than that of DCM. This behaviour between solvent and solute was identified by White *et al.* [2] and Zheng *et al.* [9,33], who found higher recoveries and lower permeability for the bulky molecules due to a larger steric presence.

As illustrated in Figure 4.7, lower solute fractions in the feed provide lower rejections. Hexadecane has a molecular weight of $226.45 \text{ g}\cdot\text{mol}^{-1}$, which should in theory not allow it to permeate through the membrane. Although Duramem™ 150 is classified as a membrane that rejects 90% of molecules with the molecular weight of $150 \text{ g}\cdot\text{mol}^{-1}$ or greater, this rejection is not complete. MEK has a higher purity in the permeate than DCM, as is shown in Figure 4.7. Although DCM has a higher pure species permeance, the MEK solvent provides better rejection due to less steric hindrance in the MEK-hexadecane feed mixture. Both MEK and DCM have similar properties, which makes it difficult to justify how the behavioural properties of these two solvents influence the transport of hexadecane through the membrane.

Membrane flux and rejection are two important output variables that are used to describe the recovery of a desired species. In Figure 4.8 rejection is plotted against membrane flux, demonstrating how these two recovery outputs are inter-linked with one another.

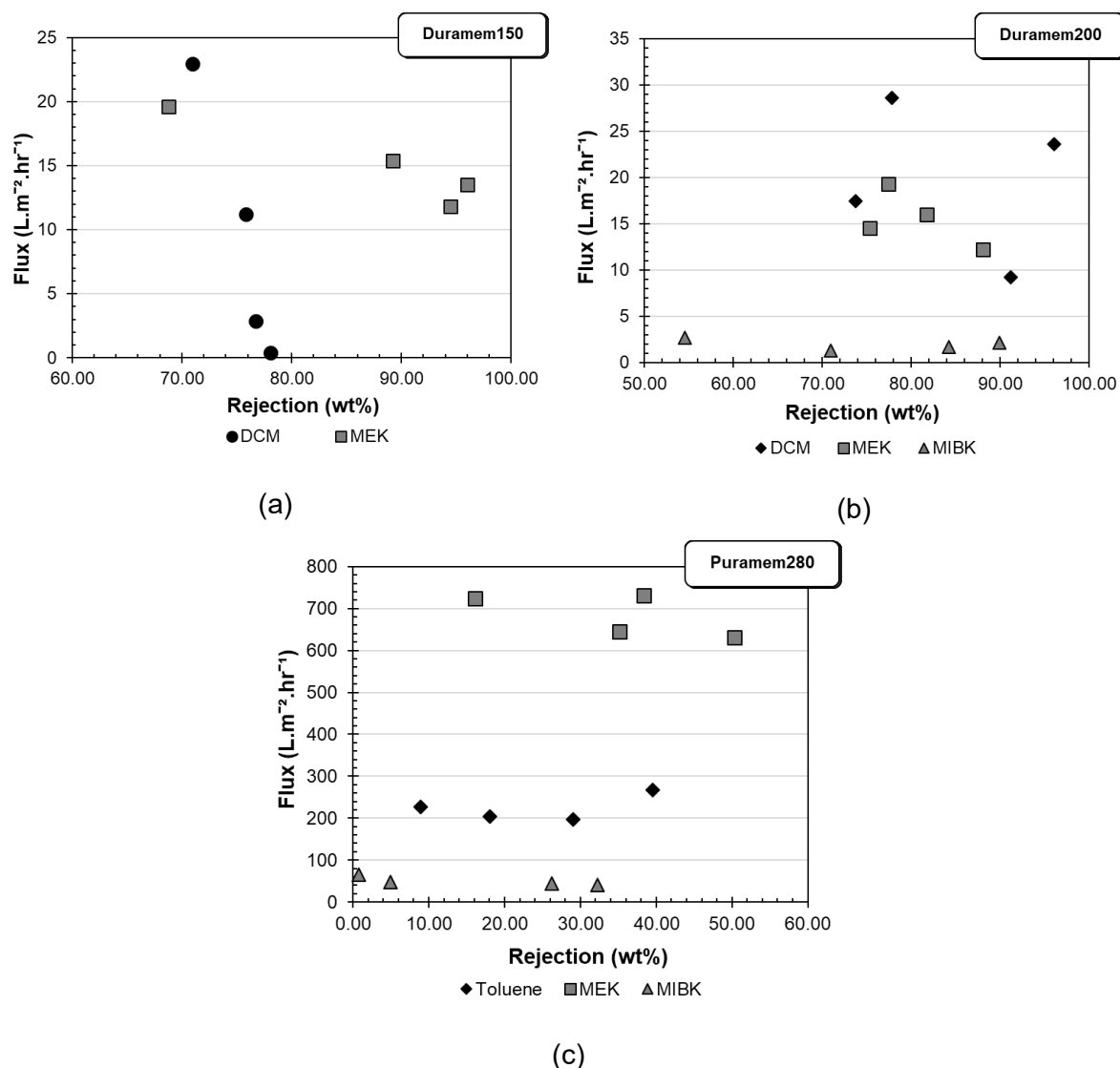


Figure 4.8: Flux vs rejection performances for (a) Duramem™150, (b) Duramem™200 and (c) Puramem™280 at 30 bar and room temperature.

Figure 4.8 shows that the flux performance parameter decreases as the rejection of solute increases. This trend is most clearly illustrated in Figure 4.8(a), where DCM flux has a steep decrease as rejection of hexadecane increases, however this trend is less predominant for DCM through Duramem™200. The main cause of this is the build-up of solute on the membrane surface, contributing to the lower flow of solvent through the membrane due to the many steric hindrances. MIBK and toluene do not show strong resemblance to the trends followed by DCM and MEK. This is due to the challenges in determining the permeate flux of these solvents. The sensitivity of the mass scale that was used to obtain readings for the accumulative mass of very slow permeating species, resulted in error in the readings for the solute-solvent mixtures of the solvent species toluene and MIBK. Comparison between the recovery performance variables provides a good indication as to which would be a better choice for recovery. Ideally high rejection and high permeate flux are desired.

4.6. Concluding remarks

In this chapter, the recovery of solvent through OSN membranes has been demonstrated to be influenced by a number of factors.

Experimental validation for all species besides DCM demonstrated good reproducibility of the experimental results, . The experimental error was taken as an arithmetic mean, taking into account pressure drop, experimental rejections and recorded accumulated mass readings and was shown to be 2.5 % at a feed pressure of 30 Bar. The break-in procedure, which was used to acquire steady state in this study, was shown to be a viable procedure for use in this study. It was also shown that steady state conditions were achieved using the dead end cell setup. The equipment validation, which was performed using 1-octene, demonstrated good similarities with literature fluxes.

Permeation tests performed for pure species through Duramem™150, Duramem™200 and Puramem™280 membranes provided results that illustrated how properties from both membrane and permeating species have an effect on flux. MEK and DCM provide higher fluxes overall due to their molecular size, polarity and solubility. However, toluene provides two orders of magnitude greater fluxes through Puramem™280 than Duramem™200, which demonstrates the influence of membrane interaction as well. DCM has been shown to be detrimental to membranes in general including the Duramem™ series membranes, which are classified to be polar stable membranes. This study has shown that DCM is not recommended as a suitable solvent to be used in lube oil dewaxing processes using Duramem™ and Puramem™ series membranes, due to the fact that it is a chlorinated species.

A binary solvent-solute mixture, representing the feed solution in membrane operation, was also investigated. Solvent recovery was successfully demonstrated through membrane permeation and rejection of solute, which were determined through analytical analysis.

The most notable results obtained for membrane performance for binary feedstock was that, at solute feed weight fractions lower than 15 wt/wt%, the rejection of solute was poor. It was found that solute feed weight fractions ranging between 20 – 25 wt/wt% provided rejections of solute as high as 95%, thus resulting in the recovery of higher purity solvent in the permeate.

MEK and toluene are the preferred solvents used in industries for the recovery of solvent using dead-end cell equipment, as was also shown through the experimentation performed in this study.

4.7. References

- [1] P. Silva, S. Han, A.G. Livingston, *J. Membr. Sci.* **262** (2005) 49.
- [2] L.S. White, A.R. Nitsch, *J. Membr. Sci.* **179** (2000) 267.
- [3] J. Whu, B. Baltzis, K. Sirkar, *J. Membr. Sci.* **170** (2000) 159.
- [4] P. van der Gryp, A. Barnard, J. Cronje, D. de Vlieger, S. Marx, H.C. Vosloo, *J. Membr. Sci.* **353** (2010) 70.
- [5] Y. Zhao, Q. Yuan, *J. Memb. Sci.* **279** (2006) 453–458.
- [6] A. Jeżowska, T. Schipolowski, G. Wozny, *Desal.* **189** (2006) 43.
- [7] P. Marchetti, M.F.J. Solomon, G. Szekely, A.G. Livingston, *Am. Chem. Soc.* **114** (2015) 10735-10806.
- [8] S. Darvishmanesh, L. Firoozpour, J. Vanneste, P. Luis, J. Degrevé, B. Van der Bruggen, *Green Chem.* **13** (2011) 3476–3483.
- [9] F. Zheng, C. Li, Q. Yuan, F. Vriesekoop, *J. Memb. Sci.* **318** (2008) 114–122.
- [10] S. Darvishmanesh, J. Vanneste, E. Tocci, J. Jansen, F. Tasseli, J. Degrevé, E. Drioli, B. Van der Bruggen, *J. Phys. Chem. B.* **115** (2011) 14507–14517.
- [11] L.S. White, *J. Memb. Sci.* **205** (2002) 191–202.
- [12] S. Aerts, A. Buekenhoudt, H. Weyten, L.E.M. Gevers, I.F.J. Vankelecom, P.A. Jacobs, *J. Memb. Sci.* **280** (2006) 245–252.
- [13] M.F.J. Dijkstra, S. Bach, K. Ebert, *J. Memb. Sci.* **286** (2006) 60–68.
- [14] S. Zeidler, U. Kätzel, P. Kreis, *J. Memb. Sci.* **429** (2013) 295–303.
- [15] D. Bhanushali, S. Kloos, C. Kurth, D. Bhattacharyya, *J. Membr. Sci.* **189** (2001) 1.
- [16] J. Geens, B. Van der Bruggen, C. Vandecasteele, *Sep. Purif. Technol.* **48** (2006) 255–263.
- [17] S. Darvishmanesh, J. Degrevé, B. Van der Bruggen, *Phys. Chem. Chem. Phys.* **12** (2010) 13333–13342.
- [18] E.S. Tarleton, J.P. Robinson, C.R. Millington, A. Nijmeijer, M.L. Taylor, *J. Memb. Sci.* **278** (2006) 318–327.
- [19] E.S. Tarleton, J.P. Robinson, S.J. Smith, J.J.W. Na, *J. Memb. Sci.* **261** (2005) 129-135.

- [20] J.P. Robinson, E.S. Tarleton, C.R. Millington, A. Nijmeijer, *J. Memb. Sci.* **230** (2004) 29–37.
- [21] A. Miyagi, H. Nabetani, M. Nakajima, *Sep. Purif. Technol.* **88** (2012) 216–226.
- [22] J. Li, M. Wang, Y. Huang, B. Luo, *RSC Adv.* **4** (2014) 37375–37380.
- [23] Y.S. Toh, X. Loh, K. Li, A. Bismarck, A. Livingston, *J. Membr. Sci.* **291** (2007) 120.
- [24] <https://duramem.evonik.com/product/duramem-puramem/en/Pages/membrane-properties.aspx>
- [25] W. Lau, A. Ismail, N. Misdan, M. Kassim, *Desal.* **287** (2012) 190.
- [26] S. Konagaya, H. Kuzumoto, O. Watanabe, *J. Appl. Polym. Sci.* **75** (2000) 1357–1364.
- [27] P.R. Buch, D. Jagan Mohan, A.V.R. Reddy, *J. Membr. Sci.* **309** (2008) 36–44.
- [28] J. Geens, B. Van der Bruggen, C. Vandecasteele, *Sep. Purif. Technol.* **48** (2006) 255–263.
- [29] S. Darvishmanesh, A. Buekenhoudt, J. Degève, B. Van der Bruggen, *J. Memb. Sci.* **334** (2009) 43–49.
- [30] I. Kim, J. Jegal, K. Lee, *J. Polym. Sci. Part B Polym. Phys.* **40** (2002) 2151–2163.
- [31] X.J. Yang, A.G. Livingston, L. Freitas Dos Santos, *J. Memb. Sci.* **190** (2001) 45–55.
- [32] Y. Kong, D. Shi, H. Yu, Y. Wang, J. Yang, Y. Zhang, *Desal.* **191** (2006) 254.
- [33] F. Zheng, Z. Zhang, C. Li, Q. Yuan, *J. Memb. Sci.* **332** (2009) 13–23.

Chapter 5: Results and Discussion - OSN Characterization and Modelling

Overview

This chapter describes the transport through membranes using transport models, such as pore-flow and solution-diffusion models. A brief explanation is provided for each model's uses. Thereafter, a discussion of the applicability of each model to the prediction of the fluxes of permeating species follows in Section 5.2 and 5.3. Concluding remarks, in Section 5.4, are provided which discuss the overall predictions and make statements regarding the selection of solution-diffusion or pore-flow models in general.

5.1. Introduction

There has been a lot of focus on the modelling of membrane transport over the past few years. This chapter aims to contribute to the knowledge database that has been built up on the modelling of membrane transport. According to Wang *et al.* [1], a trial and error approach is often taken in modelling membrane transport since there exists a lack of insight resulting from a lack of developed predictive models. The modelling of the transport of the solvent-solute system originates from basic pore-flow and solution-diffusion models, which were later developed into models that are more complex.

The solution-diffusion and pore-flow models are known to be most applicable to OSN transport, due to the models' parameters, which involve chemical and physical properties of the membrane and the specific permeating species [2]. Equations 5.1 and 5.2, respectively, represent the solution-diffusion and pore-flow models described in Section 2.2.

$$J_i = P_i^{SD} \left[w_{i,M} - \frac{J_i}{J_i + J_k} \exp \left(-\frac{v_i \Delta p}{RT} \right) \right] \quad (5.1)$$

Where:

- $J_{i,k}$ – Partial mass flux of species i and k ($\text{kg} \cdot \text{m}^{-2} \cdot \text{s}^{-1}$)
- P_i^{SD} – Permeance term for solution-diffusion for species i ($\text{kg} \cdot \text{m}^{-2} \cdot \text{s}^{-1}$)
- w_i – Mass fraction in feed for species i
- v_i – The molar volume of species i ($\text{m}^3 \cdot \text{mol}^{-1}$)
- ΔP – Pressure across membrane (Pa)
- R – Universal gas constant ($\text{m}^3 \cdot \text{Pa} \cdot \text{mol}^{-1} \cdot \text{K}^{-1}$)
- T – Temperature (K)

For a binary species system, Equation 5.1 is solved simultaneously for species i and j , knowing each species' permeance. The pore-flow model, that was investigated (given in Equation 5.2), demonstrates other parameters that are required than those of the solution-diffusion model.

$$J_v = \left(\frac{\varepsilon_m \cdot d_{pore}^2}{32 \cdot l \cdot \tau} \right)_{mix} \left(\frac{\Delta P}{\eta_{mix}} \right) = P_{mix}^{PF} \left(\frac{\Delta P}{\eta_{mix}} \right) \quad (5.2)$$

Where:

- J_v – The volumetric flux of total permeate ($\text{L} \cdot \text{m}^{-2} \cdot \text{s}^{-1}$)
- ε – The membrane surface porosity
- τ – The membrane tortuosity
- d_{pore} – The membrane pore size
- l – The membrane thickness
- P_{mix} – The permeability of solution ($\text{kg} \cdot \text{m}^{-2} \cdot \text{bar}^{-1}$)

The pore-flow model, represented in Equation 5.2, can be described as a one-parameter model where the permeability term $P^{PF} = \left(\frac{\varepsilon d_{pore}^2}{32l\tau}\right)$ for each solvent was determined by arithmetic averages. The viscosity for the binary mixture of species i and j are determined using the Kendall and Monroe correlation [2], which is fairly well suited for hydrocarbon mixtures and is described in Equation 5.3.

$$\eta_{mix} = \left(x_i \eta_i^{\frac{1}{3}} + x_j \eta_j^{\frac{1}{3}}\right)^3 \quad (5.3)$$

Where

$x_{i,j}$ – The weight fraction of species i and j.

$\eta_{i,j}$ – The theoretical viscosity for species i and j ($\text{Pa}\cdot\text{s}^{-1}$)

Pure species permeance can be determined using experimental pure species permeation data and the solution-diffusion and pore-flow models, provided in Equation 5.1 and 5.2, respectively. In this study, the permeability term for pure solvents has been derived and sample calculations are given in Appendix C. Table 5.1 provides a general summary of the pure species permeability terms for both solution-diffusion and pore-flow models.

Table 5.1: Pure species permeance for solvents used in this study

(P^{SD}) Solution-diffusion Permeability ($\text{kg}\cdot\text{m}^{-2}\cdot\text{s}^{-1}$)			
Species	DuramemTM150	DuramemTM200	PuramemTM280
DCM	3.26×10^{-1}	3.11×10^{-1}	-
MEK	8.86×10^{-2}	7.58×10^{-2}	1.95
MIBK	7.97×10^{-3}	5.92×10^{-3}	1.35×10^{-1}
Toluene	2.31×10^{-3}	4.00×10^{-3}	6.33×10^{-1}
(P^{PF}) Pore-flow Permeability ($\text{kg}\cdot\text{m}^{-2}$)			
Species	DuramemTM150	DuramemTM200	PuramemTM280
DCM	3.49×10^{-12}	3.34×10^{-12}	-
MEK	1.28×10^{-12}	1.09×10^{-12}	2.81×10^{-11}
MIBK	2.22×10^{-13}	1.65×10^{-13}	3.75×10^{-12}
Toluene	5.37×10^{-14}	9.31×10^{-14}	1.47×10^{-11}

5.2. Pore-flow model

The pore-flow model as given in Equation 5.2, requires a number of parameters that can be used to model the solvent mixture through the membrane. The permeance term used in the one-term pore-flow model described the transport based on the permeating species. A later two-parameter pore-flow model, known as the two-term Hagen-Poiseuille pore-flow model as

given in Equation 5.4, describes the transport through a membrane using membrane parameters as well as the permeating species parameters.

$$J = \left(\frac{\Delta P}{\eta_{mix}} \right) \left[v_1 c_{1(m)} \left(\frac{\varepsilon d_{pore}^2}{32 l \tau} \right)_1 + v_2 c_{2(m)} \left(\frac{\varepsilon d_{pore}^2}{32 l \tau} \right)_2 \right] \quad (5.4)$$

Where

$c_{i(m)}$ – is the concentration of species i through the membrane (mol.m^{-3})

v_i – is the partial molar volume of species i ($\text{m}^3.\text{mol}^{-1}$)

The Hagen-Poiseuille pore-flow model, as mentioned by Silva *et al.* [3], was based on the assumption that the concentration values were those of the pure species investigated, assuming no viscous selectivity and a linear pressure profile through the membrane.

The one-term model (PF-1) and two-term (PF-2) pore-flow model are shown in Figure 5.1 to describe the transport of the solvent-solute mixture accurately.

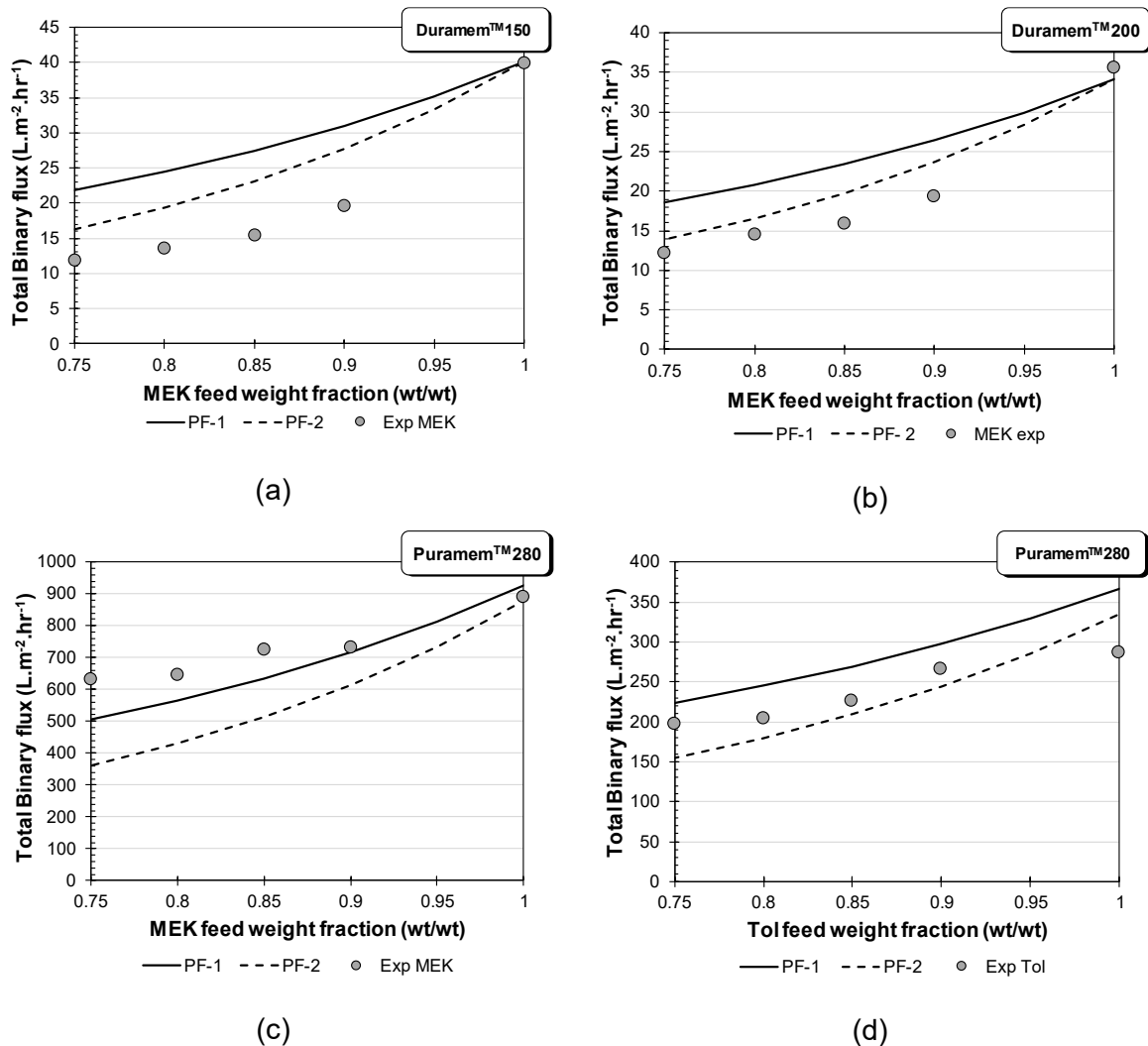


Figure 5.1: One-term and two-term pore-flow models describing MEK-hexadecane mixture at 30 bar through Duramem™ and Puramem™ series at ambient room temperature.

The models are compared at the upper range of the solvent weight fraction, where the experimental data is based on realistic solvent-to-solute ratios. Therefore, the scope of the models are assumed to be applicable in the solvent fraction ranges of 75 – 100 wt %, which is similar to the solvent fractions in industry.

Both pore-flow models illustrated in Figure 5.1 demonstrated good fits for the modelling of binary flux in a solvent oil system. The models demonstrate very good correlation to the experimental results by visual inspection. Figure 5.1 (a, b and d) also shows that the Hagen-Poiseuille two-term pore-flow model provides a more accurate fit to the experimental data for polar solvents permeating through polar stable membranes, as well as non-polar solvents permeating through non-polar stable membranes. In the case of polar solvents permeating through a non-polar stable membrane (i.e. Puramem™280), the Hagen-Poiseuille one-term pore-flow model provides a more accurate fit to the experimental data.

The Hagen-Poiseuille two-term pore-flow model (PF-2) takes into account the solvent-membrane and solute-membrane interactions by including the concentration of solute-solvent mixtures and their molecular shapes. The Hagen-Poiseuille one-term pore-flow model (PF-1), which provides a less accurate fit to experimental data, supports the argument that transport through a membrane is influenced by more than just a specific solvent property, such as viscosity. It is also influenced by the concentration of permeating species, which is related to the membrane swelling.

The parameters in the PF-1 and PF-2 models that influence the models the most, are the pure species permeability (P^{PF}) parameters. Varying the permeability shifts the model up and down along the vertical axis. However, since the permeability of a pure species is fixed based on the specific membrane system, it is important to note that the model mostly relies on the system itself.

5.3. Solution-diffusion model

The solution-diffusion model, as discussed in Section 2.2, was applied in this study to model the binary species fluxes through Duramem™ series and Puramem™ series membranes. The solution-diffusion model, as given in Equation 5.1, uses two parameters, namely the permeances of both the solute and the solvent species in question. Permeance values are shown in Table 5.1 and the solvent and solute properties are discussed in Chapter 4.

The solution-diffusion permeance is based on diffusive and sorption properties and is shown in Equation 5.5.

$$p^{SD} = \frac{D_i K_i}{l} \quad (5.5)$$

The permeance term is thus determined from the experimental permeance values and is incorporated into a modified model. This modified model combines the Hagen-Poiseuille two-term pore-flow model (PF-2), shown in Equation 5.4, and the proposed solution-diffusion model from Bhanushali *et al.* [4], provided in Equation 5.6, to form a new modified solution-diffusion model (SD-2) given in Equation 5.7.

$$J \propto A \propto \left(\frac{v_i}{\eta}\right) \left(\frac{1}{\phi^n \gamma_{sv}}\right) \quad (5.6)$$

$$J_v = \frac{\Delta P}{\eta_{mix} \phi^n} \left(v_i c_{i,m} \left(\frac{\varepsilon d_{pore}^2}{32 \tau l} \right)_i + v_j c_{j,m} \left(\frac{\varepsilon d_{pore}^2}{32 \tau l} \right)_j \right) \quad (5.7)$$

Where:

ΔP – Pressure across membrane (Pa)

η_{mix} – Viscosity of species (or mixture) (Pa.s)

ϕ^n – Sorption value of solvent, where n is empirical constant

v_i – Molar volume of species ($\text{m}^3 \cdot \text{mol}^{-1}$)

$c_{i,m}$ – Concentration of species i through the membrane ($\text{mol} \cdot \text{m}^{-3}$)

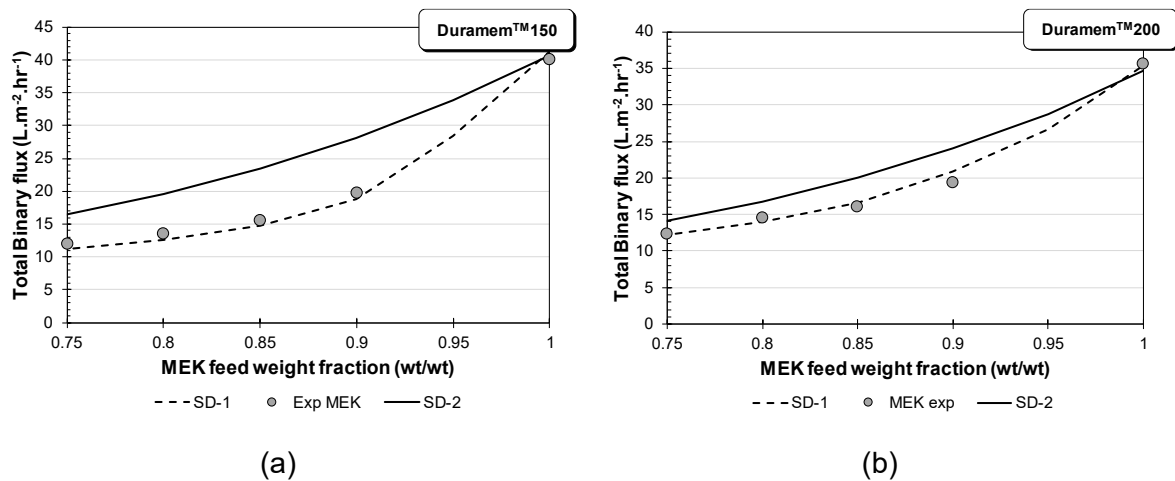
γ_{sv} – Surface tension

d_{pore}^2 – Diameter of pore in membrane

ε – Porosity of membrane

τ – Torosity factor of membrane

The proposed Bhanushali model introduces four existing parameters, which are also used in similar pore-flow models, namely viscosity, sorption value, molar volume and surface tension [5]. This proposed model by the Bhanushali *et al.* group is classified as a solution-diffusion model. Figure 5.2 illustrates the Matlab determination of the binary total flux for solvent-solute species using the solution-diffusion model (SD-1), provided in Equation 5.1, and the initial modified solution-diffusion model (SD-2), provided in Equation 5.6.



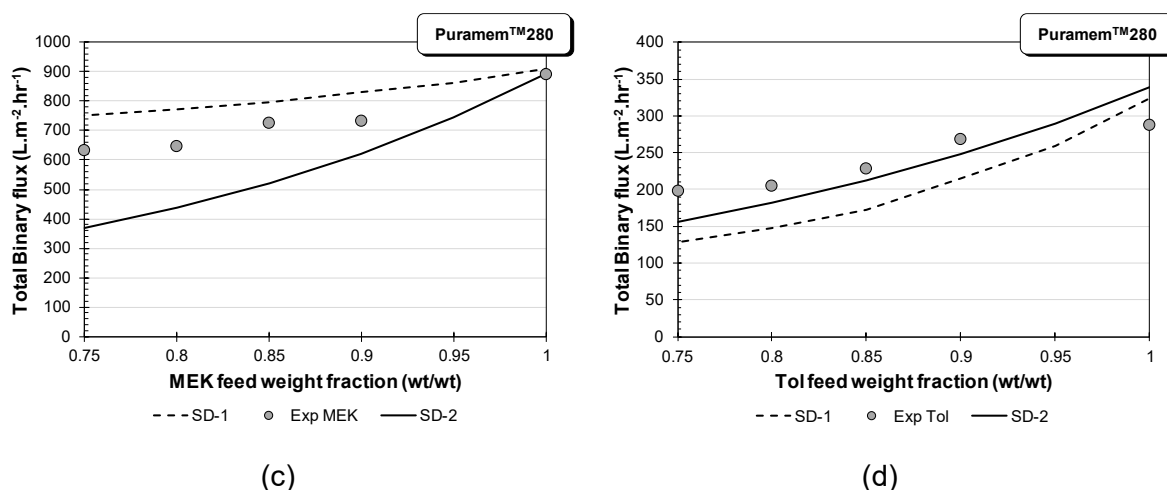


Figure 5.2: SD-1 and SD-2 models describing MEK-hexadecane and toluene-hexadecane mixtures at 30 bar through DuramemTM and PuramemTM series at ambient room temperature.

It is clear from Figure 5.2 that the solution-diffusion models provided a better fit to the experimental data, referring specifically to the solution-diffusion modified model (SD-1) which had already been regressed to obtain the optimal permeability parameter for hexadecane. The SD models fit well with the DuramemTM membranes using a polar solvent, while they provided less accurate results for the PuramemTM series membranes. SD-2 and PF-2 models for toluene as solvent, yielded the best fit for non-polar species through PuramemTM280, as shown in Figure 5.1 (d) and Figure 5.2 (d).

The solution-diffusion models model the data better than the pore-flow models with prior knowledge to the permeance parameters and molecular size (i.e. geometry, volumetric shape). The diffusion parameters model the interaction between permeating species through polar stable membranes, such as DuramemTM series membranes. Pore-flow models, which are preferably used to model non-polar solvent stable membranes such as the PuramemTM series membranes, illustrate that the interaction between membrane and permeating species are not that relevant. Therefore, the assumption can be made that pore-flow models describe only solvent- solute interactions and properties for a system using a non-polar solvent stable membrane.

5.4. Regression of P^{SD}_{c16}

In order to find the best fit for the solution diffusion model, a regression function in Matlab was used to determine the optimal permeability parameter for the hexadecane solute. The regression function makes use of a Matlab function called Fminsearch, which functions as an unconstrained non-linear optimization. The function finds the minimum of a scalar function containing several variables.

The regression focuses on finding the smallest difference between the modelled total flux and the experimental total flux through solving two partial solution diffusion equations (i.e. Equation 5.1) simultaneously.

Initially the permeability parameter was estimated for the SD-1 model, which provided a specific curve. Once regressed, the new permeability parameter was used to fit the curve. As illustrated in Figure 5.3, the estimated and regressed SD-model was fitted to the experimental data for a MEK-hexadecane and DCM-hexadecane binary mixture through Duramem™150.

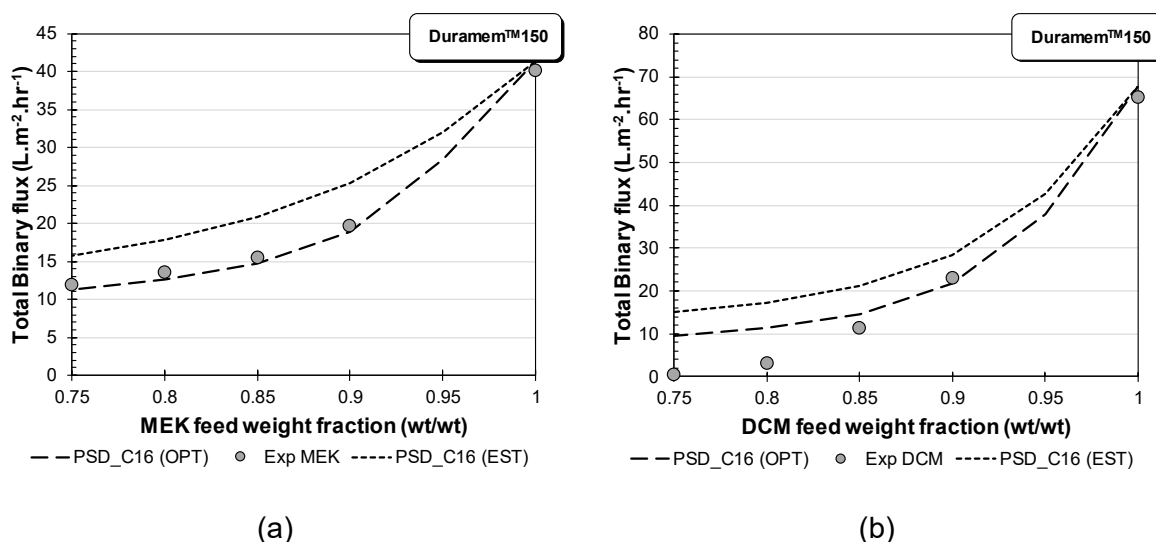


Figure 5.3: Comparison between optimized and estimated hexadecane permeability through Duramem™150 at 30 bar in a binary mixture using the solution-diffusion model with (a) MEK and (b) DCM.

As illustrated in Figure 5.3, regression on the permeability variable provides improved modelling results for the binary mixtures of MEK-hexadecane and DCM-hexadecane in the weight fraction range of 0.75 – 1.00 wt/wt. These improved results using the solution diffusion model and regressed parameters make the model more robust and preferable compared to the other models.

With regard to Figure 5.3 (a), the Pearson correlation improves from 0.9963 to 0.9995, while at the same time changing the permeability parameter of hexadecane from 0.0006 to 0.00036272 kg.m⁻².s⁻¹. Results of the application of this regression using another solvent through Duramem™150, to find the optimized permeability of hexadecane, are shown in Figure 5.3(b). The permeability was found to be similar to the regressed $P_{\text{hexadecane}}^{\text{SD}}$ using MEK as solvent.

5.5. Concluding remarks

The transport through the commercial membranes used in this study was successfully predicted using pore-flow and solution-diffusion models adapted from literature. The focus was on the most commercially used solvents (i.e. MEK and toluene) as well as the evaluation of all the membranes that were used in this study by modelling the transport through them.

The transport through Duramem™ series membranes can be modelled with both the two-parameter pore-flow and classic solution-diffusion models to predictions as high as 0.985 Pearson coefficients for polar stable membranes. For Puramem™280, the pore-flow models (PF-1) have been shown to provide the most adequate results. Overall, it is concluded that the transport through the membranes can be modelled using both the solution-diffusion and pore-flow models based on the parameters of each model. The properties of the solvent and solute as well as membrane permeability are major factors that influence transport through the membrane and the predictive modelling of this process.

In general, the classic solution-diffusion models (SD-1 and SD-2) would be considered better predictive models, as illustrated in Figure 5.2. However, the pore-flow models are better choices for the modelling of a membrane system where the solvent is highly polar and the membrane is stable for non-polar systems. After regressing the P_{C16}^{SD} parameter, which illustrated the effect of solute permeability on the model, a best fit was demonstrated by using the SD-1 model, as shown in Figure 5.3.

It was shown that the diffusive and viscous properties of solvent and solute species play a very important role in predicting the transport through polar stable membranes, such as the Duramem™ series membranes.

5.6. References

- [1] J. Wang, D.S. Dlamini, A.K. Mishra, M.T.M. Pendergast, M.C.Y. Wong, B.B. Mamba, V. Freger, *et al.*, *J. Memb. Sci.* **454** (2014) 516–537.
- [2]. B. Zhmud, Viscosity blending equations. *Lube Magazine* **6** (2014) 24.
- [3] P. Silva, S. Han, A.G. Livingston, *J. Membr. Sci.* **262** (2005) 49
- [4] D. Bhanushali, S. Kloos, C. Kurth, D. Bhattacharyya, *J. Memb. Sci.* **189** (2001) 1–21.
- [5] P. Van der Gryp. Separation of Grubbs-based catalysts with nanofiltration, Doctoral dissertation, North-West University. (2008)

Chapter 6: Cost and Energy Evaluation

Overview

This chapter investigates the feasibility of OSN compared to distillation by performing a preliminary techno-economic evaluation. A simulation of OSN and distillation was performed in Aspen Plus V8.8. A brief background on the two separation systems are given, after which a design basis is provided for the cost evaluation in Section 6.2. Both systems are compared with regard to energy usage, capital cost and operating cost. In Section 6.4, results are shown and discussed which provide a better understanding of why there is still a debate as to which system is better.

6.1. Introduction

OSN systems have already been shown to be beneficial in terms of using less energy and providing an adequate return on working capital costs (e.g. Max Dewax process) [1]. Additionally, a few authors have published data that demonstrates that OSN membrane separation is a lower energy alternative to conventional separation processes [2 – 4]. Other researchers have performed energy and cost evaluation on the recovery of solvent [5,6], while comprehensive studies on the sustainability of OSN systems have been done by the Vankelecom and Livingston Groups [7,8].

For this study, the OSN system was simulated using Aspen Plus™. Figure 6.1 represents the OSN unit used in the feasibility analysis.

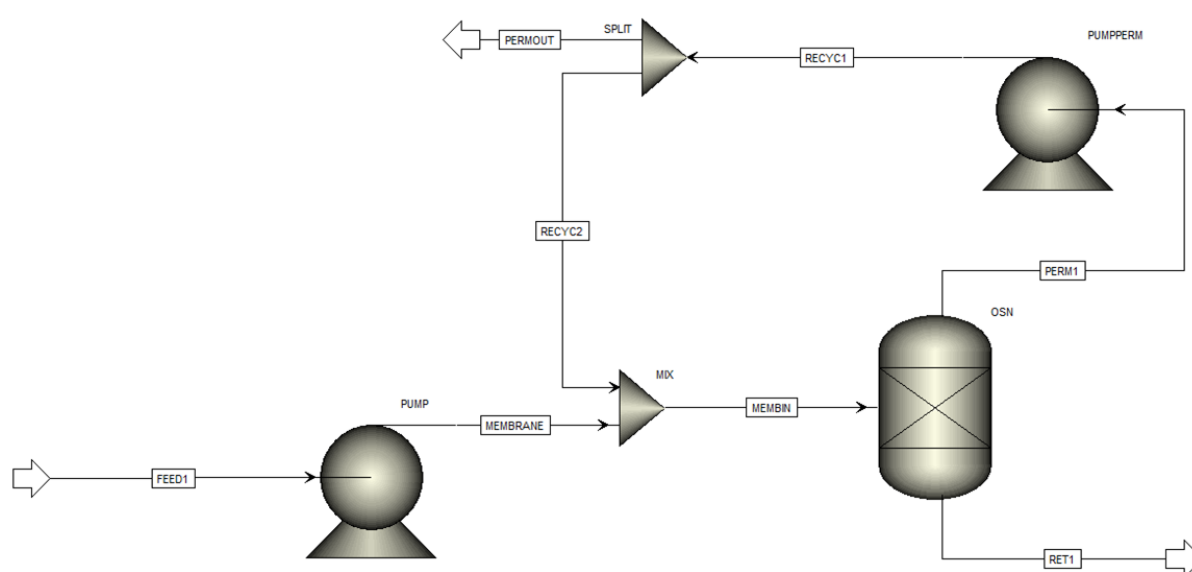


Figure 6.1. Aspen flowsheet of OSN membrane system

The OSN unit consists of two pumps; one for pumping the feed to the membrane; another for pumping the permeate. The membrane system was assumed to be continuous with a recycle stream pumping back a split fraction (split ratio of 1:1) of the permeate into the feed stream.

The distillation column was simulated using Aspen Plus™ software. The use of the RadFrac distillation column has already been demonstrated to recover solvents as documented in literature [9,17]. Therefore, in this study, the RadFrac distillation unit was used to determine the energy requirements to separate the MEK from n-hexadecane for this system. Thermodynamic properties were predicted using the Soave-Redlich-Kwong equation of state, since the system involved polar components, with operating pressures of around 30 Bar [18]. The column is specified to have 15 trays, where the feed enters the column at stage 8. The column consists of a kettle reboiler and a total condenser, as illustrated in Figure 6.2.

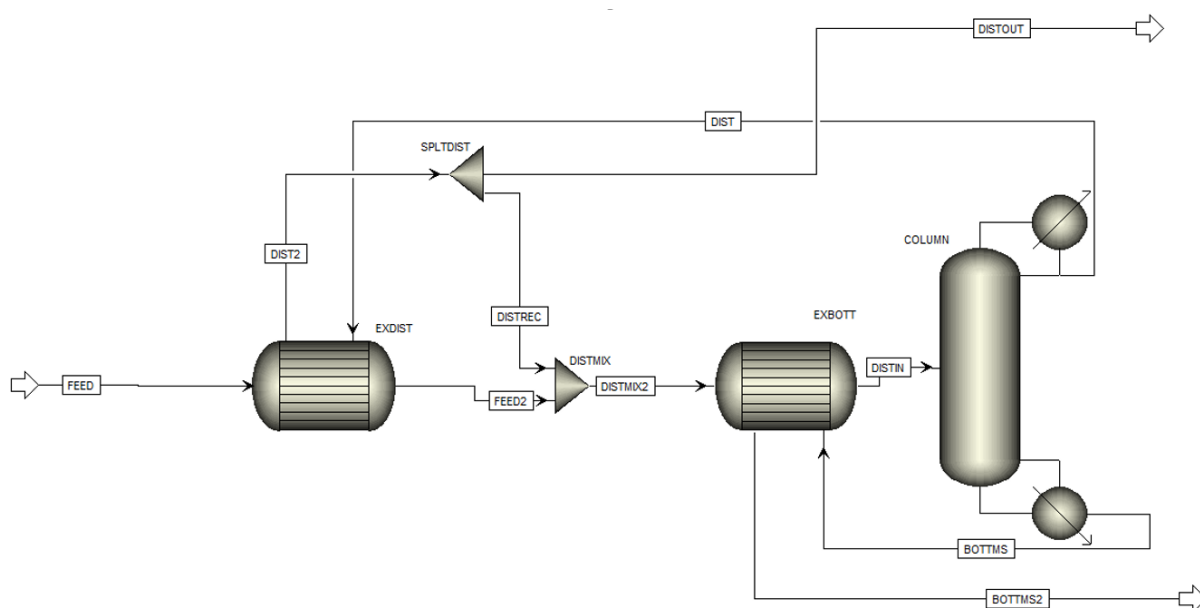


Figure 6.2: RadFrac distillation column simulation process flowsheet.

For consistency reasons, the distillation column illustrated in Figure 6.2 also contains a recycle stream at a split ratio that allows the product stream to have the same characteristics as those of the OSN permeate. The mass and energy balances could be determined for both OSN and distillation units in Aspen Plus™. Energy was recovered by heat integration of the bottoms and distillate streams with the feed stream as shown in Figure 6.2.

6.2. Design base case

The design basis focuses mainly on the energy consumption and cost of OSN and distillation systems for the recovery of solvents (i.e. MEK) from n-hexadecane. The selected membrane for OSN operation is Duramem™ 150 based on membrane performance observed during the experimental investigations in this study. It also focuses on small-scale operation over a two-year period. Furthermore, investigations on the lifespan and upscaling of membranes were proposed by Schmidt *et al.* [10], providing the base case assumption that a membrane unit area costs \$295.14 m⁻².yr⁻¹. Assuming this is a continuous process operation, the process operating time, which is based on the Douglas method [11], was taken to be 8150 hr.yr⁻¹. The operating time includes scheduled and unplanned shutdowns. The design base that was used consists of a few assumptions and is summarized in Table 6.1.

Table 6.1: Summary of design parameters used in cost and energy evaluation

Design Parameters		Source
Currency used in cost evaluation	American Dollar (\$)	
Operating time (t_{op})	8150 hr.yr ⁻¹ .	[11]

Design Parameters		Source
Feed-stream		
Total mass Flowrate (\dot{m}_{feed})	1000 kg/hr	[8]
Solute species	n-hexadecane	
Solvent Species	Methyl-ethyl-ketone	
Solute weight Fraction (C_{solute})	25.0 wt/wt %	
Pressure (ΔP)	30 Bar	
Temperature	20 °C	
Costs		
Membrane (C_{mem})	\$295.14 m ⁻² .yr ⁻¹	[10]
Solvent ($C_{solvent}$)	\$38.99 kg ⁻¹	[20]
Solute (C_{solute})	\$319.05 .kg ⁻¹	[21]
Experimental Binary Flux	10.1 kg.m ⁻² .hr ⁻¹	
Target Rejection	95.0%	[1]

The above parameters were taken from experimental as well as literature data in order to provide a simplistic analysis of the operational cost and energy requirements for the recovery of solvent. The approach used to compare OSN operation to distillation was based on a target separation where a 95 wt% rejection of solute was required. The constraint that was used to evaluate both technologies was:

“Feed and product streams for both OSN and distillation separation were to be kept the same”

This constraint allowed the evaluation of both technologies by mainly focussing on their performance to produce a specific product specification for a given input feed stream.

6.3. Design approach

The design approach, which has been discussed in Chapter 2.3, were based on the works of Szeleky *et al.* [8] as well as Schmidt *et al.* [10]. Both these groups have performed a feasibility study on general OSN and distillation operations for recovery of desired species.

6.3.1. Solvent recovery by distillation

6.3.1.1. Capital cost

The capital cost for installing a distillation column can be determined by following Hand's method. This method gives a quick estimate of the capital cost of the column in those cases

where the installation includes a condenser, kettle reboiler and the column. The costing data was obtained from Coulson and Richardson *et al.* [14] and is shown in Table 6.2.

Table 6.2: Capital cost of distillation column.

Equipment	2007	2015 ^(a)
Condenser	\$30,200	\$34,400
Kettle reboiler	\$48,370	\$55,000
Column shell	\$2,600,000	\$3,200,000
Column trays ^(b)	\$55,700	\$68,800
Total column cost	\$2,734,270	\$3,358,200

(a) Prices are based on Nelson-Farrar cost indices in year 2007 NF-index = 2054.1 (2015 NF-index = 2544)

(b) Cost of 15 trays

Table 6.2 illustrates that based on the data provided by Coulson *et al.* [14], the capital costs required for the distillation column, which was used to recover the solvent, is approximately \$3.358 million. The major contributor to the cost is the column shell. It should be noted that the costing of the column shell is equivalent to the costing of a vertical vessel of stainless steel material. Since this study used highly polar solvents, such as MEK, stainless steel is an adequate material for construction. Additionally, the capital cost for the heat exchangers (EXBOTT and EXDIST) that were used for heat integration in the distillation unit (Figure 6.2) are illustrated in Table 6.3.

Table 6.3: Capital cost of heat exchangers.

Year	Equipment	Index ^(a)	Area (m ²)	Capital cost (\$)
2001		722.0	100	\$ 25,000
2015	EXBOTT	1305	1.31	\$ 3,353
2015	EXDIST	1305	1.32	\$ 3,371
Total heat exchanger cost:				\$ 6,724

(a) Based on the Nelson-Farrar Cost index

The capital costs obtained for the heat exchangers as shown in Table 6.3 are approximately < 1% of the total capital cost of \$ 3.364 million for the distillation unit. Heat transfer areas and the log mean temperature difference (LMTD) were obtained through Aspen Plus™ and are recorded in Appendix E.3.

6.3.1.2. Operating costs

The energy required for a distillation throughput operation was determined using Equations 2.17(a-c). The values for these equations can be obtained through Aspen Plus as well as the values for heat transfer through each heat exchanger. All three variables were obtained in Aspen Plus™.

Assuming no heat loss to the atmosphere, the energy required to recover a ton of solvent in the distillate is $135 \text{ kWh.ton}_{\text{solvent_product}}^{-1}$, while rejecting 95 % of hexadecane from the feed to the bottoms. Table 6.4 summarizes the input and output variables that were used in the simulation.

Table 6.4: Summary of RadFrac Distillation input and output variables

Column operating variables	
Stages	15
Feed inlet Stage	8
Condenser	
Condenser type:	Total Condenser
Temperature	239.00 °C
Reflux ratio	0.050
Heat duty	-67.78 kW
Reboiler	
Reboiler type	Kettle Reboiler
Temperature	301.8 °C
Boil-up ratio	4.09
Heat duty	153.91 kW
Total energy required:	$135 \text{ kWh.ton}_{\text{solvent_product}}^{-1}$

Table 6.4 shows that the total energy input required to recover a ton of MEK solvent for an initial combined feed and recycle flowrate of 1600 kg.hr^{-1} was determined to be $135 \text{ kWh.ton}_{\text{solvent_product}}^{-1}$, which is a result of the condenser and reboiler operating at high temperatures ranging over 200 °C . This high energy requirement is due to the phase separation approach that distillation columns implement while separating species from each other. Heat integration was used in order to lower the condenser and reboiler loads through preheating of the feed stream.

Literature from both Abejón *et al.* [15] and Turton *et al.* [12] were used in accordance with Equations 2.18(a-e) to determine the operating costs for the distillation unit. In this study, the assumption that the costs of raw materials are ignored. The operating costs for the distillation unit are summarized in Table 6.5.

Table 6.5: Operating costs determined for distillation

Parameters (Abejón <i>et al.</i>)		Contribution of total costs
$C_{\text{energy}} (\$, \text{day}^{-1})$	165.39	36 %
$C_{\text{maint}} (\$, \text{day}^{-1})$	99.09	21 %
$C_{\text{lab}} (\$, \text{day}^{-1})$	192.00	42 %
$C_{\text{Total}} (\$ \text{ Mil. yr}^{-1})$	0.155	100 %

From Table 6.5 labour costs and energy costs are major contributors to the operating costs for distillation operation. The result of obtaining high energy costs for the distillation unit determined in this study, is within reason as supported by literature [1,8].

6.3.2. Solvent recovery by OSN

6.3.2.1. Capital cost

An economic capital costing for an OSN membrane module follows a simplistic approach. Turton *et al.* [13] illustrates a short-cut method based on process indices that can be used to determine capital costs and this is given in Equation 6.1.

$$C_2 = C_1 \left(\frac{I_2}{I_1} \right) \left(\frac{A_2}{A_1} \right)^n \quad (6.1)$$

Where:

C – Purchased cost (\$)

I – Cost index

A – Capacity of equipment

n – Cost exponent

Subscripts: “1” refers to base time when cost is known, “2” refers to time when cost is desired.

For this study, the Nelson-Farrar cost indexes were used due to the availability of index for the year 1998.

The capital cost in this study was determined with reference to the Max DeWax process that started up in the year 1998, where the capital cost for the Beaumont Refinery membrane unit was \$5.5 million [1]. The capital cost for the membrane unit used in this study is shown in Table 6.6.

Table 6.6 Capital cost for a membrane unit

Year	Index ^(a)	Area (m ²)	Capital cost (\$)
1998	1477.6	3285	\$ 5 500 000
2015	2544.0	60	\$ 857 691

(a) Based on the Nelson-Farrar Cost index

The membrane area shown in Table 6.6 is based on the assumption that the flux for both the Max DeWax and the membrane unit investigated in this study are $10.1 \text{ kg.m}^{-2}.\text{hr}^{-1}$ and that the capital cost of the Max DeWax process is based only on the total membrane area (i.e. 3285 m^2). Using the permeate flowrate from the Max DeWax process mentioned by Gould *et al.* [1] of $40 \text{ m}^3.\text{hr}^{-1}$ after membrane compaction had occurred, the area for the Max DeWax process can be determined. Additionally, Gould *et al.* [1] also mentions that the oil content in the permeate was at most 0.8 wt%, indicating that the permeate consisted of 99.2 wt% solvent. According to White *et al.* [19], the variation in the range of solvent ratios (MEK/toluene) that were tested by them (i.e. MEK/toluene ratios between 0.96 – 1.82) did not appear to have a major influence in their investigations. Assuming that the solvent used in the Max DeWax membrane operation were MEK and toluene [1] and that the ratio of MEK/toluene = 1.5 (60/40), the total membrane area can be determined using Equation 4.1 found in chapter 4. A sample calculation was performed for both the Max DeWax membrane area as well as the membrane area used in the economic evaluation.

In order to obtain a flux of $10.1 \text{ kg.m}^{-2}.\text{hr}^{-1}$, the membrane modules need to have a total area of 60 m^2 . According to Evoniks [13] the membrane modules come in standard sizes ranging from 0.1 m^2 – 24 m^2 . Thus, thirty 2 m^2 size modules were used in the membrane unit for this economic evaluation, which is due to it being the largest spiral wound Duramem™150 membrane which can be used to provide a total area of 60 m^2 .

6.3.2.2. Operating costs

The energy required for OSN can be based on the operation of the feed pump to the membrane unit, which requires energy to provide a pressure difference for a feed flow to the membrane. The energy requirement of the pump, described by Equation 6.2, was taken from literature [8].

$$Q_{OSN} = \frac{F_f \Delta P_{TM}}{\varepsilon_{pump}} \quad (6.2)$$

Where:

F_f - Feed flow through membrane

ΔP_{TM} - Pressure difference over trans-membrane

ε_{Pump} - Pump efficiency

The energy requirements determined from Equation 6.2 in Aspen Plus™ were found to be 1.636 kW and 1.5811 kW, respectively. For consistency purposes, the net work required by the pump (assuming efficiency of 0.66), as determined from Aspen Plus™, was used and is summarized in Table 6.7.

Table 6.7: Summary of energy requirements determined for OSN operation

OSN unit operating variables

Transmembrane Pressure (ΔP)	29 Bar
Temperature	21 °C
Net work required	1.58 kW

Energy per ton solvent: 2.5 kWh.ton_{solvent_product}⁻¹

The energy required to recover a ton of MEK solvent in the permeate (PERMOUT stream) for OSN operation with a combined feed and recycle flowrate of 1600 kg.hr⁻¹ was approximately 2.48 kWh.ton_{solvent_product}⁻¹. The determination of total operating costs (TOC) was done using Equation 2.18(a-e), making use of the parameters obtained from Abejón *et al.* [15] as well as values obtained from membrane manufacturers. These total operating costs with the assumption of negligible costs of raw material, are summarized in Table 6.8.

Table 6.8: Operating costs determined for membrane system

Parameters (Abejón <i>et al.</i>)		Contribution of total costs
C _{energy} (\$/day ⁻¹)	3.03	1 %
C _{maint} (\$/day ⁻¹)	50.35	22 %
C _{lab} (\$/day ⁻¹)	168.00	75 %
C_{Total} (\$ Mil.yr⁻¹)	0.075	100 %

The energy expense shown in Table 6.8 is the lowest fraction of the operating expenses while labour costs provide the highest fraction of the operating expenses. Comparison of OSN and distillation operating costs reveal that OSN operation uses significantly less energy to recover MEK solvent (2.5 kWh.ton_{solvent_product}⁻¹) compared to distillation (135 kWh.ton_{solvent_product}⁻¹). This massive difference is due to the temperature increase and phase change associated with distillation during the separation process. However, maintenance and labour forms a reasonably large fraction of the operating costs for both systems.

6.4. Results and feasibility analysis

By investigating energy requirements, capital costs as well as cost of production for both distillation and OSN membrane operation, the two separation systems could be compared in terms of their economic viability. In order to compare the two separation units it is important to keep in mind that both systems have an objective function to recover solvent at a specific rejection of solute. The boundaries of these unit operations have been discussed in sections 6.1 and 6.2. The results for the cost and energy evaluation are summarized in Table 6.9.

Table 6.9: Summary of cost and energy evaluation using Aspen Plus™ for solvent recovery

Comparative variables	OSN	Distillation
Feed Flowrate (kg.hr ⁻¹)	1000	1000
Solute Rejection Obtained (%)	97	>96
Energy required (kWh. ton _{solvent_product} ⁻¹)	2.48	135
Flowrate (permeate/distillate) (kg.hr ⁻¹)	594	592
Capital Costs (\$ Million)	0.85	3.36
Operating Costs (\$ Million.yr ⁻¹)	0.075	0.155
Energy	1.370 %	36.23 %
Maintenance	22.74 %	21.71 %
Labour	75.89 %	42.06 %

From Table 6.9 it is clear that recovery by OSN and distillation both provided high rejections. Capital costs for the OSN membrane unit was shown to be 1/4th of the cost of a distillation column. Additionally, distillation operation demands a higher energy input than OSN membrane operation. Also what is to be noted, is that the rejection of n-hexadecane through OSN is higher than that for distillation operation. The OSN operation in this study thus provided higher rejections at lower costs and fewer capital requirements.

The data provided in Table 6.9 accentuates the massive difference in energy cost between OSN and distillation. The Total Operating Costs (TOC) for OSN and distillation operation were determined to be \$0.075 Million.yr⁻¹ and \$0.155 Million.yr⁻¹, respectively. Based on the operating costs in Table 6.9, it is clear that more than twice the cost of OSN operation is required for distillation operation. It is clear that it would be more practical to use OSN separation because this would save high volumes of energy, which can be used elsewhere in the plant.

6.5. Concluding remarks

A detailed economic evaluation of a process requires more in-depth understanding of such a process. Therefore, a preliminary techno-economic evaluation with its accompanying assumptions was performed. Aspen PlusV8.8 was used to generate the simulated data, which was necessary for this economic evaluation.

Comparison of the cost and energy consumption of the OSN membrane system with that of the distillation system for the recovery of solvent from oil, illustrated which process is more economically viable. The OSN system requires 50 times less energy relative to distillation. This finding is in alignment with those of Geens *et al.* [6] and Szekely *et al.* [8], who provided relative energy outputs between OSN and distillation similar to this study.

Additionally, operating costs for OSN were minimized based on low energy consumption, while providing MEK purity of 97 wt% in the permeate. OSN capital costs were shown to be \$850 000.00 which is approximately 1/4th of the capital cost for distillation. The distillation unit has high energy inputs, while providing high solvent purities above 96 wt% (i.e. >96%) at reflux ratios below 0.3.

Without recycling of solvent the expenses of raw material are enormous, which is why it is important to recover the solvent and return it to the feed stream at as little cost as possible. Furthermore, OSN separation provides the solvent recovered at similar temperatures as the solvent feed. In contrast, the solvent recovered from distillation has to be cooled down from temperatures above 200°C to the feed temperature of 20°C through heat integration in order to recover energy as well as cool down the solvent recovery streams. After heat integration is introduced to preheat the feed into the distillation column, high energy costs were still determined relative to OSN.

6.6. References

- [1] R.M. Gould, L.S. White, C.R. Wildemuth, *Enviro. Prog.* **20** (2001) 12-16.
- [2] D. Bhanushali, D. Bhattacharyya, *Ann. N. Y. Acad. Sci.* **984** (2003) 159.
- [3] M. Buonomenna, J. Bae, *Sep. Purif. Rev.* **44** (2015) 157.
- [4] A.P.B. Ribeiro, J.M. de Moura, L.A. Gonçalves, J.C.C. Petrus, L.A. Viotto, *J. Membr. Sci.* **282** (2006) 328.
- [5] S. Darvishmanesh, J. Vanneste, E. Tocci, J.C. Jansen, F. Tasselli, J. Degrevé, *et al.*, *J. Phys. Chem. B* **115** (2011) 14507.
- [6] J. Geens, B. De Witte, B. Van der Bruggen, *Sep. Sci. Technol.* **42** (2007) 2435.
- [7] P. Vandezande, L.E. Gevers, I.F. Vankelecom, *Chem. Soc. Rev.* **37** (2008) 365.
- [8] G. Szekely, M.F. Jimenez-Solomon, P. Marchetti, J.F. Kim, A.G. Livingston, *Green Chem.* **16** (2014) 4440.
- [9] S. Darvishmanesh, L. Firoozpour, J. Vanneste, P. Luis, J. Degrevé, B. Van der Bruggen, *Green Chem.* **13** (2011) 3476–3483.
- [10] P. Schmidt, E.L. Bednarz, P. Lutze, A. Górak, *Chem. Eng. Sci.* **115** (2014) 115.
- [11] J.M. Douglas, **Conceptual Design of Chemical Processes**, McGraw-Hill, Singapore, 1988.
- [12] R. Turton, R.C. Bailie, W.B. Whiting, J.A. Schaeiwitz, **Analysis, Synthesis, and Design of Chemical Processes**, 3rd Ed., Prentice Hall, Boston, 2009.
- [13] <https://duramem.evonik.com/product/duramem-puramem/en/Pages/membrane-properties.aspx>
- [14] D. Peacock, J.F. Richardson, *Chemical Engineering, Volume 3: Chemical and Biochemical Reactors and Process Control*, Elsevier, 2012.
- [15] R. Abejón, A. Garea, A. Irabien. *Chem. Eng. Res. Design* **90** (2012) 442.
- [16] W.L. Peddie, J.N. Van Rensburg, H.C. Vosloo, P. Van der Gryp, *Chem. Eng. Res. Design* **121** (2017) 219.
- [17] M.H.M. Chowdhury, *Simulation, Design and Optimization of Membrane Gas Separation, Chemical Absorption and Hybrid Processes for CO₂ Capture* (Ph.D. thesis), University of Waterloo, 2011.

- [18] J. Fang, H. Jin, T. Ruddy, K. Pennybaker, D. Fahey, B. Subramaniam, *Ind. Eng. Chem. Res.* **46** (2007) 8687-8692.
- [19] L.S. White, A.R. Nitsch, *J. Memb. Sci.* **179** (2000) 267-274.
- [20] Methyl – Ethyl – Ketone online purchase: <https://www.sigmaaldrich.com/>
- [21] n – hexadecane online purchase: <https://www.sigmaaldrich.com/>

Chapter 7: Conclusions and Recommendations

Overview

This chapter discusses the overall results obtained through experimentation, modelling and economic evaluation which relates to the recovery of solvent from dewaxed oil feed solutions. Section 7.1 forms the introduction to this chapter, followed by a discussion of the contributions that have been made by this study (Section 7.2.). Conclusions and recommendations for future research work on OSN separation and solvent recovery are discussed in Section 7.3 and Section 7.4, respectively.

This study involved the demonstration of solvent recovery from novel OSN membranes through experimentation. The transport through membranes was further investigated using the experimental data that was obtained in this study, to develop models for the transport through OSN membranes. Additionally, a preliminary feasibility evaluation of OSN compared to conventional processes has been done through energy and cost analysis. In this chapter the overall viability for the use of OSN membranes in separation is discussed and conclusions are made pertaining to this.

The organic solvents that were investigated in this study for recovery through Duramem™ and Puramem™ series membranes were toluene, MEK, MIBK and DCM. The solute component that represented the dewaxed lube oil mixture was n-hexadecane.

7.1. Solvent recovery

Experimental investigations for pure solvent recovery and solvent recovery from binary mixtures found that MEK was the solvent that was recovered the best of all solvents tested. Recovery of MEK was especially high through Duramem™150 and Duramem™200 series membranes. DCM has been shown to be the most incompatible solvent, which should not be used in lube-oil dewaxing and separating processes. Based on experimentation it was found that:

- Pure species permeation of all solvents through membranes are linearly proportional to the pressure applied.
- Solvent properties such as viscosity, polarity (i.e. dielectric constant, dipole moments), solubility and surface tension as well as physical properties such as molar volume, molecular shape, molecular size and molecular weight influence membrane performance. Membrane performance influences the recovery of solvent. Non-homogeneous feed mixtures, demonstrating interactions between each species and the membrane, are required to identify the major contributing solvent parameter influencing membrane performance.
- DCM solvent permeation through Puramem™280 was shown to be detrimental to the membrane. Chlorinated solvents perforate the membrane, which is undesirable. Perforation causes the membrane to provide little to no separation and in the process the membrane is damaged.

The binary mixtures that were evaluated in this study were MEK/n-hexadecane, toluene/n-hexadecane, MIBK/n-hexadecane and DCM/n-hexadecane. The solute concentrations were varied between 10,15, 20 and 25 wt% at 30 bar applied pressure. In this study, it was found that:

- Binary feed mixture permeation through the Duramem™ and Puramem™ series membranes results in non-linear proportional behaviour with increasing feed solute concentration. Steric hindrance and interactions of solute and solvent species with each another as well as with the membrane are associated with the non-linear behaviour.
- Concentration polarization was also shown to affect the permeation through membranes by resulting in a continuous slow decrease in permeation through membranes, especially Duramem™150 where the MWCO is 150 Da. Puramem™ 280 provided poor rejection of solute and demonstrated that toluene is an adequate solvent for Puramem™280, but is not recommended for the Duramem™ series membranes.
- Good recovery of MEK through Duramem™150 and Duramem™200 was found, with permeations ranging around 11 L.m⁻².hr⁻¹.Bar⁻¹ and rejections reaching 95%. DCM showed the second best recovery after MEK, with rejections ranging around 78% and membrane permeation similar to MEK. Toluene was shown to provide extremely low permeation rates through the Duramem™ series membranes and standard permeation rates through the Puramem™280 membrane.

7.2. OSN transport modelling

MEK and toluene were selected from the experimental results as solvents to be used to compare models and experimental data. Two pore-flow models (i.e. the one-term (PF-1) and two-term (PF-2) Hagen-Poiseuille pore-flow models) and two solution-diffusion models (i.e. classical solution-diffusion model (SD-1) and the modified solution-diffusion model (SD-2)) were adapted from literature and used to describe the transport through OSN membranes. Using experimental pure flux and binary flux data, and comparing it to transport models, it was found that:

- The classic solution-diffusion model provided the best prediction for the permeation of MEK through both Duramem™ series membranes, which demonstrates that the membrane can be described through diffusive properties, such as permeability of solvent. The permeability for MEK was determined through pure species permeation. The SD-1 model (i.e. Equation 7.1) provides Pearson coefficients ranging from around 0.997

$$J_i = P_i^{SD} \left[w_{i,M} - \frac{J_i}{J_i + J_j} \exp \left(-\frac{v_i \Delta p}{RT} \right) \right] \quad (7.1)$$

- The SD-1 Model predicted transport through Puramem™280 poorly for both polar and non-polar solvents.

- The PF-2 model yielded fair predictions for MEK and toluene through all three membranes. The additional inclusion of the solute properties, demonstrated the importance of solute interactions and that it is important to take into account their effect.
- The SD-2 model provided similar predictions to those of the PF-2 transport models, due to inclusion of the concentration of solute and viscosity parameters.
- Regressing $P_{\text{hexadecane}}^{\text{SD}}$ provided a better fit for the Duramem™ membrane series.

7.3. Energy and economic evaluation.

In this study, energy usage was investigated and a preliminary economic evaluation with regard to feasibility was done for OSN by comparing this alternative technology to conventional technologies, such as distillation. An energy analysis, capital cost analysis as well as operating cost analysis were done and it was found that:

- For both OSN and distillation systems assumed to have negligible raw material costs and a feed flowrate of $1000 \text{ kg}\cdot\text{hr}^{-1}$, the energy required to recover a ton of MEK solvent through OSN (i.e. $2.5 \text{ kWh}\cdot\text{ton}_{\text{solvent_product}}^{-1}$) and ca 50 times less than that of distillation (i.e. $135 \text{ kWh}\cdot\text{ton}_{\text{solvent_product}}^{-1}$). This is due to the fact that distillation operates at temperatures ranging around 240°C , which requires high amounts of energy.
- Capital costs for OSN instalment was $1/4^{\text{th}}$ of the capital cost for distillation. Capital costs were determined using heuristics from Turton *et al.* [1]. The cost index used was the Nelson-Ferrar cost index.

7.4. Recommendations for future work

Through experimentation, modelling and economic evaluation, it was shown that OSN technology has potential to be favourable over distillation. However, there are certain issues relating to OSN technology which need to be addressed. Based on the conclusions and results provided in this study, certain recommendations can be made for future research on possible improvements to the OSN process. These recommendations are as follows:

- The use of the dead-end cell operation does not reflect the industrial conditions for OSN process operation, such as membrane life span. This is due to the fact that dead-end cell operation is a batch-wise process in contrast to the continuous operation done in industry. Cross-flow set-ups are recommended as better reflections of industrial conditions, in order to provide better OSN knowledge to the OSN technology database.
- There is a lack of knowledge in modern research articles on the recovery of typical industrial solvents from lube-oil through the commercially available Duramem™ and Puramem™ membrane series. Thus, future research should focus on improving the knowledge database on the compatibility of solvents with these various membranes.

- Due to the influence which solvents have on the dewaxing process, it would be beneficial to determine the influence of various solvents on the permeation by using various binary solvents with a solute.
- The models provided good predictions in describing the transport for a binary mixture. However, incorporating the models into simulation of the OSN system is still recommended for future work. This will provide an improved understanding of the process with models incorporated into simulation.
- A full economic and energy evaluation is recommended due to the many solute species that have not been taken into account in this work. The long chain paraffin profile provides a much more difficult transport and recovery from a theoretical point of view. However, it would be preferred if future research investigations on the various solutes could focus on novel membrane performance.
- The scope of the study can be expanded to include a more complex heat integration for both OSN and distillation separation units to re-evaluate effective energy usage.

7.5. References

- [1] R. Turton, R.C. Bailie, W.B. Whiting, J.A. Schaeiwitz, **Analysis, Synthesis, and Design of Chemical Processes**, 3rd Ed., Prentice Hall, Boston, 2009.

Appendices

Appendix A: Detailed experimental procedure

A.1. Step-by-step procedure for OSN experiments

A.1.1. Membrane pre-treatment and steady state characterization.

1. Load cell with 150 mL of toluene.
2. Fasten cell with flange.
3. Place membrane cell on magnetic stirrer and adjust speed.
4. Position the permeate outlet pipe towards the permeate collection flask.
5. Place the permeate collection flask on an electric scale.
6. Make sure all valves, except the dead end cell feed valve, are closed and then connect the nitrogen gas line to the cell inlet.
7. Open cell inlet valve from the nitrogen gas line.
8. Pressurize cell to 30 bar.
9. Allow 50 mL toluene to permeate with impurities such as preservation oil.
10. Once 50 mL has permeated, depressurize cell, open cell and then add fresh toluene.
11. Close and pressurize the cell to desired pressure.
12. Allow two thirds of the feed volume in the cell to permeate.
13. During the permeation, measure the flux as mass or volume of permeate collected over a time interval and membrane active area. The pre-treatment is stopped once a constant flux is obtained.
14. The cell can be depressurized.

A.1.2. Solvent recovery from oil-solvent mixture

1. Make up an oil-solvent mixture containing 10 – 25 wt/wt% solution.
2. Load cell with 150 mL of toluene.
3. Fasten cell with flange.
4. Place membrane cell on magnetic stirrer and adjust speed.
5. Position the permeate outlet pipe towards the permeate collection flask.
6. Place the permeate collection flask on an electric scale.
7. Make sure all valves are closed and then connect the nitrogen gas line to the cell inlet.
8. Open cell inlet valve from the nitrogen gas line.
9. Pressurize cell to 30 bar.
10. Allow 40% of initial feed mixture volume to permeate in order to remove preservative oils.
11. Depressurize cell, refill the cell with new feedstock.
12. Take an 80 μ L feed sample used for analysis and then pressurize cell to desired pressure.

13. During permeation, measure the flux as mass or volume of permeate collected per unit time and membrane active area.
14. For a feed of 10 wt/wt% solute and 150 feed solution, take an 80 μL permeate sample at a permeate volume of 10 -15 ml of permeate.
15. Put the permeate flask aside and introduce a new empty flask to collect the following 10 – 15 ml. At the 10-15 ml mark, take another 80 μL permeate sample.
16. Repeat steps 13 – 14 four times and then return all permeate in each flask back to the feed solution in the cell.
17. Depressurise and open cell.

Appendix B: Analytical procedures and calibrations

B.1. Start-up, operational and shutdown procedures

Start-up

1. Open up the hydrogen, oxygen and helium line valves at the tanks against the wall.
2. Make sure the air cylinder is open (located underneath the lab in parking lot).
3. Switch on PC and go into GC program.
4. Close the oven, switch on GC (switch is located behind the GC).
5. Make sure the flow is at the correct pressure.
6. Once GC is on, make sure GC solvent vial (i.e. DCM) is not empty.
7. Open method used for analysis and make sure it is the method which is chosen for the run.
8. Run a blank sample to clean up the column (the auto-sampler will then perform a GC analysis on the blank vial).
9. Next, insert the diluted samples in the concentration ranges of the GC.
10. Run the auto-sampler sequence and queue all samples prepared for sampling.
11. Once in queue, operation has started.

Operational

1. Do not touch the detector while the operation is running.
2. After each sample has been analysed, let the GC run a blank sample before following the shut-down procedure.

Shut-down

1. Change GC method to the shutdown method provided during GC training.
2. Once the method has been changed to the shut-down method, let the system reach the initial conditions set by the method, such as oven temperature and FID temperature.
3. Once the column has reached the method initial state, switch off the oven using the switch.
4. The FID may be left on if the instrument is used on a weekly basis.
5. Close the hydrogen, helium and air valves as it was opened in that order. (Only close the air valve and other valves if no other GC is running from the same gas line).
6. Close the air valve on the air cylinder in the parking lot.

B.2. Calibration curves and data

Prepare standards as follows:

1. Five standard solutions were prepared (i.e. 10 μ L, 20 μ L, 30 μ L, 50 μ L, 80 μ L) by taking n-hexadecane and weighing each standard vial at those volumes.

2. Place those volumes in DCM with 30 μ L of decane added to each of the five vials.
3. Make 2 extra replicates of each standard by following steps 1 and 2 above, which is used for reproducibility purposes.
4. Make sure the dilution concentration is within the limits of the GC before placing standards into the sample vial.
5. Once the standards are in the sample vials, take the samples to the GC for analysis.

The Calibration Curve for n-hexadecane is illustrated in Figure B.1.

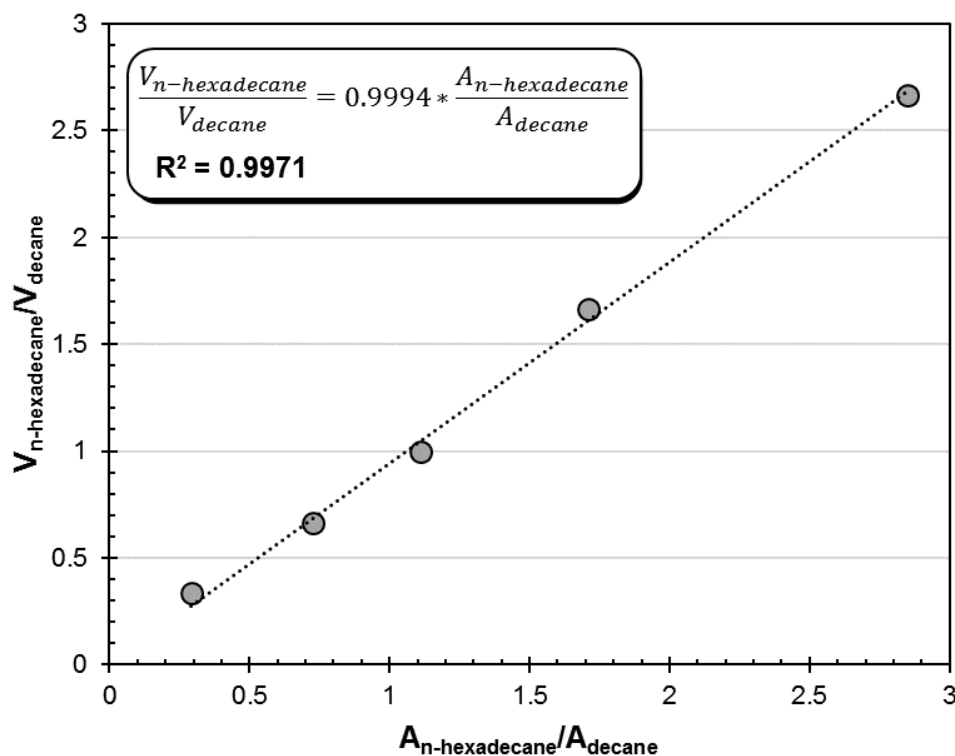


Figure B.1: GC calibration curve for n-hexadecane

Appendix C: Sample calculations

C.1. Experimental flux and rejection

C.1.1. Experimental flux

Initial Parameters:

$$V_{feed} = 150 \text{ ml}$$

$$\rho_{MEK} = 804.9 \text{ kg.m}^{-3} (@ 20^{\circ}\text{C})$$

$$A_{active} = 0.00159 \text{ m}^2$$

Experimental Data noted:

Data set 1:

Permeate mass (m_{p1}): 5 g

Time interval (t_{p1}): 521 s

Data set 2:

Permeate mass (m_{p1}): 10 g

Time interval (t_{p1}): 1012 s

Calculations:

$$\Delta m_{1 \rightarrow 2} = m_{p2} - m_{p1} = 10 \text{ (g)} - 5 \text{ (g)} = 5 \text{ g}$$

$$\Delta t_{1 \rightarrow 2} = t_{p2} - t_{p1} = 1012 \text{ (s)} - 521 \text{ (s)} = 491 \text{ (s)}$$

$$\Delta V_{1 \rightarrow 2} = \frac{\Delta m_{1 \rightarrow 2}}{\rho_{MEK}} = \frac{5 \text{ (g)}}{804.9 \frac{\text{kg}}{\text{m}^3}} \times \frac{1 \text{ kg}}{1000 \text{ g}} \times \frac{1000 \text{ L}}{1 \text{ m}^3} \times \frac{1000 \text{ mL}}{1 \text{ L}} = 6.212 \text{ mL}$$

$$\text{experimental flux (J}_v\text{)} = \frac{\Delta V_{1 \rightarrow 2}}{A \cdot \Delta t_{1 \rightarrow 2}} = \frac{6.212 \text{ mL}}{0.00159 \text{ m}^2 \cdot 491 \text{ s}} \times \frac{1 \text{ L}}{1000 \text{ mL}} \times \frac{3600 \text{ s}}{1 \text{ hr}}$$

$$\text{experimental flux (J}_v\text{)} = 28.645 \text{ L.m}^{-2}.\text{hr}^{-1}$$

C.1.2. Determining rejection of solute from GC data

For MEK-n-Hexadecane at 10 wt% concentration:

Feed sample:

Area of hexadecane (A_{C16}): 3243702

Area of decane (A_{C10}): 12728769

$$V_{C16} = RF \times \left(\frac{A_{C16}}{A_{C10}} \right) \times V_{C10} = 0.994 \times \left(\frac{3243702}{12728769} \right) \times (30 \text{ } \mu\text{L}) = 7.60 \text{ } \mu\text{L}$$

$$m_{C16} = V_{C16} \times \left(\frac{1 \text{ mL}}{1000 \text{ } \mu\text{L}} \right) \times \rho_{C16} = (7.60 \text{ } \mu\text{L}) \times \left(\frac{1 \text{ mL}}{1000 \text{ } \mu\text{L}} \right) \times 733.44 \text{ (mg.mL}^{-1}\text{)} =$$

$$m_{C16} = 5.57 \text{ mg}$$

$$C_{C16(feed)} = \frac{m_{C16}}{V_{Mix\ solution}} \times \left(\frac{1000\ \mu L}{1\ mL} \right) \times \left(\frac{1000\ mL}{1\ L} \right) = \frac{5.57\ mg}{80\ \mu L} \times 1000 \times 1000 = 0.06966\ \frac{mg}{L}$$

Permeate sample:

Area of hexadecane (A_{C16}): 1091704

Area of decane (A_{C10}): 9419201

$$V_{C16} = RF \times \left(\frac{A_{C16}}{A_{C10}} \right) \times V_{C10} = 0.994 \times \left(\frac{1091704}{9419201} \right) \times (30\ \mu L) = 3.46\ \mu L$$

$$m_{C16} = V_{C16} \times \left(\frac{1\ mL}{1000\ \mu L} \right) \times \rho_{C16} = (3.46\ \mu L) \times \left(\frac{1\ mL}{1000\ \mu L} \right) \times 733.44\ (mg.\ mL^{-1}) =$$

$$m_{C16} = 2.53\ mg$$

$$C_{C16(Perm)} = \frac{m_{C16}}{V_{Mix\ solution}} \times \left(\frac{1000\ \mu L}{1\ mL} \right) \times \left(\frac{1000\ mL}{1\ L} \right) = \frac{2.53\ mg}{80\ \mu L} \times 1000 \times 1000 =$$

$$C_{C16(Perm)} = 0.03168\ \frac{mg}{L}$$

Rejection:

$$R_{C16} = \left(1 - \left(\frac{C_{C16(Perm)}}{C_{C16(feed)}} \right) \right) \times 100\ \% = \left(1 - \left(\frac{0.03168\ \frac{mg}{L}}{0.06966\ \frac{mg}{L}} \right) \right) \times 100\ \% = 54.52\ \%$$

C.2. Transport modelling

C.2.1. Pore-flow models

Binary one-term Pore-flow model:

$$J_v = P_{mix}^{PF} \left(\frac{\Delta P}{\eta_{mix}} \right) \times \left(\frac{1}{\rho_{mix}} \right)$$

$$\eta_{mix} = \left(w_i \eta_i^{\frac{1}{3}} + w_j \eta_j^{\frac{1}{3}} \right)^3$$

$$\rho_{mix} = w_i \rho_i + w_j \rho_j$$

$$P_{mix}^{PF} = \frac{(P_i^{PF} + P_j^{PF})}{\frac{P_i^{PF}}{P_i^{PF} + P_j^{PF}} + \frac{P_j^{PF}}{P_i^{PF} + P_j^{PF}}}$$

$$J_v = P_{mix}^{PF} \left(\frac{\Delta P}{\eta_{mix}} \right) \times \left(\frac{1}{\rho_{mix}} \right) = \left[\frac{(P_i^{PF} + P_j^{PF})}{\frac{P_i^{PF}}{P_i^{PF} + P_j^{PF}} + \frac{P_j^{PF}}{P_i^{PF} + P_j^{PF}}} \right] \times \left[\frac{\Delta P}{\left(w_i \eta_i^{\frac{1}{3}} + w_j \eta_j^{\frac{1}{3}} \right)^3 \times (w_i \rho_i + w_j \rho_j)} \right]$$

For species i = MEK and species j = n-hexadecane(C16) through Duramem™ 150:

$$\eta_{mix} = \left(0.75 \left(\frac{kg_{mek}}{kg_{total}} \right) ((4.28E^{-4})(Pa.s))^{\frac{1}{3}} + 0.25 \left(\frac{kg_{C16}}{kg_{total}} \right) ((3.00E^{-3})(Pa.s))^{\frac{1}{3}} \right)^3$$

$$\eta_{mix} = 7.93E^{-4} Pa.s$$

$$\rho_{mix} = 0.75 \left(\frac{kg_{mek}}{kg_{total}} \right) \times 804.9 \left(\frac{kg_{mek}}{m^3_{MEK}} \right) + 0.25 \left(\frac{kg_{C16}}{kg_{total}} \right) \times 773.44 \left(\frac{kg_{C16}}{m^3_{C16}} \right) = 797.04 \frac{kg_{mix}}{m^3_{mix}}$$

$$J_v = \left[\frac{(1.28E^{-12} + 1.49E^{-15})}{\frac{1.28E^{-12}}{1.28E^{-12} + 1.49E^{-15}} + \frac{1.49E^{-15}}{1.28E^{-12} + 1.49E^{-15}}} (kg_{mix} \cdot m^{-2}) \right] \times \left[\frac{30 Bar \times \frac{100\,000 Pa}{1 Bar}}{7.93E^{-4}(Pa.s) \times 797.04 \left(\frac{kg_{mix}}{m^3_{total}} \right)} \right] \times \frac{3600 s}{1 hr}$$

$$J_v = 21.89 L \cdot m^{-2} \cdot hr^{-1}$$

Binary Two-term Pore-flow model:

$$J = \left(\frac{\Delta P}{\eta_{mix}} \right) [v_i c_{i(m)} P_i^{PF} + v_j c_{j(m)} P_j^{PF}]$$

$$v(frac)_i = \frac{\left(\frac{w_i}{\rho_i} \right)}{\left(\frac{w_i}{\rho_i} \right) + \left(\frac{w_j}{\rho_j} \right)} = \frac{\left(\frac{0.75 \frac{kg_{mek}}{kg_{total}}}{804.9 \frac{kg_{mek}}{m^3_{MEK}}} \right)}{\left(\frac{0.75 \frac{kg_{mek}}{kg_{total}}}{804.9 \frac{kg_{mek}}{m^3_{MEK}}} \right) + \left(\frac{0.25 \frac{kg_{C16}}{kg_{total}}}{773.44 \frac{kg_{C16}}{m^3_{C16}}} \right)} = 0.742 \frac{m^3_{mek}}{m^3_{total}}$$

$$v(frac)_j = \frac{\left(\frac{w_j}{\rho_j} \right)}{\left(\frac{w_i}{\rho_i} \right) + \left(\frac{w_j}{\rho_j} \right)} = \frac{\left(\frac{0.25 \frac{kg_{C16}}{kg_{total}}}{773.44 \frac{kg_{C16}}{m^3_{C16}}} \right)}{\left(\frac{0.75 \frac{kg_{mek}}{kg_{total}}}{804.9 \frac{kg_{mek}}{m^3_{MEK}}} \right) + \left(\frac{0.25 \frac{kg_{C16}}{kg_{total}}}{773.44 \frac{kg_{C16}}{m^3_{C16}}} \right)} = 0.258 \frac{m^3_{C16}}{m^3_{total}}$$

$$C_{i(m)} = (v(frac)_i \times V_{solution}) \times \frac{\rho_i \times \left(\frac{1}{Mw_i} \right)}{V_{solution}}$$

$$C_{i(m)} = \left[\left(0.742 \frac{m^3_{mek}}{m^3_{total}} \right) (150 mL) \left(\frac{1 L}{1000 mL} \right) \left(\frac{1 m^3_{total}}{1000 L} \right) \right] \times \frac{\left[\left(804.9 \frac{kg_{mek}}{m^3_{MEK}} \right) \left(\frac{1}{72.11 \frac{g}{mol}} \right) \left(\frac{1000 g}{1 kg} \right) \right]}{150 mL \left(\frac{1 L}{1000 mL} \right) \left(\frac{1 m^3_{total}}{1000 L} \right)}$$

$$C_{i(m)} = C_{MEK(m)} = 8.287E^{+3} \frac{mol}{m^3}$$

$$C_{j(m)} = \left[\left(0.258 \frac{m^3_{C16}}{m^3_{total}} \right) (150 mL) \left(\frac{1 L}{1000 mL} \right) \left(\frac{1 m^3_{total}}{1000 L} \right) \right] \times \frac{\left[\left(773.44 \frac{kg_{C16}}{m^3_{C16}} \right) \left(\frac{1}{226.45 \frac{g}{mol}} \right) \left(\frac{1000 g}{1 kg} \right) \right]}{150 mL \left(\frac{1 L}{1000 mL} \right) \left(\frac{1 m^3_{total}}{1000 L} \right)}$$

$$C_{j(m)} = C_{C16(m)} = 879.66 \frac{mol}{m^3}$$

$$J_v = \left(\frac{30 \text{ Bar} \times \frac{100\,000 \text{ Pa}}{1 \text{ Bar}}}{7.93E^{-4} (\text{Pa.s})} \right) \left[\left(8.944E^{-5} \frac{\text{m}^3_{mek}}{\text{mol}_{mek}} \right) \left(8.287E^{+3} \frac{\text{mol}_{mek}}{\text{m}^3_{total}} \right) \left(1.28E^{-12} \frac{\text{kg}}{\text{m}^2} \right) + \right. \\ \left. \left(2.92E^{-4} \frac{\text{m}^3_{C16}}{\text{mol}_{C16}} \right) \left(8.79E^{+2} \frac{\text{mol}_{C16}}{\text{m}^3_{total}} \right) \left(1.49E^{-15} \frac{\text{kg}}{\text{m}^2} \right) \right] \times \frac{3600 \text{ s}}{1 \text{ hr}} \times \frac{1}{797.04 \frac{\text{kg}_{mix}}{\text{m}^3_{mix}}} \times \frac{1000 \text{ L}}{1 \text{ m}^3}$$

$$J_v = 16.86 \text{ L.m}^{-2}.\text{hr}^{-1}$$

C.2.2 Solution Diffusion models

Classic Solution-diffusion Model (SD-1):

This model involves many iterative calculations performed in Matlab R2016a. A convenient way to show how the calculation steps are done, is by providing a block diagram shown in Figure C.1. This helps to visually illustrate the calculation steps during each iteration.

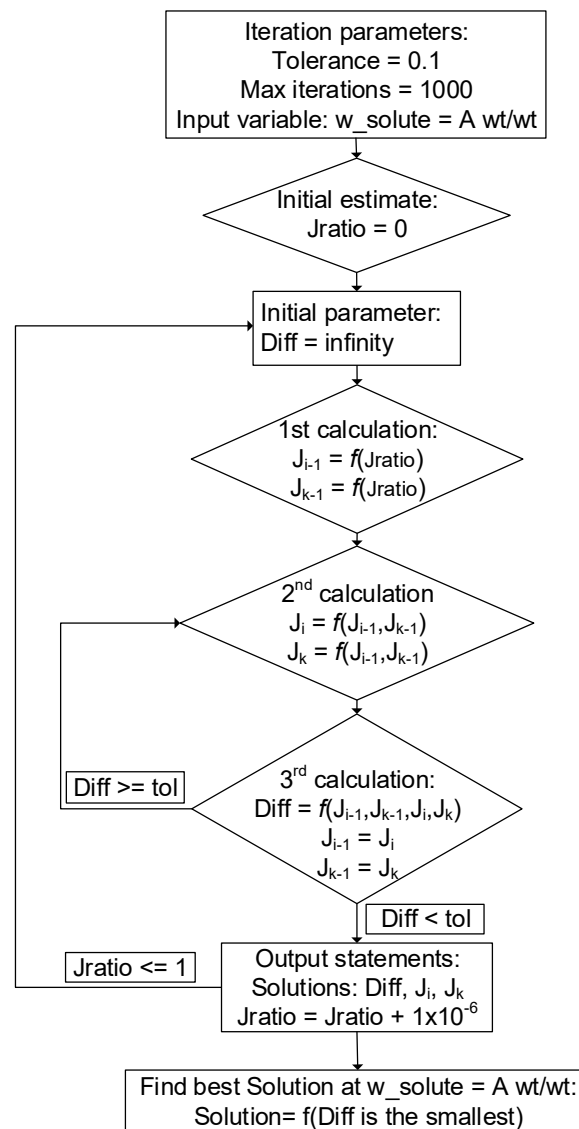


Figure C.1: Block diagram for iteration step in the solution-diffusion model (SD-1)

Determining the total flux for MEK at a weight fraction of 0.75 wt/wt % with the solution diffusion model is shown as follows for the first iteration:

Starting at a guessed $J_{ratio} = 0.81274$

Determining J_{i-1} and J_{k-1} using J_{ratio} :

$$J_i = P_i^{SD} \left[w_{i,M} - \frac{J_i}{J_i + J_k} \exp \left(-\frac{v_i \Delta p}{RT} \right) \right]$$

$$J_k = P_k^{SD} \left[w_{i,M} - \frac{J_k}{J_i + J_k} \exp \left(-\frac{v_k \Delta p}{RT} \right) \right]$$

1st Calculation: $J_{mek-1} = P_{mek}^{SD} (w_{mek} - J_{ratio} \times \exp \frac{v_{mek} \Delta p}{R.T})$

$$J_{mek-1} = \left(8.86E - 2 \frac{kg}{m^2 s^1} \right) \left(0.75 \frac{kg_{mek}}{kg_{tot}} - \left(0.81274 \frac{\frac{kg_{tot}}{m^2 hr^1}}{\frac{kg_{tot}}{m^2 hr^1}} \right) \times \exp \frac{\left(\frac{8.944E-5 \frac{m^3_{mek}}{mol} \right) (30E+5 Pa)}{\left(\frac{8.314 \frac{Pa.m^3}{K.mol}} \right) (293.15 K)} \right)$$

$$J_{mek-1} = 0.001948 \frac{kg}{m^3.s}$$

$$J_{C16-1} = \left(0.0036 \frac{kg}{m^2 s^1} \right) \left(0.25 \frac{kg_{C16}}{kg_{tot}} - \left(1 - 0.81274 \frac{\frac{kg_{tot}}{m^2 hr^1}}{\frac{kg_{tot}}{m^2 hr^1}} \right) \times \exp \frac{\left(\frac{2.92E-4 \frac{m^3_{C16}}{mol} \right) (30E+5 Pa)}{\left(\frac{8.314 \frac{Pa.m^3}{K.mol}} \right) (293.15 K)} \right)$$

$$J_{C16-1} = 0.0004298 \frac{kg}{m^3.s}$$

2nd Calculation: $J_i = P_i^{SD} \left[w_{i,M} - \frac{J_{i-1}}{J_{i-1} + J_{k-1}} \exp \left(-\frac{v_i \Delta p}{RT} \right) \right]$

$$J_{mek} = \left(8.86E - 2 \frac{kg}{m^2 s^1} \right) \left(0.75 \frac{kg_{mek}}{kg_{tot}} - \left(0.8192 \frac{\frac{kg_{tot}}{m^2 hr^1}}{\frac{kg_{tot}}{m^2 hr^1}} \right) \times \exp \frac{\left(\frac{8.944E-5 \frac{m^3_{mek}}{mol} \right) (30E+5 Pa)}{\left(\frac{8.314 \frac{Pa.m^3}{K.mol}} \right) (293.15 K)} \right)$$

$$J_{mek} = 0.001432 \frac{kg}{m^3.s} \times \frac{kg}{m^2.s} \times \frac{1}{\rho_{mek}}$$

$$J_{mek} = 0.001432 \frac{kg}{m^2.s} \times \frac{3600 s}{1 hr} \times \frac{1}{804.9 \left(\frac{kg_{mek}}{m^3_{MEK}} \right)} \times \frac{1000 L}{1 m^3} = 6.408 L.m^{-2}.hr^{-1}$$

$$J_{C16} = \left(0.0036 \frac{kg}{m^2 s^1} \right) \left(0.25 \frac{kg_{C16}}{kg_{tot}} - \left(1 - 0.8192 \frac{\frac{kg_{tot}}{m^2 hr^1}}{\frac{kg_{tot}}{m^2 hr^1}} \right) \times \exp \frac{\left(\frac{2.92E-4 \frac{m^3_{C16}}{mol} \right) (30E+5 Pa)}{\left(\frac{8.314 \frac{Pa.m^3}{K.mol}} \right) (293.15 K)} \right)$$

$$J_{C16} = 0.000446 \frac{kg}{m^2.s} \times \frac{1}{\rho_{C16}}$$

$$J_{C16} = 0.000446 \frac{kg}{m^2.s} \times \frac{3600 s}{1 hr} \times \frac{1}{773.44 \left(\frac{kg_{C16}}{m^3_{C16}} \right)} \times \frac{1000 L}{1 m^3} = 2.076 L.m^{-2}.hr^{-1}$$

$$\mathbf{3^{rd} Calculation: Diff} = (J_{mek} - J_{mek-1})^2 + (J_{C16} - J_{C16-1})^2$$

$$Diff = (J_{mek} - J_{mek-1})^2 + (J_{C16} - J_{C16-1})^2$$

$$Diff = (6.408 - 0.001948)^2 + (2.076 - 0.0004298)^2 = 45.35$$

Since Diff > Tolerance, $J_{mek-1} = J_{mek}$ & $J_{C16-1} = J_{C16}$ thus repeating **2nd Calculation** step.

Final solution for MEK through Duramem™150 at C16 weight fraction of 0.15 wt/wt:

$$J_{mek} = 8.7128 L.m^{-2}.hr^{-1}$$

$$J_{C16} = 2.00075 L.m^{-2}.hr^{-1}$$

$$J_{tot} = J_{mek} + J_{C16} = 8.7128 L.m^{-2}.hr^{-1} + 2.00075 L.m^{-2}.hr^{-1} = 10.713 L.m^{-2}.hr^{-1}$$

C.3. Determining energy required for OSN

$$Q_{OSN} = \frac{F_f \Delta P_{TM}}{\epsilon_{pump}} = \frac{(129.54 L.hr^{-1}) \times (30 bar)}{0.66} \times \left(\frac{100 kPa}{1 Bar} \right) = 0.163 kW$$

C.4. Determining the capital cost of membrane

$$\rho_{mix} = \rho_{MEK} \cdot 0.6 + \rho_{tol} \cdot 0.4 = \left(804.9 \frac{kg_{mek}}{m^3} \right) (0.6) + \left(866.9 \frac{kg_{tol}}{m^3} \right) (0.4) = 829.34 \frac{kg}{m^3}$$

$$J_{v,Maxdwx} = \frac{\dot{v}_{perm}}{A_{mem}} \rightarrow A_{mem} = \frac{\dot{v}_{perm}}{J_v} \times \rho_{mix} = \left(\frac{40 \frac{m^3}{hr}}{10.1 \frac{kg}{m^2.hr}} \right) \left(829.34 \frac{kg}{m^3} \right) = 3284.51 \sim 3285 m^2$$

$$J_{v,study} = \frac{\dot{v}_{perm}}{A_{mem}} \rightarrow A_{mem} = \frac{\dot{v}_{perm}}{J_v} = \left(\frac{600 \frac{kg}{hr}}{10.1 \frac{kg}{m^2.hr}} \right) = 59.4 \sim 60 m^2$$

$$C_2 = C_1 \left(\frac{I_2}{I_1} \right) \left(\frac{A_2}{A_1} \right)^n = (\$5,500\ 000) \times \left(\frac{2544}{1477.6} \right) \times \left(\frac{60}{3285} \right)^{0.6} = \$857\ 691.14$$

C.5. Determining operating costs using heuristics from Turton *et al.*

$$TOC = C_{raw} + C_{labour} + C_{energy} + C_{maint}$$

$$C_{raw} = FY_{raw} = 75 MEK \frac{kg}{hour} \times 24 \frac{hour}{day} \times 315 MEK \frac{\$}{kg} = \$ 574,296.00 \text{ per day}$$

$$C_{labour} = 24Y_{labour} = 24 \times 7 = \$ 168.00 \text{ per day}$$

$$C_{energy} = \frac{\Sigma(Q_{INI}\Delta P)}{36\eta} Y_{elec} = 0.15 \text{ kW} \times 0.08 \frac{\$}{\text{kWh}} \times 24 \frac{\text{hours}}{\text{day}} = \$ 0.30336 \text{ per day}$$

$$C_{maint} = 0.05 C_{capital} = 0.05 \times \frac{\$ 25,000,000.00}{8150 \frac{\text{hours}}{\text{year}}} \times 24 \frac{\text{hours}}{\text{day}} = \$ 3680.98 \text{ per day}$$

$$TOC = \frac{(\$ 574,296.00 + \$ 168.00 + \$ 0.30336 + \$ 3680.98) \text{ day}^{-1}}{24 \frac{\text{hours}}{\text{day}}} \times 8150 \frac{\text{hours}}{\text{year}}$$

$$TOC = \$ 196 \text{ million per year}$$

Appendix D: Raw experimental data

D.1. Pure species flux tests

Table D.1.1: MEK flux data through Puramem™280 at 40 Bar

Test:	permeability tests		Room temperature	19.3	oC					
Date	2017-05-11		Ambient pressure	1.02	Bar					
Time	morning		Gas pressure	40	Bar					
Solvent	MEK		Vinitial charge	150	mL					
Density	804.9	kg/m3	membrane area	0.00159	m2					
membrane ID	Puramem		thickness	0.002	m					
MWCO	280	Da								
Mass of permeate (g)	Time (hr:min:sec)	Δmass permeate (g)	Δvolume permeate (ml)	hours	Totalminutes	cuml Seconds	cum time (hr)	Delta t (hr)	Flux (g.m ⁻² .hr ⁻¹)	Flux (L.m ⁻² .hr ⁻¹)
1	00:00:03.21	1	1.242	0.0	0	3	0.0008	0.00083	754716.98	937.65
5	00:00:15.80	4	4.970	0.0	0	16	0.0044	0.00361	696661.83	865.53
10	00:00:31.83	5	6.212	0.0	0	32	0.0089	0.00444	707547.17	879.05
13	00:00:51.11	3	3.727	0.0	0	51	0.0142	0.00528	357497.52	
21	00:00:53.06	8	9.939	0.0	0	53	0.0147	0.00056	9056603.77	
25	00:01:02.97	4	4.970	0.0	1	3	0.0175	0.00278	905660.38	1125.18
30	00:01:13.19	5	6.212	0.0	1	13	0.0203	0.00278	1132075.47	1406.48
40	00:01:38.47	10	12.424	0.0	1	38	0.0272	0.00694	905660.38	1125.18
50	00:02:04.76	10	12.424	0.0	2	5	0.0347	0.00750	838574.42	1041.84
60	00:02:31.57	10	12.424	0.0	2	32	0.0422	0.00750	838574.42	1041.84

Table D.1.2: MEK flux data through Puramem™280 at 30 Bar

Test:	permeability tests		Room temperature	20	oC					
Date	2017-05-11		Ambient pressure	1.02	Bar					
Time	morning		Gas pressure	30	Bar					
Solvent	MEK		Vinitial charge	150	mL					
Density	804.9	kg/m3	membrane area	0.00159	m2					
membrane ID	Puramem		thickness	0.002	m					
MWCO	280	Da								
Mass of permeate (g)	Time (hr:min:sec)	Δmass permeate (g)	Δvolume permeate (ml)	hours	Totalminutes	cuml Seconds	cum time (hr)	Delta t (hr)	Flux (g.m ⁻² .hr ⁻¹)	Flux (L.m ⁻² .hr ⁻¹)
1	00:00:15.90	1	1.242	0.0	0	16	0.004	0.004	141509.43	175.81
5	00:00:25.37	4	4.970	0.0	0	25	0.007	0.003	1006289.31	1250.20
10	00:00:41.26	5	6.212	0.0	0	41	0.011	0.004	707547.17	879.05
15	00:00:55.97	5	6.212	0.0	0	56	0.016	0.004	754716.98	937.65
20	00:01:14.43	5	6.212	0.0	1	14	0.021	0.005	628930.82	781.38
25	00:01:28.35	5	6.212	0.0	1	28	0.024	0.004	808625.34	1004.63
30	00:01:46.14	5	6.212	0.0	1	46	0.029	0.005	628930.82	781.38
40	00:02:22.00	10	12.424	0.0	2	22	0.039	0.010	628930.82	781.38
50	00:02:56.29	10	12.424	0.0	2	56	0.049	0.009	665926.75	827.34
60	00:03:32.68	10	12.424	0.0	3	33	0.059	0.010	611932.69	760.26

Table D.1.3: MEK flux data through Puramem™280 at 20 Bar

Test:	permeability tests		Room temperature	20	oC					
Date	2017-05-11		Ambient pressure	1.02	Bar					
Time	morning		Gas pressure	20	Bar					
Solvent	MEK		Vinitial charge	130	mL					
Density	804.9	kg/m3	membrane area	0.00159	m2					
membrane ID	Puramem		thickness	0.002	m					
MWCO	280	Da								
Mass of permeate (g)	Time (hr:min:sec)	Δmass permeate (g)	Δvolume permeate (ml)	hours	Totalminutes	cuml Seconds	cum time (hr)	Delta t (hr)	Flux (g.m ⁻² .hr ⁻¹)	Flux (L.m ⁻² .hr ⁻¹)
1	00:00:17.14	1	1.242	0.0	0	17	0.005	0.005	133185.35	165.47
5	00:00:32.77	4	4.970	0.0	0	33	0.009	0.004	566037.74	703.24
10	00:00:55.23	5	6.212	0.0	0	55	0.015	0.006	514579.76	639.31
15	00:01:18.77	5	6.212	0.0	1	19	0.022	0.007	471698.11	586.03
20	00:01:42.35	5	6.212	0.0	1	42	0.028	0.006	492206.73	611.51
25	00:02:05.74	5	6.212	0.0	2	6	0.035	0.007	471698.11	586.03
30	00:02:31.31	5	6.212	0.0	2	31	0.042	0.007	452830.19	562.59
40	00:03:17.54	10	12.424	0.0	3	18	0.055	0.013	481734.24	598.50
50	00:04:08.67	10	12.424	0.0	4	9	0.069	0.014	443951.17	551.56
60	00:05:00.60	10	12.424	0.0	5	1	0.084	0.014	435413.64	540.95

Table D.1.4: MEK flux data through Puramem™280 at 10 Bar

Test:	permeability tests		Room temperature	20	oC					
Date	2017-05-11		Ambient pressure	1.02	Bar					
Time	morning		Gas pressure	10	Bar					
Solvent	MEK		Vinitial charge	130	mL					
Density	804.9	kg/m3	membrane area	0.00159	m2					
membrane ID	Puramem		thickness	0.002	m					
MWCO	280	Da								
Mass of permeate (g)	Time (hr:min:sec)	Δmass permeate (g)	Δvolume permeate (ml)	hours	Totalminutes	cuml Seconds	cum time (hr)	Delta t (hr)	Flux (g.m ⁻² .hr ⁻¹)	Flux (L.m ⁻² .hr ⁻¹)
1	00:00:21.10	1	1.242	0.0	0	21	0.006	0.006	107816.71	133.95
5	00:00:52.25	4	4.970	0.0	0	52	0.014	0.009	292148.51	362.96
10	00:01:32.25	5	6.212	0.0	1	32	0.026	0.011	283018.87	351.62
15	00:02:14.21	5	6.212	0.0	2	14	0.037	0.012	269541.78	334.88
20	00:02:56.63	5	6.212	0.0	2	57	0.049	0.012	263273.37	327.09
25	00:03:38.37	5	6.212	0.0	3	38	0.061	0.011	276115.97	343.04
30	00:04:20.77	5	6.212	0.0	4	21	0.073	0.012	263273.37	327.09
41	00:05:55.18	11	13.666	0.0	5	55	0.099	0.026	264953.83	329.18
51	00:07:21.67	10	12.424	0.0	7	22	0.123	0.024	260247.23	323.33
60	00:08:42.59	9	11.182	0.0	8	43	0.145	0.023	251572.33	312.55

Table D.1.5: Toluene flux data through Puramem™280 at 40 Bar

Test:	permeability tests		Room temperature	14	oC					
Date	2017-06-13		Ambient pressure	1.006	Bar					
Time	Afternoon		Gas pressure	40	Bar					
Solvent	Toluene		Vinitial charge	150	mL					
Density	866.9	kg/m3	membrane area	0.0016619	m2					
membrane ID	Puramem		thickness	0.002	m					
MWCO	280	Da								
Mass of permeate (g)	Time (hr:min:sec)	Δmass permeate (g)	Δvolume permeate (ml)	hours	Totalminutes	cuml Seconds	cum time (hr)	Delta t (hr)	Flux (g.m ⁻² .hr ⁻¹)	Flux (L.m ⁻² .hr ⁻¹)
1	00:00:34.08	1	1.15	0.0	0	34	0.009	0.009	63711.53	79.15
5	00:00:56.10	4	4.61	0.0	0	56	0.016	0.006	393853.10	489.32
10	00:01:26.53	5	5.77	0.0	1	27	0.024	0.009	349385.81	434.07
23	00:02:50.30	13	15.00	0.0	2	50	0.047	0.023	339283.09	421.52
32	00:03:42.48	9	10.38	0.0	3	42	0.062	0.014	374917.85	465.79
40	00:04:37.15	8	9.23	0.0	4	37	0.077	0.015	315082.48	391.46
60	00:06:46.60	20	23.07	0.0	6	47	0.113	0.036	333260.31	414.04
80	00:09:03.75	20	23.07	0.0	9	4	0.151	0.038	316232.41	392.88

Table D.1.6: Toluene flux data through Puramem™280 at 30 Bar

Test:	permeability tests		Room temperature	24	oC					
Date	2017-06-13		Ambient pressure	0.997	Bar					
Time	Afternoon		Gas pressure	30	Bar					
Solvent	Toluene		Vinitial charge	130	mL					
Density	866.9	kg/m3	membrane area	0.0016619	m2					
membrane ID	Puramem		thickness	0.002	m					
MWCO	280	Da								
Mass of permeate (g)	Time (hr:min:sec)	Δmass permeate (g)	Δvolume permeate (ml)	hours	Totalminutes	cuml Seconds	cum time (hr)	Delta t (hr)	Flux (g.m ⁻² .hr ⁻¹)	Flux (L.m ⁻² .hr ⁻¹)
1	00:00:27.00	1	1.15	0.0	0	27	0.008	0.008	80229.33	92.55
5	00:00:57.16	4	4.61	0.0	0	57	0.016	0.008	288825.61	333.17
10.3	00:01:43.04	5.3	6.11	0.0	1	43	0.029	0.013	249583.00	287.90
20	00:03:03.75	9.7	11.19	0.0	3	4	0.051	0.023	259408.18	299.24
30	00:04:29.80	10	11.54	0.0	4	30	0.075	0.024	251882.80	290.56
41	00:06:04.51	11	12.69	0.0	6	5	0.101	0.026	250822.24	289.33
60	00:08:48.31	19	21.92	0.0	8	48	0.147	0.045	252500.91	291.27
80	00:11:47.11	20	23.07	0.0	11	47	0.196	0.050	242032.63	279.19

Table D.1.7: Toluene flux data through Puramem™280 at 20 Bar

Test:	permeability tests		Room temperature	24	oC					
Date	2017-06-13		Ambient pressure	0.998	Bar					
Time	Afternoon		Gas pressure	20	Bar					
Solvent	Toluene		Vinitial charge	110	mL					
Density	866.9	kg/m3	membrane area	0.0016619	m2					
membrane ID	Puramem		thickness	0.002	m					
MWCO	280	Da								
Mass of permeate (g)	Time (hr:min:sec)	Δmass permeate (g)	Δvolume permeate (ml)	hours	Totalminutes	cuml Seconds	cum time (hr)	Delta t (hr)	Flux (g.m ⁻² .hr ⁻¹)	Flux (L.m ⁻² .hr ⁻¹)
2	00:00:46.11	2	2.31	0.0	0	46	0.013	0.013	94182.26	108.64
5	00:01:13.84	3	3.46	0.0	1	14	0.021	0.008	232092.00	267.73
10	00:02:18.47	5	5.77	0.0	2	18	0.038	0.018	169233.75	195.22
20	00:04:17.28	10	11.54	0.0	4	17	0.071	0.033	182032.94	209.98
30	00:06:17.85	10	11.54	0.0	6	18	0.105	0.034	179024.14	206.51
40	00:08:21.46	10	11.54	0.0	8	21	0.139	0.034	176113.17	203.15
62	00:12:52.43	22	25.38	0.0	12	52	0.214	0.075	175853.23	202.85
80.4	00:16:46.77	18.4	21.23	0.0	16	47	0.280	0.065	169608.23	195.65

Table D.1.8: Toluene flux data through Puramem™280 at 10 Bar

Test:	permeability tests		Room temperature	10	oC					
Date	2017-06-13		Ambient pressure	1.02	Bar					
Time	Afternoon		Gas pressure	10	Bar					
Solvent	Toluene		Vinitial charge	130	mL					
Density	866.9	kg/m3	membrane area	0.00159	m2					
membrane ID	Puramem		thickness	0.002	m					
MWCO	280	Da								
Mass of permeate (g)	Time (hr:min:sec)	Δmass permeate (g)	Δvolume permeate (ml)	hours	Totalminutes	cuml Seconds	cum time (hr)	Delta t (hr)	Flux (g.m ⁻² .hr ⁻¹)	Flux (L.m ⁻² .hr ⁻¹)
1	00:00:38.26	1	1.15	0.0	0	38	0.011	0.011	59582.92	74.03
5	00:02:20.36	4	4.61	0.0	2	20	0.039	0.028	88790.23	110.31
11.3	00:04:16.61	6.3	7.27	0.0	4	17	0.071	0.033	121915.82	151.47
22	00:08:16.28	10.7	12.34	0.0	8	16	0.138	0.066	101365.75	125.94
30.6	00:11:30.26	8.6	9.92	0.0	11	30	0.192	0.054	100369.58	124.70
40	00:15:13.42	9.4	10.84	0.0	15	13	0.254	0.062	95439.55	118.57
60	00:22:48.32	20	23.07	0.0	22	48	0.380	0.126	99523.12	123.65
78	00:30:39.81	18	20.76	0.0	30	40	0.511	0.131	86344.74	107.27
100	03:43:33.00	22	25.38	3.0	43	33	3.726	3.215	4304.10	5.35
120	04:43:33.00	20	23.07	4.0	43	33	4.726	1.000	12578.62	15.63
140	05:43:33.00	20	23.07	5.0	43	33	5.726	1.000	12578.62	15.63

Table D.1.9: MEK flux data through Duramem™200 at 40 Bar

Test:	permeability tests		Room temperature	19.3	oC					
Date	2017-07-17		Ambient pressure	1.02	Bar					
Time	morning		Gas pressure	40	Bar					
Solvent	MEK		Vinitial charge	150	mL					
Density	804.9	kg/m3	membrane area	0.0016619	m2					
membrane ID	Duramem200		thickness	0.002	m					
MWCO	200	Da								
Mass of permeate (g)	Time (hr:min:sec)	Δmass permeate (g)	Δvolume permeate (ml)	hours	Totalminutes	cuml Seconds	cum time (hr)	Delta t (hr)	Flux (g.m ⁻² .hr ⁻¹)	Flux (L.m ⁻² .hr ⁻¹)
1	00:01:41.87	1	1.24	0.0	1	42	0.028	0.028	21237.18	26.38
5.3	00:05:48.76	4.3	5.34	0.0	5	49	0.097	0.069	37711.04	46.85
12.5	00:12:51.64	7.2	8.95	0.0	12	52	0.214	0.118	36871.35	45.81
16.4	00:16:40.75	3.9	4.85	0.0	16	41	0.278	0.064	36891.48	45.83
20.5	00:20:40.96	4.1	5.09	0.0	20	41	0.345	0.067	37005.78	45.98
25.8	00:26:14.71	5.3	6.58	0.0	26	15	0.438	0.093	34373.71	42.71
30	00:30:16.90	4.2	5.22	0.0	30	17	0.505	0.067	37595.07	46.71
37.8	00:38:14.98	7.8	9.69	0.0	38	15	0.638	0.133	35347.90	43.92

Table D.1.10: MEK flux data through Duramem™200 at 30 Bar

Test:	permeability tests		Room temperature	20	oC					
Date	2017-07-17		Ambient pressure	1.02	Bar					
Time	morning		Gas pressure	30	Bar					
Solvent	MEK		Vinitial charge	150	mL					
Density	804.9	kg/m3	membrane area	0.0016619	m2					
membrane ID	Duramem200		thickness	0.002	m					
MWCO	200	Da								
Mass of permeate (g)	Time (hr:min:sec)	Δmass permeate (g)	Δvolume permeate (ml)	hours	Totalminutes	cuml Seconds	cum time (hr)	Delta t (hr)	Flux (g.m ⁻² .hr ⁻¹)	Flux (L.m ⁻² .hr ⁻¹)
1.7	00:03:20.07	1.7	2.11	0.0	3	20	0.056	0.056	18412.63	22.88
5	00:07:24.47	3.3	4.10	0.0	7	24	0.123	0.068	29296.86	36.40
11	00:15:55.24	6	7.45	0.0	15	55	0.265	0.142	25434.74	31.60
15	00:19:49.08	4	4.97	0.0	19	49	0.330	0.065	37028.92	46.00
21	00:27:14.00	6	7.45	0.0	27	14	0.454	0.124	29207.08	36.29
27	00:34:51.68	6	7.45	0.0	34	52	0.581	0.127	28378.06	35.26
31.5	00:40:33.11	4.5	5.59	0.0	40	33	0.676	0.095	28586.11	35.52
35.4	00:45:30.89	3.9	4.85	0.0	45	31	0.759	0.083	28349.49	35.22

Table D.1.11: MEK flux data through Duramem™200 at 20 Bar

Test:	permeability tests		Room temperature	20	oC					
Date	2017-07-17		Ambient pressure	1.02	Bar					
Time	morning		Gas pressure	20	Bar					
Solvent	MEK		Vinitial charge	130	mL					
Density	804.9	kg/m3	membrane area	0.0016619	m2					
membrane ID	Duramem200		thickness	0.002	m					
MWCO	200	Da								
Mass of permeate (g)	Time (hr:min:sec)	Δmass permeate (g)	Δvolume permeate (ml)	hours	Totalminutes	cuml Seconds	cum time (hr)	Delta t (hr)	Flux (g.m ⁻² .hr ⁻¹)	Flux (L.m ⁻² .hr ⁻¹)
1	00:00:17.14	1	1.24	0.0	0	17	0.005	0.005	127423.06	158.31
5	00:00:32.77	4	4.97	0.0	0	33	0.009	0.004	541548.01	672.81
10	00:00:55.23	5	6.21	0.0	0	55	0.015	0.006	492316.37	611.65
15	00:01:18.77	5	6.21	0.0	1	19	0.022	0.007	451290.01	560.68
20	00:01:42.35	5	6.21	0.0	1	42	0.028	0.006	470911.31	585.06
25	00:02:05.74	5	6.21	0.0	2	6	0.035	0.007	451290.01	560.68
30	00:02:31.31	5	6.21	0.0	2	31	0.042	0.007	433238.41	538.25
40	00:03:17.54	10	12.42	0.0	3	18	0.055	0.013	460891.92	572.61
50	00:04:08.67	10	12.42	0.0	4	9	0.069	0.014	424743.54	527.70
60	00:05:00.60	10	12.42	0.0	5	1	0.084	0.014	416575.39	517.55

Table D.1.12: MEK flux data through Duramem™200 at 10 Bar

Test:	permeability tests		Room temperature	20	oC					
Date	2017-07-17		Ambient pressure	1.02	Bar					
Time	morning		Gas pressure	10	Bar					
Solvent	MEK		Vinitial charge	130	mL					
Density	804.9	kg/m3	membrane area	0.0016619	m2					
membrane ID	Duramem200		thickness	0.002	m					
MWCO	200	Da								
Mass of permeate (g)	Time (hr:min:sec)	Δmass permeate (g)	Δvolume permeate (ml)	hours	Totalminutes	cuml Seconds	cum time (hr)	Delta t (hr)	Flux (g.m ⁻² .hr ⁻¹)	Flux (L.m ⁻² .hr ⁻¹)
1	00:00:21.10	1	1.24	0.0	0	21	0.006	0.006	103152.00	128.16
5	00:00:52.25	4	4.97	0.0	0	52	0.014	0.009	279508.65	347.26
10	00:01:32.25	5	6.21	0.0	1	32	0.026	0.011	270774.01	336.41
15	00:02:14.21	5	6.21	0.0	2	14	0.037	0.012	257880.01	320.39
20	00:02:56.63	5	6.21	0.0	2	57	0.049	0.012	251882.80	312.94
25	00:03:38.37	5	6.21	0.0	3	38	0.061	0.011	264169.76	328.20
30	00:04:20.77	5	6.21	0.0	4	21	0.073	0.012	251882.80	312.94
41	00:05:55.18	11	13.67	0.0	5	55	0.099	0.026	253490.56	314.93
51	00:07:21.67	10	12.42	0.0	7	22	0.123	0.024	248987.59	309.34
60	00:08:42.59	9	11.18	0.0	8	43	0.145	0.023	240688.00	299.03

Table D.1.12: Toluene flux data through Duramem™200 at 40 Bar

Test:	permeability tests		Room temperature	14	oC						
Date	2017-07-18		Ambient pressure	1.006	Bar						
Time	morning		Gas pressure	40	Bar						
Solvent	Toluene		Vinitial charge	150	mL						
Density	866.9	kg/m3	membrane area	0.0016619	m2						
membrane ID	Duramem200		thickness	0.002	m						
MWCO	200	Da									
Mass of permeate (g)	Time (hr:min:sec)	Δmass permeate (g)	Δvolume permeate (ml)	hours	Totalminutes	cuml Seconds	cum time (hr)	Delta t (hr)	Flux (g.m ⁻² .hr ⁻¹)	Flux (L.m ⁻² .hr ⁻¹)	
0.5	00:11:47.50	0.5	0.58	0.0	11	47	0.196	0.196	1531.96	1.77	
1	00:19:10.08	0.5	0.58	0.0	19	10	0.319	0.123	2444.91	2.82	
1.4	00:26:39.58	0.4	0.46	0.0	26	40	0.444	0.125	1925.50	2.22	
2	00:35:30.53	0.6	0.69	0.0	35	31	0.592	0.148	2447.67	2.82	

Table D.1.13: Toluene flux data through Duramem™200 at 30 Bar

Test:	permeability tests		Room temperature	24	oC						
Date	2017-07-18		Ambient pressure	0.997	Bar						
Time	morning		Gas pressure	30	Bar						
Solvent	Toluene		Vinitial charge	130	mL						
Density	866.9	kg/m3	membrane area	0.0016619	m2						
membrane ID	Duramem200		thickness	0.002	m						
MWCO	200	Da									
Mass of permeate (g)	Time (hr:min:sec)	Δmass permeate (g)	Δvolume permeate (ml)	hours	Totalminutes	cuml Seconds	cum time (hr)	Delta t (hr)	Flux (g.m ⁻² .hr ⁻¹)	Flux (L.m ⁻² .hr ⁻¹)	
1	00:30:27.00	1	1.15	0.0	30	27	0.508	0.508	1185.66	1.37	
2	00:50:27.00	1	1.15	0.0	50	27	0.841	0.333	1805.16	2.08	
3	01:12:43.00	1	1.15	1.0	12	43	1.212	0.371	1621.40	1.87	
4	01:34:04.00	1	1.15	1.0	34	4	1.568	0.356	1691.02	1.95	
5	01:55:04.00	1	1.15	1.0	55	4	1.918	0.350	1719.20	1.98	
6	02:17:04.00	1	1.15	2.0	17	4	2.284	0.367	1641.05	1.89	

Table D.1.14: Toluene flux data through Duramem™ 200 at 20 Bar

Test:	permeability tests		Room temperature	24	oC					
Date	2017-07-18		Ambient pressure	0.998	Bar					
Time	Afternoon		Gas pressure	20	Bar					
Solvent	Toluene		Vinitial charge	110	mL					
Density	866.9	kg/m3	membrane area	0.0016619	m2					
membrane ID	Duramem200		thickness	0.002	m					
MWCO	200	Da								
Mass of permeate (g)	Time (hr:min:sec)	Δmass permeate (g)	Δvolume permeate (ml)	hours	Totalminutes	cuml Seconds	cum time (hr)	Delta t (hr)	Flux (g.m ⁻² .hr ⁻¹)	Flux (L.m ⁻² .hr ⁻¹)
1	00:30:27.00	1	1.15	0.0	30	27	0.508	0.508	1185.66	1.37
2	01:00:26.00	1	1.15	1.0	0	26	1.007	0.500	1204.11	1.39
3	01:32:43.00	1	1.15	1.0	32	43	1.545	0.538	1118.32	1.29
4	02:03:04.00	1	1.15	2.0	3	4	2.051	0.506	1189.56	1.37
5	02:34:59.00	1	1.15	2.0	34	59	2.583	0.532	1131.17	1.30
6	03:06:44.00	1	1.15	3.0	6	44	3.112	0.529	1137.11	1.31
7	03:38:30.00	1	1.15	3.0	38	30	3.642	0.529	1136.51	1.31

Table D.1.15: Toluene flux data through Duramem™ 200 at 10 Bar

Test:	permeability tests		Room temperature	10	oC					
Date	2017-07-18		Ambient pressure	1.02	Bar					
Time	Afternoon		Gas pressure	10	Bar					
Solvent	Toluene		Vinitial charge	130	mL					
Density	866.9	kg/m3	membrane area	0.0016619	m2					
membrane ID	Duramem200		thickness	0.002	m					
MWCO	200	Da								
Mass of permeate (g)	Time (hr:min:sec)	Δmass permeate (g)	Δvolume permeate (ml)	hours	Totalminutes	cuml Seconds	cum time (hr)	Delta t (hr)	Flux (g.m ⁻² .hr ⁻¹)	Flux (L.m ⁻² .hr ⁻¹)
1	00:55:27.00	1	1.15	0.0	55	27	0.924	0.924	651.09	0.75
2	01:50:32.00	1	1.15	1.0	50	32	1.842	0.918	655.43	0.76
3	02:52:43.00	1	1.15	2.0	52	43	2.879	1.036	580.59	0.67
4	03:55:14.00	1	1.15	3.0	55	14	3.921	1.042	577.50	0.67
5	04:58:04.00	1	1.15	4.0	58	4	4.968	1.047	574.59	0.66
6	06:00:55.00	1	1.15	6.0	0	55	6.015	1.048	574.43	0.66
7	07:03:55.00	1	1.15	7.0	3	55	7.065	1.050	573.07	0.66

Table D.1.16: MEK flux data through Duramem™150 at 40 Bar

Test:	permeability tests		Room temperature	20	oC					
Date	2016-07-11		Ambient pressure	1.02	Bar					
Time	Morning		Gas pressure	40	Bar					
Solvent	MEK		Vinitial charge	150	mL					
Density	804.9	kg/m3	membrane area	0.0016619	m2					
membrane ID	Duramem150		thickness	0.002	m					
MWCO	150	Da								
Mass of permeate (g)	Time (hr:min:sec)	Δmass permeate (g)	Δvolume permeate (ml)	hours	Totalminutes	cuml Seconds	cum time (hr)	Delta t (hr)	Flux (g.m ⁻² .hr ⁻¹)	Flux (L.m ⁻² .hr ⁻¹)
1	00:01:57.00	1	1.24	0.0	1	57	0.033	0.033	18514.46	23.00
5.5	00:05:28.02	4.5	5.59	0.0	5	28	0.091	0.059	46198.41	57.40
10.2	00:09:13.99	4.7	5.84	0.0	9	14	0.154	0.063	45049.13	55.97
15.2	00:13:24.48	5	6.21	0.0	13	24	0.223	0.069	43323.84	53.83
22.12	00:19:17.62	6.92	8.60	0.0	19	18	0.322	0.098	42344.77	52.61
30.2	00:25:50.31	8.08	10.04	0.0	25	50	0.431	0.109	44650.08	55.47
40.02	00:34:11.87	9.82	12.20	0.0	34	12	0.570	0.139	42374.51	52.65
50.04	00:42:30.24	10.02	12.45	0.0	42	30	0.708	0.138	43584.83	54.15
60	00:50:43.96	9.96	12.37	0.0	50	44	0.846	0.137	43674.64	54.26
70	00:58:54.09	10	12.42	0.0	58	54	0.982	0.136	44208.00	54.92
80	01:07:10	10	12.42	1.0	7	10	1.119	0.138	43673.23	54.26

Table D.1.17: MEK flux data through Duramem™150 at 30 Bar

Test:	permeability tests		Room temperature	18	oC					
Date	2016-07-11		Ambient pressure	1.02	Bar					
Time	Morning		Gas pressure	30	Bar					
Solvent	MEK		Vinitial charge	150	mL					
Density	804.9	kg/m3	membrane area	0.0016619	m2					
membrane ID	Duramem150		thickness	0.002	m					
MWCO	150	Da								
Mass of permeate (g)	Time (hr:min:sec)	Δmass permeate (g)	Δvolume permeate (ml)	hours	Totalminutes	cuml Seconds	cum time (hr)	Delta t (hr)	Flux (g.m ⁻² .hr ⁻¹)	Flux (L.m ⁻² .hr ⁻¹)
1.1	00:02:06.97	1.1	1.37	0.0	2	7	0.035	0.035	18762.29	23.31
5	00:06:34.55	3.9	4.85	0.0	6	35	0.110	0.074	31522.94	39.16
10.32	00:12:27.02	5.32	6.61	0.0	12	27	0.208	0.098	32739.04	40.67
15.34	00:18:02.63	5.02	6.24	0.0	18	3	0.301	0.093	32363.94	40.21
20.82	00:24:12.80	5.48	6.81	0.0	24	13	0.404	0.103	32083.06	39.86
30.1	00:34:29.00	9.28	11.53	0.0	34	29	0.575	0.171	32633.54	40.54
40.21	00:45:53.34	10.11	12.56	0.0	45	53	0.765	0.190	32017.84	39.78
51.7	00:58:42.97	11.49	14.28	0.0	58	43	0.979	0.214	32324.09	40.16
60.6	01:08:45.19	8.9	11.06	1.0	8	45	1.146	0.167	32025.10	39.79
70	01:19:23.00	9.4	11.68	1.0	19	23	1.323	0.177	31915.68	39.65

Table D.1.18: MEK flux data through Duramem™150 at 20 Bar

Test:	permeability tests		Room temperature	20	oC					
Date	2016-07-11		Ambient pressure	1.02	Bar					
Time	Morning		Gas pressure	20	Bar					
Solvent	MEK		Vinitial charge	130	mL					
Density	804.9	kg/m3	membrane area	0.0016619	m2					
membrane ID	Duramem150		thickness	0.002	m					
MWCO	150	Da								
Mass of permeate (g)	Time (hr:min:sec)	Δmass permeate (g)	Δvolume permeate (ml)	hours	Totalminutes	cuml Seconds	cum time (hr)	Delta t (hr)	Flux (g.m ⁻² .hr ⁻¹)	Flux (L.m ⁻² .hr ⁻¹)
1.1	00:03:29.84	1.1	1.37	0.0	3	30	0.058	0.058	11346.72	14.10
5	00:10:14.21	3.9	4.85	0.0	10	14	0.171	0.112	20911.26	25.98
10	00:18:45.30	5	6.21	0.0	18	45	0.313	0.142	21195.62	26.33
16.5	00:30:05.71	6.5	8.08	0.0	30	6	0.502	0.189	20675.84	25.69
20.8	00:37:20.07	4.3	5.34	0.0	37	20	0.622	0.121	21462.27	26.66
30.1	00:53:25.86	9.3	11.55	0.0	53	26	0.891	0.268	20854.64	25.91
40.55	01:11:28.33	10.45	12.98	1.0	11	28	1.191	0.301	20921.17	25.99
56.06	01:38:27.50	15.51	19.27	1.0	38	28	1.641	0.450	20739.28	25.77

Table D.1.19: MEK flux data through Duramem™150 at 10 Bar

Test:	permeability tests		Room temperature	20	oC						
Date	2016-07-11		Ambient pressure	1.02	Bar						
Time	Afternoon		Gas pressure	10	Bar						
Solvent	MEK		Vinitial charge	130	mL						
Density	804.9	kg/m3	membrane area	0.0016619	m2						
membrane ID	Duramem150		thickness	0.002	m						
MWCO	150	Da									
Mass of permeate (g)	Time (hr:min:sec)	Δmass permeate (g)	Δvolume permeate (ml)	hours	Totalminutes	cuml Seconds	cum time (hr)	Delta t (hr)	Flux (g.m ⁻² .hr ⁻¹)	Flux (L.m ⁻² .hr ⁻¹)	
1.05	00:07:35.86	1.05	1.30	0.0	7	36	0.127	0.127	4987.94	6.20	
5.3	00:27:14.33	4.25	5.28	0.0	27	14	0.454	0.327	7815.21	9.71	
10.1	00:49:24.98	4.8	5.96	0.0	49	25	0.824	0.370	7811.96	9.71	
15.44	01:14:14.50	5.34	6.63	1.0	14	14	1.237	0.414	7768.61	9.65	
20.42	01:37:15.01	4.98	6.19	1.0	37	15	1.621	0.384	7811.47	9.70	

D.2. Summary of all experimental calculated data

Table D.2.1: Experimental result summary for MEK solvent

membrane	C16 Frac solute (wt/wt %)	Pressure (bar)	Average Flux (L.m ⁻² .hr ⁻¹)	Rejection (%)
Duramem™150	-	40	54.55	-
	-	30	39.96	-
	-	20	26.05	-
	-	10	9.69	-
	10	30	19.59	68.78
	15	30	15.40	89.21
	20	30	13.51	95.98
	25	30	11.84	94.47
Duramem™200	-	40	45.16	-
	-	30	35.57	-
	-	20	22.38	-
	-	10	10.00	-
	10	30	19.30	77.42
	15	30	15.96	81.79
	20	30	14.50	75.33
	25	30	12.21	88.11
Puramem™280	-	40	1148.10	-
	-	30	889.25	-
	-	20	597.75	-
	-	10	341.11	-
	10	30	730.88	38.38
	15	30	724.80	16.11
	20	30	645.56	35.18
	25	30	630.91	50.37

Table D.2.1: Experimental result summary for DCM solvent

membrane	C16 Frac solute (wt/wt %)	Pressure (bar)	Average Flux (L.m ⁻² .hr ⁻¹)	Rejection (%)
Duramem™150	-	40	89.70	-
	-	30	65.05	-
	-	20	40.85	-
	-	10	16.92	-
	10	30	22.95	70.95
	15	30	11.19	75.83
	20	30	2.89	76.76
	25	30	0.37	78.10
Duramem™200	-	40	70.33	-
	-	30	55.76	-
	-	20	33.43	-
	-	10	16.12	-
	10	30	28.60	77.81
	15	30	23.62	96.06
	20	30	17.43	73.71
	25	30	9.23	91.23
Puramem™280	-	40	n/a	n/a
	-	30	n/a	n/a
	-	20	n/a	n/a
	-	10	n/a	n/a
	10	30	n/a	n/a
	15	30	n/a	n/a
	20	30	n/a	n/a
	25	30	n/a	n/a

Table D.2.1: Experimental result summary for MIBK solvent

membrane	C16 Frac solute (wt/wt %)	Pressure (bar)	Average Flux (L.m ⁻² .hr ⁻¹)	Rejection (%)
Duramem™150	-	40	6.61	-
	-	30	4.69	-
	-	20	3.50	-
	-	10	-	-
	10	30	-	-
	15	30	-	-
	20	30	-	-
	25	30	-	-
Duramem™200	-	40	4.89	-
	-	30	3.48	-
	-	20	2.39	-
	-	10	1.28	-
	10	30	2.67	54.52
	15	30	2.11	89.92
	20	30	1.69	84.24
	25	30	1.32	70.98
Puramem™280	-	40	107.27	-
	-	30	83.16	-
	-	20	61.60	-
	-	10	28.04	-
	10	30	65.38	0.74
	15	30	47.49	4.95
	20	30	44.50	26.19
	25	30	39.88	32.22

Table D.2.1: Experimental result summary for toluene solvent

membrane	C16 Frac solute (wt/wt %)	Pressure (bar)	Average Flux (L.m ⁻² .hr ⁻¹)	Rejection (%)
Duramem™150	-	40	1.55	-
	-	30	1.11	-
	-	20	0.72	-
	-	10	-	-
	10	30	-	-
	15	30	-	-
	20	30	-	-
	25	30	-	-
Duramem™200	-	40	2.62	-
	-	30	1.96	-
	-	20	1.32	-
	-	10	0.66	-
	10	30	n/a	n/a
	15	30	n/a	n/a
	20	30	n/a	n/a
	25	30	n/a	n/a
Puramem™280	-	40	429.87	-
	-	30	287.59	-
	-	20	202.04	-
	-	10	123.21	-
	10	30	267.57	39.58
	15	30	227.64	8.91
	20	30	204.90	18.07
	25	30	197.77	29.06

Appendix E: Simulation data

E.1 OSN stream data

Stream Properties		Streams							
		FEED1	MEMBRANE	MEMBIN	PERM1	PERMOUT	RET1	RECYC1	RECYC2
Phase:		Liquid	Liquid	Liquid	Liquid	Liquid	Liquid	Liquid	Liquid
Comp Mole Flow									
MEK	KMOL/HR	10.40	10.40	18.58	16.36	8.180	2.220	16.36	8.180
hexadecane	KMOL/HR	1.104	1.104	1.122	0.037	0.018	1.085	0.037	0.018
Comp Mass Flow									
MEK	KG/HR	750.00	750.00	1339.85	1179.71	589.85	160.146	1179.706	589.853
hexadecane	KG/HR	250.00	250.00	254.20	8.414	4.207	245.792	8.414163	4.207
Comp Mass Fraction									
MEK		0.750	0.750	0.840	0.992	0.992	0.394	0.992	0.992
hexadecane		0.250	0.250	0.1594	0.007	0.007	0.605	0.007	0.007
Mole Flow	KMOL/HR	11.505	11.505	19.704	16.397	8.198	3.306	16.397	8.198
Mass Flow	KG/HR	1000.0	1000.0	1594.06	1188.12	594.060	405.939	1188.12	594.060
Volume Flow	CUM/HR	1.295	1.290	2.038	1.493	0.746	0.534	1.493	0.746
Temperature	C	20.00	21.124	20.592	20.592	20.592	20.592	20.592	20.592
Pressure	BAR	1.00	30.00	30.00	30.00	30.00	30.00	30.00	30
Liquid Fraction		1.00	1.00	1.00	1.00	1.00	1.00	1.00	1
Molar Enthalpy	KJ/HR	-291.660	-291.166	-284.538	-275.250	-275.250	-332.250	-275.250	-275.23
Mass Enthalpy	KJ/KG	-3355.467	-3349.775	-3516.99	-3798.651	-3798.651	-2706.068	-3798.651	-3798.46
Enthalpy Flow	KW	-932.083	-930.5	-1557.305	-1253.694	-626.833	-305.138	-1253.694	-626.805
Molar Density	KG/CUM	0.0088	0.0090	0.0097	0.0109	0.0109	0.0062	0.0109	0.0109
Mass Density	KG/CUM	771.942	774.864	781.949	795.444	795.444	759.252	795.444	795.444
Ave Molecular Weight	g/mol	86.916	86.916	80.900	72.457	72.457	122.773	72.456	72.456

E.2 Distillation stream data

Stream data		Streams									
		BOTTOMS	BOTTOMS2	DIST	DIST2	DISTIN	DISTMIX2	DISTOUT	DISTREC	FEED	FEED2
Comp Mole Flow											
MEK	kmol/hr	2.249	2.249	16.304	16.304	18.553	18.553	8.152	8.152	10.401	10.401
HEX	kmol/hr	1.083	1.083	0.042	0.042	1.125	1.125	0.021	0.021	1.104	1.104
Comp Mass Flow											
MEK	kg/hr	162.20	162.20	1175.59	1175.59	1337.79	1337.79	587.79	587.79	750.00	750.00
HEX	kg/hr	245.29	245.29	9.40	9.40	254.70	254.70	4.70	4.70	250.00	250.00
Comp Mass Frac											
MEK		0.398	0.398	0.992	0.992	0.840	0.840	0.992	0.992	0.750	0.750
HEX		0.602	0.602	0.008	0.008	0.160	0.160	0.008	0.008	0.250	0.250
Mole Flow	kmol/hr	3.333	3.333	16.345	16.345	19.678	19.678	8.173	8.173	11.505	11.505
Mass Flow	kg/hr	407.5	407.5	1185	1185	1592.5	1592.5	592.5	592.5	1000	1000
Volume Flow	cum/hr	1.022	0.657	3.079	1.850	2.959	2.629	0.925	0.925	1.289	1.699
Temperature	c	301.9	171.1	239.0	141.1	197.0	161.1	141.1	141.1	20.0	173.2
Pressure	bar	30	30	30	30	30	30	30	30	30	30
Liquid Fraction		1	1	1	1	1	1	1	1	1	1
Molar Enthalpy	kw	-28.60	-34.41	-27.74	-30.42	-29.76	-30.75	-30.42	-30.42	-34.79	-30.98
Mass Enthalpy	kJ/kg	-1958	-2356	-3204	-3514	-3080	-3182	-3514	-3514	-3352	-2985
Enthalpy Flow	kw	-221.68	-266.72	-1054.53	-1156.58	-1362.36	-1407.39	-578.30	-578.30	-931.13	-829.08
Molar Density	kg/cum	0.204	0.317	0.331	0.551	0.415	0.467	0.551	0.551	0.557	0.423
Mass Density	kg/cum	398.68	620.52	384.92	640.38	538.13	605.86	640.38	640.38	775.87	588.70
Ave Mol Wt	g/mol	122.27	122.27	72.50	72.50	80.93	80.93	72.50	72.50	86.92	86.92

E.3. Heat exchanger Aspen Plus™ data

Equipment parameters	units	EXBOTT	EXDIST
Calculated heat duty	kW	45.04	102.06
Required exchanger area	sqm	1.31	1.32
Average U (Dirty)	kJ/sec-sqm-K	0.85	0.85
UA	kJ/sec-K	1.12	1.13
LMTD (Corrected)	C	40.37	90.66
LMTD correction factor		1	1
Number of shells in series		1	1

